Proceedings of the 16th International Conference on Soil Mechanics and Geotechnical Engineering

doi:10.3233/978-1-61499-656-9-251

Development of geotechnical earthquake engineering in Japan

Développement de l'ingénierie sismique géotechnique au Japon

I. Towhata
Department of Civil Engineering, The University of Tokyo

ABSTRACT

Japan is one of the regions which are most prone to natural hazards. Among such disasters as indeced by heavy rainfalls, typhoons, and volcanic actions, earthquakes have been causing a variety of bad consequences in the history. Under this hard natural environment, technologies have developed historically and in modern times in a variety of directions in order to prevent or mitigate natural hazards. The earliest examples of those developments are the famous seismic coefficient method of seismic design and Mononobe-Okabe earth pressure theory. Repeated strong earthquakes in densely populated area have kept showing new kinds of problems. Under many disasters, it was often possible to demonstrate the effectiveness of new mitigative technologies. Problems related with soil liquefaction is one of the examples of this type. Starting with the assessment of liquefaction potential and prevention of the onset of liquefaciotn, geotechnical engineering in the recent decades is shifting to the performance-based approach in which the consequence of liquefaction is assessed and, if the consequence is not allowable, it is mitigated. This situation has provided significant research topics, which are extremely difficult, and important achievements have been accomplished. The latest problem to be solved is the introduction of broader viewpoints in which the seismic resistance of individual structurea is studied and determined so that the seismic vulnerability of the whole public may be minimized. This would be a combination of geotechnical engineering and regional economic planning.

RÉSUMÉ

Le Japon est l'une des régions au monde les plus sujettes aux risques naturels. Parmi ces calamités naturelles citons les pluies torrentielles, les typhons, les éruptions volcaniques et les tremblements de terre qui ont été la cause de nombreuses catastrophes historiques. Dans cet environnement naturel difficile, les technologies se sont développées au fil du temps dans de nombreux domaines dans le but d'arriver aujourd'hui à prévenir ou minimiser ces risques naturels. Un des plus anciens exemples de ces développements est la fameuse méthode du coefficient sismique de design sismique et la théorie de pression des sols de Mononobe-Okabe. Des tremblements de terre importants à répétition dans des zones fortement peuplées ont apporté leur lot de nouvelles sortes de problèmes. Suite à de nombreuses catastrophes, il a souvent été possible de prouver l'efficacité des nouvelles technologies de prévention. Les problèmes liés à la liquéfaction des sols illustrent bien ces améliorations. A l'origine, préoccupée par l'évaluation des potentiels de liquéfaction des sols et par la prévention de ses conséquences, l'ingénierie géotechnique évolue maintenant vers une approche où les conséquences de la liquéfaction sont évaluées, et si ces conséquences ne sont pas tolérables, les actions sont alors entreprises pour les prévenir. Cette évolution a été l'occasion de nombreux sujets de recherche particulièrement complexes qui ont permis de nombreuses avancées. La problématique qu'il reste à résoudre est l'introduction d'une vision plus large dans laquelle la résistance sismique spécifique à chaque structure est étudiée et déterminée de telle manière que la vulnérabilité sismique de l'ensemble d'une région soit minimisée. Ce serait la combinaison de l'ingénierie géotechnique avec la planification économique régionale.

1 INTRODUCTION

Similar to many countries located in seismically active regions, Japan has been affected by strong earthquakes many times in its history. Usami (1996) made a comprehensive study on the history of seismic damages in Japan. According to him, the earliest written record of earthquake appeared in its governmental book of history in the year of 416, simply stating that ground shaking occurred. A description on any kind of damage appeared in the year of 599, which stated that houses fell down. There is a report on landslide in 679. Thus, the type of damage which attracted an official concern was a landslide together with collapse of houses and buildings. Fig.1 illustrates people's anger to a catfish after an earthquake in present Tokyo in the year of 1855. This fish was believed to be the earthquake generator. With so many experiences of earthquakes in the history, people became very sensitive to earthquake problems. Urban developments in the recent decades have led to new types of seismic damages such as lifeline breakage and liquefaction in addition to building failure and slope instability being still important.

Written history tells us many important stories about the consequence of earthquakes. According to Usami (1996), boiling of water and soil, which is probably liquefaction in the present sense, has been described many times since the year of 684. What is interesting to the author is the record in the same year of 684 in which a report was made of a regional subsidence of ground in the southern part of Shikoku Island which faces a source of repeated gigantic earthquakes in the Pacific Ocean (Fig.2). Upon the event in 684, submergence of land under sea water occurred over an area of 10 km^2. This event seems noteworthy because there are written records of similar phenomena in the same region in the years of 1099 (again 10 km^2), 1854 (1 to 1.5 m subsidence), and 1946; after 1946, 9.3 km^2 subsided near Kochi City, while 3.0 km^2 near Suzaki City (Usami, 1996).

A combination of a humid climate, heavy rainfalls, geologically young rocks, a high rate of erosion and weathering, and consequent steep mountain slopes induced and still induces slope failures as well as debris flows frequently. Fig.3 shows a result of debris flow in Minamata of Kyushu, 2003. Since such a soil flow is able to travel over hundreds of meters or even kilometers and affect local communities along the path, it is required to develop a mitigative engineering which consists not only of slope stability assessment in the source area but also quantitative understanding of flow dynamics so that travel distance and induced forces on existing structures may be evaluated.

Figure 1. People punishing catfish which caused disastrous earthquake in present Tokyo in 1855.

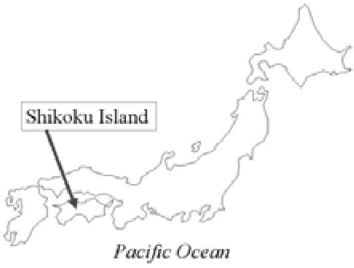

Figure 2. Location of Shikoku Island of Japan.

Figure 3. Deposit of debris flow in Minamata of Kyushu, 2003 (Photo by T.Ito).

Figure 4. Retaining structure of potentially unstable mountain slope (Tateyama, Toyama Prefecture).

The aforementioned adverse combination of climatic and geological conditions has caused gigantic slope failures many times in the history. The efforts for disaster mitigation in the recent decades, however, have drastically reduced the number of victims from thousands in one event of heavy rainfall to, for example, tens or less. The said efforts consist of slope stabilization in the source area such as retaining structures (Fig.4) and vegetation, construction of protective structures along a river channel (Fig.5), and setting-up of disaster management measures in a potentially hazardous area. Additional contribution is made during heavy rainfalls by the Meteorological Agency which issues warning against slope instability hazards based on rainfall monitoring data.

Figure 5. River channel after improvement against sedimentary transport (Joganji River).

Figure 6. Ohya site of seismically-induced slope failure.

Figure 7. Rice fields situated upon irregular surface configuration made by past landslide (Shiotani Village, Niigata).

2 EXPERIENCES DURING PAST EARTHQUAKES

Strong earthquake motion often destroys unstable mountains. Fig.6 shows the site of Ohya slope failure in Shizuoka Prefecture which was caused by an earthquake in 1707. Since then the problem has remained to continue; heavy rainfalls cause debris flow in this slope and the failed material is transported downwards by the river flow. This implies the importance of erosion control technology after such a large slope failure.

The recent 2004 Niigata-Chuetsu earthquake of magnitude (JMA scale) 6.8 demonstrated several kinds of slope problems during earthquakes. Since mountains in the affected region were made of young (tertiary) sandstones and mudstones, slope failure occurred at more than 1000 sites in total, although many of them were surficial. The potentially unstable nature of the slopes in this region has been shown by the existing topography which was made by landslides in the past (Fig.7). One of the remarkable consequences of the quake was the formation of natural dams (Fig.8) which flooded the upstream area. Probably more significant to the local community, however, was the damage in local roads. Fig.9 shows an example of collapse of a road embankment on a small valley, while Fig.10 indicates a distorted tunnel. The latter in particular reveals that problem of a tunnel in soft rock which is in contrast with an empirical knowledge of safety in a tunnel excavated through hard rock. It should be learned from the events in Figs 9 and 10 that rescue and restoration are impossible once road traffic is stopped by such geotechnical hazards.

Figure 8. Natural dam formed by slope failure (Yamakoshi Village, Niigata).

Figure 9. Failed road embankment resting upon small valley (Yamakoshi Village).

The significance of seismic liquefaction in loose and water-saturated deposit of sand came to be known to the engineering community at the time of the 1964 Niigata earthquake. Fig.11 illustrates the landscape of Niigata in 1849 in which there is a channel of Shinano River in the center. Noteworthy is a big cove or bay of the river to the right of this map. In early 20th century, this part of river was filled with clean and fine sand which was easily available in the coastal dune of the city, and was named Kawagishi Cho. Since compaction of sandy ground was not within a geotechnical scope in those days, a loose sandy deposit was formed. It is well known today that such a geotechnical condition is highly vulnerable to liquefaction as evidenced by the 1964 quake (Fig.12).

Artificial soil filling in a similar way, i.e. pouring cohesionless soils into water, was conducted as well in the city of Dagupan in Luzon Island of the Philippines and Port Island of Kobe together with many others, and very similar consequence occurred. It is meaningful to hereby inspect what happened in those sites during respective earthquakes. Fig.13 illustrates an inclined shape of a building in Niigata City which was supported by a shallow footing foundation. As is widely known, liquefaction of subsoil substantially reduced the rigidity of foundation sand, leading to subsidence and tilting of the building. It should be noted that the super structure did not have such a structural damage as cracking and buckling, suggesting that the conventional kind of safety evaluation based on breakage and material strength is not relevant. This building was considered to be damaged because of the significant extent of subsidence and tilting. It seems noteworthy further that the building tilted towards the right in Fig.13 possibly because of the load eccentricity to the same direction as suggested by the roof structure on the right side as well. Readers are advised to inspect photographs of the apartment buildings in Kawagishi-Cho of Niigata which tilted to the direction of roof structure as well. The building in Dagupan City (Fig.14) was considered to be damaged because of the extensive subsidence. This unallowable magnitude of subsidence made it impossible to use this building, although there was no structural damage.

(a) Cracking in concrete lining at the top.

(b) Distortion of pavement due to compression.

Figure 10. Collapse of tunnel in soft-rock mountain, Niigata-Chuetsu, 2004.

Figure 11. Map of Niigata City in 1849.

Figure 12. Liquefaction in Kawagishi-Cho area of Niigata city (Japanese Geotechnical Society, 2004).

In addition to subsidence which was caused by the gravity force exceeding the bearing capacity, floating of embedded structures occurred during liquefaction. Fig.15 shows floating of sewage treatment tank in Niigata, while in Fig.16 the same thing happened in Dagupan. In both cases, the gravity force of the tanks was overcome by the buoyancy force which was equal to the unit weight of water-saturated sand multiplied by the tank volume, and the reduced rigidity of liquefied sand could not prevent floating. Note that there is no structural damage such as cracking in the tank. Those tanks were considered to be damaged because the excessive vertical displacement made them out of service. Fig.17 shows floating of a manhole of a sewage pipeline which was induced by liquefaction of backfill sand. The large vertical displacement made the pipeline out of service.

Figure 13. Tilting of building resting on shallow foundation placed on loose sandy ground (Univ. Tokyo).

Figure 14. Significant subsidence of building in Dagupan.

Figure 15. Floating of embedded tank for sewage treatment in Niigata (Univ. Tokyo).

Figure 16. Floating of sewage treatment tank in Dagupan.

Figure 17. Floating of sewage manhole due to liquefaction of water-saturated backfill soil (Ojiya City of Niigata in 2004).

Figure 18. Dainichi Yama seismic landslide in Niigata, 2004.

Figure 19. Distortion of ground behind gravity quay wall in Nishinomiya Harbor (after 1995 Kobe earthquake).

Figure 20. Heavy distortion of backfill in Port Island of Kobe.

Residual displacement in the horizontal direction is often caused by ground shaking. The slope instability during earthquakes as mentioned before is certainly one of the important examples. In Fig.18 a soil mass moved and rotated along a circular slip plane, and a road which used to connect both sides of the plane was disconnected. Although the moving soil mass developed many cracks in its surface, its overall integrity was maintained. Thus, the soil mass may be idealized as a rigid mass as has been practiced in slope stability analysis. Although liquefied ground may translate in the lateral direction as well, the idea of rigid mass is not relevant. In Fig.19, many tension cracks developed on the surface of backfill behind a translating quay wall. This distortion of backfill area indicates that the movement of a quay wall may affect structural foundations and embedded structures behind it.

Fig.20 demonstrates a deformed shape of a quay wall and backfill in Port Island of Kobe. Since the service of the Kobe harbor was stopped for a long time due to significant distortion of quay walls, many clients decided to use other harbors and did not come back to Kobe again, even after the harbor structures were restored. It should be pointed out therefore that the essence of damage lay not in the structural breakage but in the closure of service which affected the harbor business significantly.

Excessive displacement due to subsoil liquefaction is taken seriously in seismic design of river dikes. Fig.21 indicates the subsidence of Yodo River dike in Osaka which was induced by the 1995 Kobe earthquake. The extent of subsidence was more than 2 m with the maximum value of 3 m (Matsuo, 1996). Liquefaction of subsoil was verified by boiling at the foot of its slope. Due to loss of rigidity in the subsoil, the dike slope moved laterally, and the top of the dike sank down. The essence of this damage lies in the excessive loss of height which might have allowed overtopping of river water. Conventionally, seismic design has hardly been practiced in river dikes. The philosophy behind this idea was that the major function of river dikes is the prevention of flooding during high water level in the river, and that earthquake and flooding were unlikely to come at the same time. Accordingly, a quick restoration of possible seismic damage was considered to be more important than costly seismic retrofitting. Although this idea is reasonable in most cases (Fig.22), an exception was the case of Yodo River which was located near the sea and had a high tidal level twice a day. Thus, there was no time to spare between earthquake and occurrence of high water level. Even worse was the ground elevation behind the dike. Being lower than the sea level, the high tidal level could have supplied an unlimited volume of water flooding into the densely populated back area, if the dike subsidence had been substantial. Accordingly, the importance of a seismic design of river dike was clearly understood. Note that, more precisely, the residual height of a dike after a strong quake is the key issue in contrast with the fact that the magnitude of displacement is the issue in buildings, embedded tanks, and others as described above.

In summary, the essential issue in liquefaction damage is the excessive magnitude of residual displacement that makes the concerned facility out of service, while structural breakage in super structures is less important. Therefore, efforts for damage mitigation should be focused on reduction of displacement induced by liquefaction. If the induced displacement exceeds the allowable limit, the function of the facility may stop for a long time and affect the local community or even a nation substantially.

Figure 21. Subsidence of Yodo River dike due to subsoil liquefaction (Photograph by Fudo Construction Company).

Figure 22. Quick restoration of seismic damage in Ushishubetsu River dike in Hokkaido in 2003.

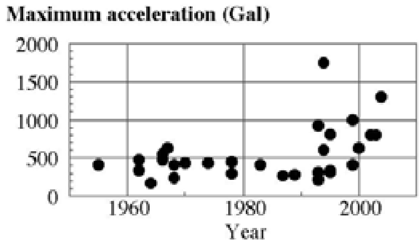

Figure 23.. Maximum horizontal accelerations recorded during recent strong earthquakes.

3 PERFORMANCE-BASED SEISMIC DESIGN OF GEOTECHNICAL STRUCTURES

The earliest version of seismic design for modern structures was developed by Sano (1916 and 1917) who investigated the earthquake-induced damage caused by the Great San Francisco earthquake in 1906. He proposed to use seismic inertia force in design, which is static and considered equivalent to shaking; seismic inertia force = (seismic coefficient) * (weight of concerned structure), and conceptually the seismic coefficient K_h = *(maximum horizontal acceleration) / (gravity acceleration)* as the d'Alembert's principle of mechanics states. This idea was universally accepted, and made a great contribution to saving human lives and structures. The Mononobe-Okabe theory of seismic active earth pressure is one of the applications of the Sano's idea (Okabe, 1924 and 1926; Mononobe and Matsuo, 1929).

Recent earthquakes have posed problems to seismic design practice. Fig.23 illustrates the magnitudes of maximum horizontal acceleration during recent earthquakes. Since the number of seismic recording stations has increased tremendously in the recent decade, the chance to obtain very strong accelerations has increased as well. For example, the 1993 Kushiro-Oki earthquake registered 9.2 m/sec^2 acceleration, and the 1995 Kobe earthquake 8.2 m/sec^2; both upon small hills. The 1999 ChiChi earthquake in Taiwan produced 10m/sec^2. Consequently, there has been a tendency in the seismic engineering discipline to increase the intensity of design earthquakes. For example, the 2002 version of the Highway Bridge Design Code (Japan Road Association, 2002) employs for seismic design of superstructures 10 to 15 m/sec^2 as the peak value of response acceleration spectrum as a very rare but strong design earthquake on soft soil conditions. On hard soils, those values become 7 to 20 m/sec^2. Sano's idea in its original form implies that 7 m/sec^2 acceleration should be converted to a static force of 70 % of the structural weight. It is too expensive or even impossible to design structures against such a strong static force. Since the real earthquake is dynamic and lasts for a short time, the seismic engineering for steel and concrete structures has adopted advanced types of philosophy in which dynamic analysis, nonlinear behavior of materials, the levels of serviceability, and collapse mechanisms are taken into account.

It is evident that geotechnical engineering has to carry out similar efforts for modernization of design principles. This is particularly important because geotechnical materials cannot resist such a strong seismic inertia force as is equivalent to 7 m/sec^2; 70 % of own weight. One attempt to solve this problem is to use the empirical formula by Noda et al. (1975) who collected the maximum horizontal accelerations, Amax, in damaged and undamaged harbor structures and compared them with the design seismic coefficient, *Kh*. Their idea was that the boundary of *Amax* between damaged and undamaged structures is equivalent to the design seismic load of *Kh*. Consequently, the following empirical formula was obtained;

$$Kh = \frac{1}{3}\left(\frac{A\max}{g}\right)^{1/3} \qquad (1)$$

in which *g* stands for the gravity acceleration. Although the above formulae can significantly reduce the level of *Kh*, from *1.0* in case of *Amax=g* to *0.33*, this magnitude of static seismic design force in combination with the static load may still make it difficult to maintain the factor of safety greater than unity. To overcome this problem, it is necessary to take into account the following two issues. Firstly, the earthquake loading is not static and the seismic factor of safety less than unity does not mean the overall failure. Therefore, the residual deformation might be reasonably small, depending upon the nature of shaking and material properties. Another issue is the idea of quick restoration. Fig.22 illustrated an example for this. It is noteworthy that earth structures in general can be restored more easily than steel and concrete structures. Figs.24 and 25 illustrate a river dike in Wufeng of Taiwan immediately after the 1999 ChiChi earthquake and six months later. This damage was caused by a fault action underlying this particular site. In contrast to many bridges and a concrete dam which were destroyed by fault actions and took much longer time for restoration, the quick restoration in this dike is remarkable. With further reference to the discussion in the previous section that the essence of liquefaction damage lies in the extensive displacement, it can be stated that a future version of seismic design for geotechnical structures should be based on the magnitude of seismically-induced deformation and/or displacement. In case the induced displacement is sufficiently small, it should be considered acceptable and further seismic reinforcement is not necessary.

The use of the residual displacement which is induced by an earthquake shaking as a design criterion appears to be in line with the development of earthquake engineering for steel and concrete structures. It is, however, very important to take into account special features of earth structures.

First of all, earth structure is less resistant against earthquakes than well-designed bridges and other steel or concrete structures. Fig.26 illustrates the subsidence of approach to a bridge after the 2004 Chuetsu earthquake in Niigata, Japan. The subsidence of the road embankment stopped the traffic although the main part of the bridge was intact. In planning an emergency action which is practiced after a strong quake, attention should be paid to the operation of not only the main structure of bridges but also associating earth structures. However, it is impossible to reinforce so many earth structures so that no distortion may be induced during strong shaking.

Secondly, as demonstrated in Figs. 24 and BC, the restoration procedure of earth structures is relatively quick as compared with steel and concrete structures. In the case of Fig. 26, a temporary earth filling at the place of subsidence allowed emergency traffics to pass. Since structures such as road embankment in particular play very important roles in emergency rescue immediately after an earthquake, their quick restoration is extremely important. Fig.27 illustrates a temporary detour which was placed next to a collapsed road embankment resting upon small valley topography. At this place, trunk lines of a railway and road were similarly damaged, and the road traffic was somehow started again within a few days, while railway took a few months. This difference is related with the fact that train service demands a perfect configuration of a railway, while car drivers can adjust themselves to defects in road conditions. Therefore, the emergency rescue and restoration activities rely on the operation of road traffic, allowing limited extent of distortion.

Figure 24. Damaged shape of river dike at Wufeng after 1999 ChiChi earthquake in Taiwan.

Figure 25. Restored shape of river dike at Wufeng 6 months after the damage.

Figure 26. Differential subsidence of bridge approach (Yamabe Bridge in Niigata, 2004).

Figure 27. Detour road which allowed emergency traffic to go (in 2004, Ojiya, Niigata).

Difficulty in post-earthquake restoration depends on the magnitude of residual distortion. In this respect, efforts have been made to take into account in seismic design codes of geotechnical structures the allowable deformation. Problems to be overcome are the lack of philosophy by which the allowable deformation is determined, and missing of practical method to assess the seismically-induced deformation. The latter means that detailed soil investigation is not carried out in most geotechnical structures and that deformation analysis with reliable soil data is difficult.

The present chapter concerns with the philosophy by which the allowable limit of seismically-induced deformation is determined. To date it appears to be difficult to determine a particular value of allowable deformation, because there seems to be no significant difference in seismic deformation of 20cm and 40cm, for example, from the viewpoint of post-earthquake activities. Thus, a study was conducted by a committee of Japan Society of Civil Engineers (JSCE) in which the author was the chairman. Efforts were made there to develop a systematic approach to determine the allowable seismic deformation that remains after shaking. For details, a report published by the JSCE (2000) is referred to.

The said research was initiated by visiting and interviewing those people who made significant efforts in restoration works after failure of many earth structures upon Japanese earthquakes in 90's. Those earthquakes include the 1993 Kushiro-Oki earthquake, the 1994 Sanriku-Haruka-Oki earthquake, and the 1995 Kobe earthquake. This direct inquiry was considered new and fruitful for future geotechnical engineering because those people had to deal with financial and engineering difficulties in a short period under strong demands for quick restoration from the public. On the contrary, the major shortcoming of this interview study was the limited number of interviewed people. Due to the time-consuming nature of interview and budget limitations, only 18 people were visited. Note that no user of the damaged structures was included among them because the opinion of users would tend to demand too much conservatism and overdesign; for instance, railway should continue service on the same day as a strong shaking, and water should be supplied as well. Another issue in the study is that the inquired people were asked to choose their answers out of prepared lists for easiness of later interpretation.

Fig.28 indicates kinds of damaged structures and types of involvement of the interviewed people. The studied earth and geotechnical structures consist of those of river dikes, small fill dams, road, embedded lifeline, port, and railway. The involved people are not only site engineers but also administrators and planners. All the people experienced a hard time in restoration of damaged structures. In spite of the limited amount of interviews, thus, it was thus attempted to cover a wide range of situation.

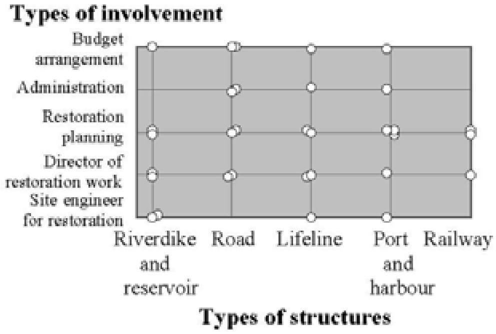

Figure 28. Kinds of damaged structures and types of human involvement in interview study.

The first output in this study is shown in Table 1 where the important issues in determination of the allowable seismic displacement are listed from No.1 to No.4. Evidently, the human life is the most important one. In reality, however, a large deformation of earth structures does not directly lead to a loss of human life. Victims are more often killed by collapse of their houses as evidenced by the 1995 Kobe and 2003 Bam earthquakes among others. Thus, it is reasonable to pay attention to the second important issue in Table 1. It is interesting in this table that the negative effects to public are considered to be very important by the interviewed people after their very hard time for restoration; none of difficulty and cost in restoration is very important. One of the reasons for this good attitude is the service spirit of the interviewed people, while the other is that those people belonged to public sectors as well as semi-public ones such as energy industries. It is very possible that those belonging to purely private sectors would have considered the cost more important.

Table 1. Factors that affect the allowable displacement.

	Factors			
	Human life	Negative effects to public	Difficulty in restoration	Cost of restoration
Importance				
No.1	14	3	0	1
2	1	12	0	1
3	1	0	4	7
4	0	0	7	5

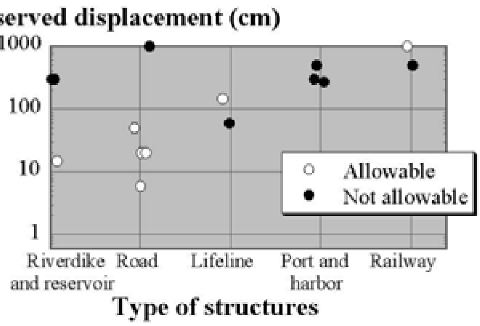

Figure 29. Relationship between extent of residual displacement and opinion.

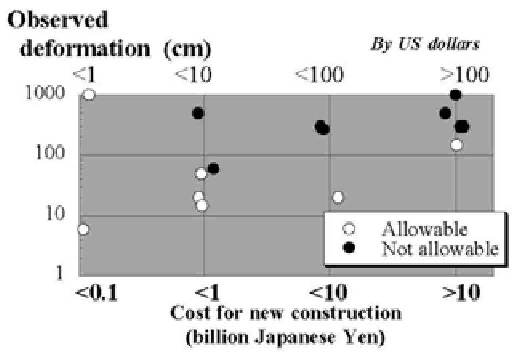

Figure 30. Relationship between residual displacement and cost for new construction.

Fig.29 illustrates the opinion of the interviewed people concerning the extent of the damage which they experienced. It is generally true that the residual displacement less than 100 cm is allowed. Fig.30 shows the relationship between the observed displacement and the cost which would be needed to reconstruct the same structure once more. Certainly, this cost is the one at the time of the present interview (1998) and does not include the cost to purchase land. It may be therein seen that the opinion on the allowable displacement is not affected by the cost. In contrast, Fig.31 manifests the effects of the time which was needed for restoration and resuming the operation of the facility. Interviewed people do not allow the operation or function of the facility to stop for more than one month. One exceptional case of one-year stop is the case of a special facility which is used only in hot summer. Since the structure was damaged in January of 1995 by the Kobe earthquake and restoration was not completed by the summer of the same year, another one year time for restoration was allowed.

The idea on effects to the public is shown in Fig.32 where the horizontal coordinate indicates the size of affected area. Municipality in Japan stands for a community with a population ranging from tens of thousand to millions, while a prefecture has a population of on average two millions in Japan. Among the data, the one from a collapse of railway embankment is considered allowable in spite of as big as 1,000 cm of displacement and the big affected area. This case should be considered exceptional in what follows because of the private judgment of the interviewed person. It may be seen then that the upper bound of the observed and allowable deformation decreases as the affected area becomes greater. Thus the interviewed people are trying to avoid the earthquake's negative effects on the public as much as possible. In summary, the opinions of the interviewed people indicate that the judgment of allowable and not-allowable deformation depends on time and area while cost is less important. Note that the size should be replaced by population or economic damage in future studies.

The discussion above somehow addressed the idea of the interviewed people on the allowable magnitude of displacement. To be clearer, the following parts are going to deal more quantitatively with the people's opinion on the allowable displacement. The conducted inquiry asked them about their idea on the magnitude of the allowable displacement after experiencing difficult times. Their idea on the allowable displacement takes somehow into account many real problems caused by big earthquakes. Fig.33 compares the observed displacement and the allowable displacement in the mind of the people. When the observed one was considered unallowable (black circles), the proposed allowable displacement is smaller than the real one, showing that the idea of the interviewed people was reasonable. On the contrary, two open circles to the right of the y=x line needs some care to be taken, because they insists the allowable displacement be even smaller, although the real displacement is considered allowable. Probably they are related to the desire of the interviewed people that such a hard time should not be repeated in future.

Fig.34 examines the relationship between the allowable displacement in the people's mind and the restoration time as experienced in reality. At the first glance, there seems to be no clear trend in this figure. Then two data on very large allowable displacement of river dikes are removed because of the different idea of allowable displacement that the remaining height, in place of the residual displacement, should be higher than the possible flooding water table. Accordingly, the upper bound of the allowable displacement increases as the restoration period becomes longer. This simply implies that the interviewed people tended to allow greater displacement when the extent of damage was greater as evidenced by the longer restoration time. Moreover, it is very possible that an alternative service such as detour of a damaged road (Fig.27) was prepared when the restoration was elongated. If this was the case, the engineers did not have to worry about the negative effects to the public and were able to make more elaborate restoration works. Due to these reasons, it seems that the "time" factor on allowable displacement may be made more clearly by Fig.35 which employs the time until an alternative service was resumed. The data on a river dike should be removed from consideration due to the aforementioned reason. Then, Fig.35 indicates that the allowable displacement is smaller when the negative effects to the public are greater as shown by the longer time prior to an initiation of an alternative service. Thus, the interviewed people wish to reduce the negative effects to the public.

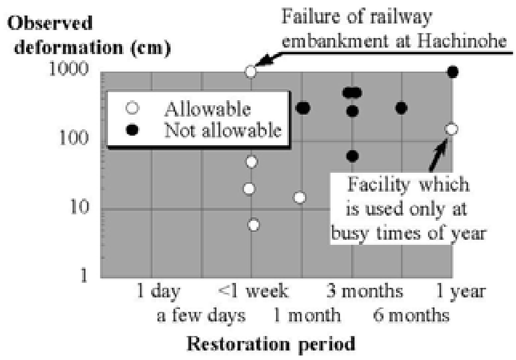

Figure 31. Relationship between residual displacement and time for restoration.

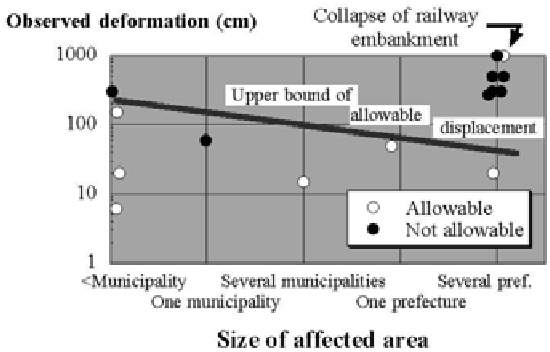

Figure 32. Relationship between residual displacement and size of affected area.

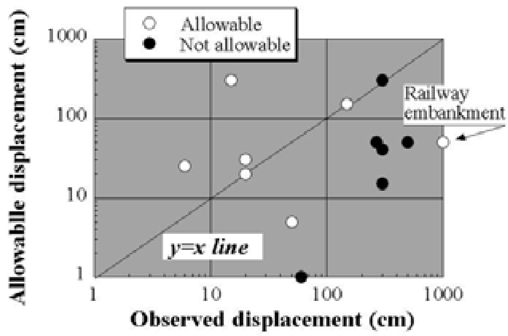

Figure 33. Comparison of allowable and real residual displacements.

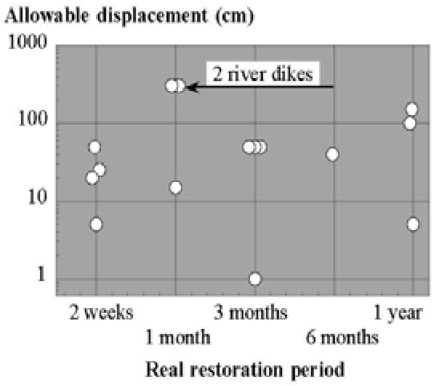

Figure 34. Relationship between restoration period in reality and idea on allowable displacement.

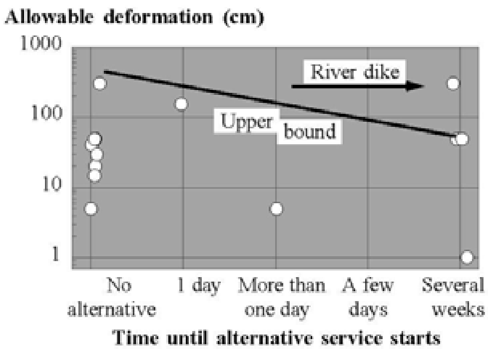

Figure 35. Relationship between idea on allowable displacement and time to find alternative service.

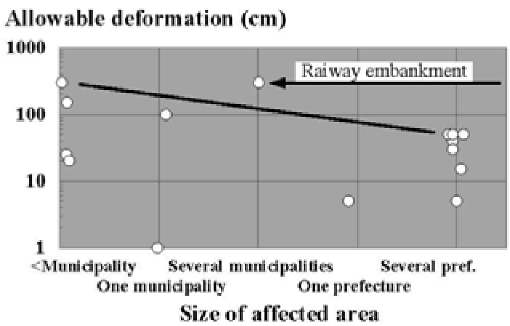

Figure 36. Relationship between idea on allowable displacement and size of affected area.

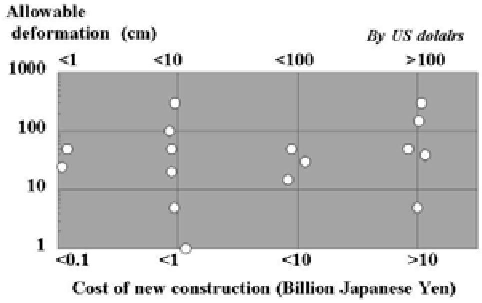

Figure 37. Relationship between idea on allowable displacement and cost for new construction of same facility.

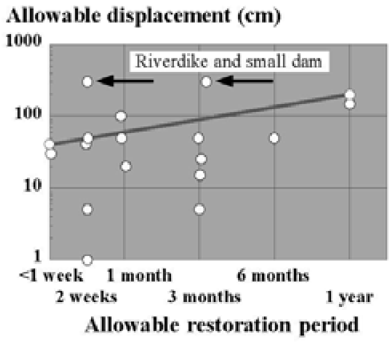

Figure 38. Relationship between allowable displacement and allowable restoration time in mind of interviewed people.

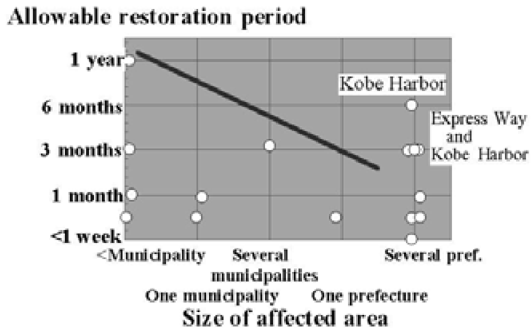

Figure 39. Relationship between allowable restoration time in mind and size of affected area.

Fig.36 demonstrates the relationship between the size of the affected area and the allowable displacement in the mind of the interviewed people. As expected, the smaller displacement is allowed when the size of the affected area is greater. This trend becomes more evident when the data from a river dike is removed from discussion due to the reason described in Fig.34. The cost of new construction is not important, conversely, because the concern is addressed to reducing negative effects to the public (Fig.37).

It has been shown thus that the idea on the extent of allowable displacement is related with the negative effects to the public which is a combination of the time needed for restoration and the size of the affected area. It should be recalled that the size of the affected area should be replaced in future studies by the affected population or the affected economic activities.

Fig.38 illustrates the relationship between the allowable displacement and the allowable restoration time as suggested by the interviewed people. Data from cases of river dike and a small dam should be removed because in these types of structures the remaining height is more important than the seismically-induced displacement. Other data remaining in Fig.38 shows that the upper bound of the allowable displacement increases with the allowable restoration period. Although the allowable displacement and the allowable restoration time are equivalent with each other, it seems that the latter is easier to decide.

Fig.39 shows firstly that the allowable restoration time decreases with the increase in the size of the affected area. This means that the interviewed people wish to reduce the negative effects to the public when the concerned damage is significant (larger affected area). Another point in Fig. 39 is that the interviewed people had to allow for a longer restoration time when the damage was as significant as to affect many prefectures. These cases are those of Kobe Harbor and an express way next to a damaged fly-over bridge. Since both cases involved more time-consuming restoration of bridges and other structures, longer restoration was needed and allowed. Other cases with shorter restoration and many affected prefectures concern river dike and railway whose restoration was the restoration of the system operation. Therefore, the solid line in Fig.39, ignoring data from express way and Kobe Harbor, is reasonable.

The combined effects of the size of the affected area and the desired restoration time on the allowable displacement are demonstrated in Fig.40. Generally, the smaller displacement is allowed by the interviewed people when the affected area is greater. The effects of the allowable restoration time is not clear in contrast, because the restarting time is also affected not only by the type of geotechnical structures but also other connected structures as mentioned above. It is, however, reasonable that the greater displacement should be allowed when the allowable restoration time is longer. Fig.40 is not contradictory to this idea. Finally, data points in Fig.40 are classified according to the allowable restoration time longer than or shorter than one month. The results in Fig.41 show the following principles and features of seismic design based on residual displacement;

1) Firstly, the size of area which is affected by the damage of a concerned structure is determined.
2) Secondly, decision is made of the allowable restoration time which is equivalent to the allowable time until the service of the facility is resumed.
3) The allowable restoration time varies with the importance of the concerned structure as well as the intensity of a design earthquake; a strong but very rare earthquake should have a longer restoration time.
4) Based on the area size and the restoration time, the allowable displacement is determined.
5) Decision on restoration time seems to be easier in a practical sense than decision of the allowable displacement. In this sense, Fig. 41 is meaningful.
6) It should be noted that Fig.41 simply stands for the idea of the interviewed people and is subject to change according to different situation. However, the basic principle shown by this figure is important.

It is interesting to point out the consistency of Fig.41 with the current practice in Japanese Railways. Seismic damage of railway embankment would affect several prefectures, and the design specification defines two types of allowable seismic displacement upon very rare and strong earthquake events; 20 to 50cm subsidence for quick restoration and more than 50cm for longer period of restoration. Fig.41 suggests similar extents of allowable displacement for the size of several prefectures.

The idea in Fig.41 is not new to the engineering discipline except that the decision is made of the allowable restoration time and that the allowable displacement is determined based on it. Its similarity to a conventional idea of seismic performance (resistance) matrix can be understood by comparing Fig.41 with the matrix in Table 2. Both Fig.41 and Table 2 show larger allowable displacement for less important structures (smaller affected area) and stronger shaking (rare event). Only one difference lies in the easy decision making on allowable restoration time.

4 PERFORMANCE-BASED DESIGN AND ASSESSMENT OF SEISMICALLY-INDUCED DISPLACEMENT

The previous chapter described that a major role is played by the assessment of residual displacement which is induced by a design earthquake motion. Calculation of displacement is, however, a difficult task in geotechnical engineering. Generally speaking, prediction of displacement under a given design earthquake loading is reasonable when the following requirements are satisfied;

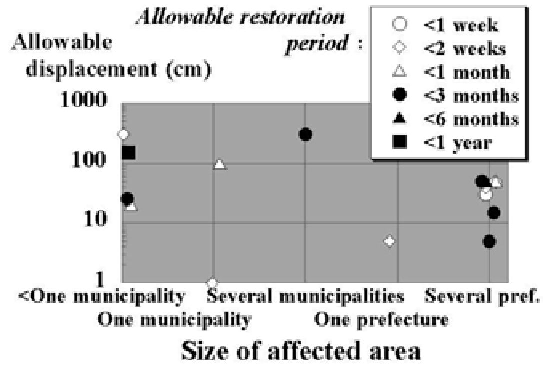

Figure 40. Relationship between allowable displacement and size of affected area for different allowable restoration time.

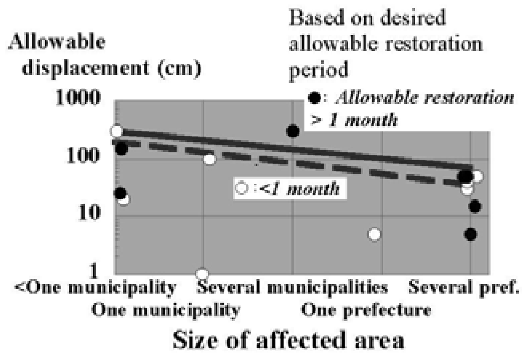

Figure 41. Determination of allowable displacement based on size of affected area and allowable restoration time.

Table 2. Concept of matrix of allowable displacement.

	Intensity of design earthquake	
Importance of structure	Very strong	Strong
More	Intermediate (avoid collapse)	Very small
Less	Larger	Smaller

- good constitutive modeling of soil,
- precise information on spatial variation of soil properties,
- sufficiently detailed testing on good soil samples in the laboratory or in situ, and
- good numerical tools.

Many efforts have been practiced in this direction, and costs for those efforts are payable in case of big projects with sufficient budgets. Examples of such a situation may be construction of big bridges, important harbors, and high-rise buildings among others. Importance and sufficient financial background make it possible to conduct detailed soil investigation, complex soil modeling, and nonlinear dynamic FE (finite element) analysis. In reality, on the contrary, there are many geotechnical projects which do not afford detailed soil investigation and analyses.

There are two ways to deal with this problem. The first way is a traditional one which relies on a good degree of compaction and does not make a special consideration of earthquake problems. Although this is simple, consequence of a rare but very strong earthquake is unknown. Since the intensity of design acceleration is becoming stronger in the recent times due to observation (Fig.23), it is unlikely that shear strength of compacted soil alone can maintain good resistance against motion. Probably the reliance on compaction is reasonable if a quick restoration is made possible by good preparedness (Fig.42). Quick restoration makes it possible for a government to save budget for retrofitting against very rare seismic events and spend money on more urgent problems such as poverty, diseases, and education. In such a case it is certainly necessary to make sure that the possible collapse of a concerned structure does not induce fatal problems to the public.

The second solution to practically assess the seismic displacement is a simplification of the whole procedure. It has been considered that the use of Newmark's rigid block analogy (Newmark, 1965) meets this requirement. The general principle proposed by Newmark was improved for practical use by Makdisi and Seed (1978). Note that care has to be taken of the choice of shear strength, considering the rate of loading and possibility of drainage as well as pore water pressure change. Since the Newmark-type analysis assumes shear failure along a well-developed slip plane, such a situation as shown in Fig. 43 fits this kind of analysis.

It should be recalled that the allowable displacement of 20-50 cm as proposed in Fig.41 may not be associated with a full development of shear strength and a generation of slip plane. In such a case it is necessary to consider accumulation of residual strain due to cyclic loading under the stress level below the shear strength. An example of such a situation is illustrated in Fig.44.

Fig.45 shows a simplified model of a soil slope which is intended to account for the accumulation of strain during cyclic loading (Mohajeri and Towhata, 2003). In this model, a column of soil taken from a soil slope is replaced by a single-degree-of-freedom model in which the displacement at the ground surface is denoted by D as a function of time, t. The nonlinear spring force, R(D), stands for the nonlinear stress-strain behavior of the soil, while two kinds of external force, F_{static} and $F_{inertia}$, produce the accumulation of displacement. The equation of motion for this model is

$$m\frac{d^2D}{dt^2} + R(D) = F_{static} + F_{inertia} \qquad (2)$$

The assumption behind this simplification is that the lateral displacement of soil, u(z), follows the fundamental mode of the soil deposit with the thickness of H, which is given by

$$u(z,t) = D(t)\sin\frac{\pi z}{2H} \qquad (3)$$

when there is no surface structure or other big mass at the surface. For illustration, see Fig.46. To convert the original soil column to a simple model in Fig.45, the theory of Lagrangian equation of motion was used. In this theory, firstly, the kinetic energy, K, the potential energy due to gravity, Pg, the potential energy concerning the inertia force, Pi, and the strain energy in the soil column, Q, are described in terms of D(t) by using the assumed displacement distribution in Eq.3. For details, refer to Mohajeri and Towhata (2003). Thereinafter, the Lagrangian equation of motion is given by

$$\frac{d}{dt}\left[\frac{\partial(K-Pi-Pg-Q)}{\partial\left(\frac{dD}{dt}\right)}\right] - \frac{\partial(K-Pi-Pg-Q)}{\partial D} = 0 \qquad (4)$$

Note that the right-hand side is zero since no viscous energy dissipation is employed. Accordingly, four terms in Eq.2 is obtained as

$$m\frac{d^2D}{dt^2} = \frac{d}{dt}\left[\frac{\partial K}{\partial\left(\frac{dD}{dt}\right)}\right]$$

$$R(D)=\frac{\partial Q}{\partial D} = \text{shear stress in soil} \qquad (5)$$

$$F_{static} = -\frac{\partial Pi}{\partial D} \quad \text{and}$$

$$F_{inertia} = -\frac{\partial Pg}{\partial D}$$

Figure 42. Quickly restored river dike after 2003 Tokachi-oki earthquake (Hokkaido of Japan, 2003).

Figure 43. Total failure of road embankment in Ojiya City of Niigata, 2004.

Figure 44. Differential movement between fill and base of house.

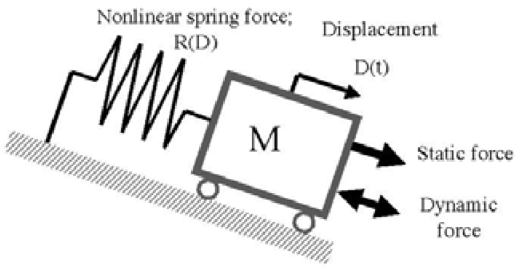

Figure 45. Single-degree-of-freedom modeling of soil column in slope.

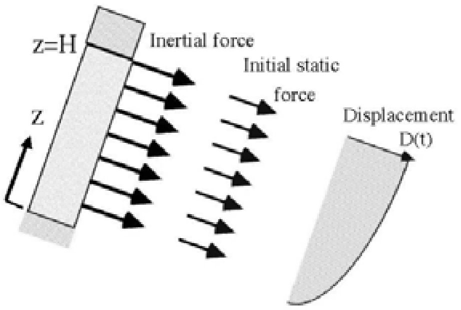

Figure 46. External force and lateral displacement along soil column.

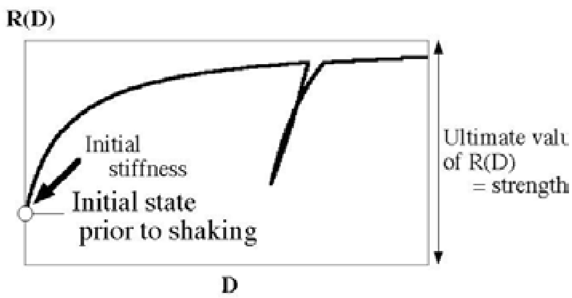

Figure 47. Conceptual drawing of nonlinear spring force, R(D).

Figure 48. Laminar box for shaking table model test.

The nonlinear feature of the spring force, R(D), is illustrated in Fig.47. Since simplification of analysis is the major requirement for ordinary earth structures, the nonlinear curve is expressed probably by a hyperbola. Since strain accumulation has to be taken into account, moreover, the unloading and reloading curves are expressed by different magnification of the monotonic loading curve. This is in contrast with the magnification of 2 as is often practiced under the name of Masing (1926). The basic parameters in a hyperbolic model are the initial stiffness and the ultimate value of R(D). They have to be determined in ordinary structures without either undisturbed soil sampling or detailed in-situ investigation. In the present case, the initial stiffness, Kmax, in a small range of D is determined by equating strain energy in the model and in a soil column;

$$\frac{K\max}{2}D^2=\int_0^H\frac{G\max}{2}\left(\frac{\partial u}{\partial z}\right)^2dz \tag{6}$$

in which Gmax is the shear modulus of soil at small strain. This value can be determined with reasonable accuracy by, for example, monitoring microtremor and determining natural period of soil without drilling bore holes. By using Eq.3,

$$K\max=\frac{\pi^2}{8H}G\max \tag{7}$$

Note that the soil modulus of Gmax is the averaged one over the whole thickness of soil. In line with this, the stress of soil at large deformation is averaged to determine the ultimate value of R. By equating energies,

$$D\times(\text{Ultimate R})=\int_0^H(\text{soil strength})\frac{\partial u}{\partial z}dz$$

$$\text{Ultimate R}=\int_0^H(\gamma z\tan\phi)\frac{\partial u}{\partial z}dz\Big/D \tag{8}$$

in which the soil strength is expressed by the Coulombic formula with γ denoting the unit weight of dry soil. For practice, the strength parameter can be determined by a variety of simple penetration tests without drilling bore holes. The integration of the equation of motion (Eq.2) is not a difficult task. With emphasis on the simplicity in both calculation and data preparation, studies in the same direction are going on at many places (Kramer et al., 2004, and Murakami et al., 2004, among others)

The model described by Eq.2 was examined against a 1-G shaking table model test in which a soil model was prepared in a laminar box in Fig.48 and tilted 10% so that horizontal shaking would produce accumulation of shear strain (Mohajeri and Towhata, 2003). The size of the model was 0.5 m in width, 1m in length, and 1m in depth. Dry Toyoura sand was compacted to the relative density of 80% for this model and was subject to harmonic horizontal shaking. Fig.49 compares the observed and calculated lateral displacements at 70-cm height from the bottom to show that this model is able to reproduce the accumulation of strain with the number of cycles.

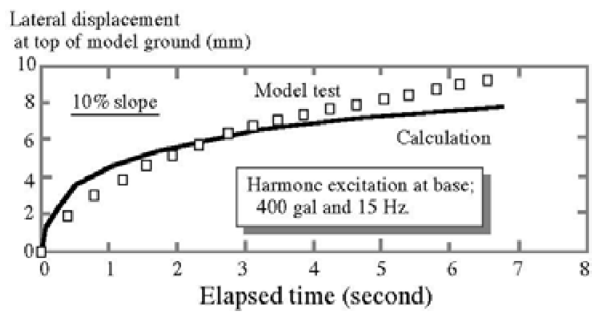

Figure 49. Calculated and observed lateral displacement of slope model in shaking table test.

5 MECHANISM OF DEVELOPMENT OF LARGE DEFORMATION IN SANDY GROUND WITH HIGH PORE WATER PRESSURE

The previous chapter reviewed liquefaction-induced damage to show that the essence of that damage does not lie in strong shaking but that the excessive displacement and deformation are the problems. Prior to the study on damage mitigation, discussion is made in this chapter on the nature of ground displacement.

Change in human civilization and technology encounters a new kind of natural disaster. Liquefaction was not considered to be a natural hazard until 1960's except by a few numbers of people such as Maslov (1957) together with Florin and Ivanov (1961). Although liquefaction did occur in the previous times, it occurred mostly in less populated area out of cities and did not attract concern.

Fig.50 manifests one of the examples of excavating sand boiling caused by a past earthquake. Being next to the Tone River channel, this site at the time of a past strong earthquake had a young soft sandy deposit created probably by flooding. Sangawa (1992) studied this kind of phenomena for a long time at many archaeological sites, and detected the occurrence of big earthquakes which were missing in the written history (Fig.51). Paleoliquefaction study is thus an important tool to determine the recurrence period of strong earthquakes in areas where written seismic records are not perfect in the historical as well as prehistoric times. Studies on paleoliquefaction have been conducted by Obermeier et al. (1985), Amick and Gelinas (1991), Clague et al. (1992 and 1997), Mori and Ikeda (1997), and Talwani and Schaeffer (2001) among others.

Concentration of population in many cities in the world became significant in the middle of 20th Century and the urban area had to be expanded outwards. This situation was frequently accompanied by filling water with sand; for example Niigata City in Fig.11. The Dagupan City in the Luzon Island of the Philippines was expanded in 1950's as well by filling dune sand on rice field and fish ponds. No densification of sand was considered necessary in those days. Another well-known example is the Port Island of Kobe Harbor. In addition to land reclamation projects as mentioned above, those of small scale have caused liquefaction problem as well.

The site in Fig.52 was a small pond in a hill area. It was turned to a residential area by filling water with dune sand which was locally abundant. Upon earthquake in 2000, liquefaction of subsoil induced subsidence and distortion in foundation of houses. The problem is that the residents of this area, who bought land but had no idea on geotechnical engineering and, in particular, liquefaction, had to take responsibility for the damage. Without legal protection from liquefaction-induced loss of properties, there seems to be only two advises that people should check, prior to purchasing land, the previous type of land use and that, if subsoil is water-saturated sand, slightly more money should be spent on reinforcing foundation than purchasing expensive furniture and interior decoration.

The role played by lifelines is becoming more and more important in the recent times and this situation will not change in the coming future. This trend became evident in 1980's and accordingly a new kind of liquefaction-induced hazard was created. When the author was allowed to join a group investigation in 1984 on liquefaction-induced damage in embedded lifelines, nothing had been known about the importance of ground displacement caused by subsurface liquefaction. Although there was a report on heavy distortion of revetment walls along the Shinano River during the 1964 Niigata earthquake (Kawasumi et al., 1968), its significance was not yet understood. It is very possible that a similar situation will occur again in future in which what the present people know but do not care will become remarkably important due to changing human culture and technology. Thus, field reconnaissance survey following a natural disaster is very important.

It has been known that many tension cracks opened near the top of a liquefied slope. This feature is evidenced by a photograph in Fig.54 where a pine tree was split into two pieces due to discontinuity of displacement.

The study further examined the vertical displacement in the concerned slope (Fig.55). In spite of limited accuracy of employed air photo surveys in measurement of vertical displacement together with the superimposed effects of consolidation settlement, it may still be seen in this figure that the upper part of the slope subsided, while the lower part heaved.

Figure 50. Sand boil as evidence of liquefaction in past times (Excavated by Tobishima Corp. at Sekiyado of Saitama, Japan).

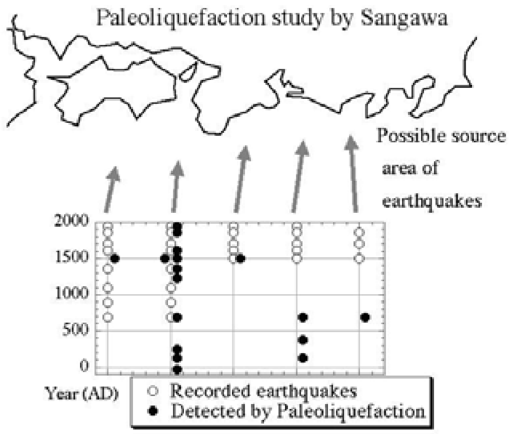

Figure 51. Big earthquakes along Pacific Coast of Japan which were missing in written history and detected by Sangawa (data plotted based on Sangawa's study); note that the source of single but gigantic earthquakes ranged over a wide area.)

Figure 52. Liquefaction in residential development area in hilly terrain (Tottori Prefecture, Japan, 2000).

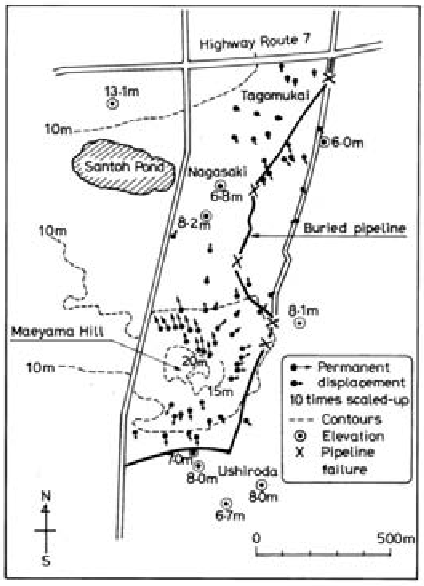

Figure 53. Liquefaction-induced ground displacement in Noshiro City, North of Japan (data by Hamada et al., 1986a and 1986b).

Figure 54. Pine tree split into two pieces at the top of liquefied slope (Photo taken by Noshiro City Government).

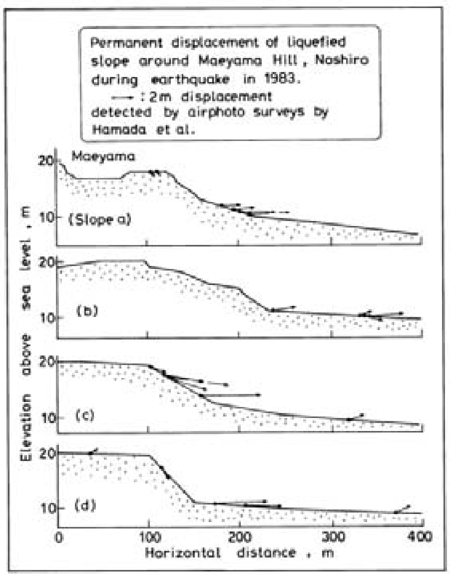

Figure 55. Vertical component of permanent displacement in liquefied slope (data by Hamada et al., 1986a and 1986b).

Effects of subsurface liquefaction on the overlying river dike are characterized by subsidence. In addition to the case of Yodo River in Osaka (Fig.21) in 1995, Fig.56 shows the excavated cross section of the Tokachi River dike after its remarkable subsidence in 1993. A sign of sand boiling was found near the bottom of the slope. Since the natural deposit of this site is composed of unliquefiable peat soil, Sasaki (1994) concluded that the significant settlement of the river dike under the gravity force loosened the sandy material of the dike, which eventually led to liquefaction in 1993.

Collecting many records of river dike subsidence in Japan since the 19th Century, then Ministry of Construction assembled data as illustrated in Fig.57. It is therein found that the subsidence of the dike does not exceed 75% of the original height, with remaining height of at least 25% above the ground surface. This empirical knowledge due to experiences of over 100 years can be understood by using the idealization in Fig.58. According to this figure, the weight or the gravity force of the river dike per unit plane area is given by

$$\textit{Gravity force} = \gamma H \tag{9}$$

where H is the height of a dike, and γ stands for the unit weight of soil. Since a dike rests above the ground water table, γ=15 kN/m^3 may be a reasonable value. Moreover, as a dike sinks into the ground, buoyancy force increases. At the subsidence of S,

$$\textit{Buoyancy force} = \gamma S \tag{10}$$

in which γ_l denotes the unit weight of subsoil. In the worst case where liquefaction occurs in all the subsoil below the ground surface, γ_l = 20 kN/m^3 for a water-saturated material is reasonable. At the ultimate stability where concerned forces are equilibrated and no more subsidence occurs, Eq.9 and Eq.10 are equal to each other and the maximum possible subsidence is derived;

$$\text{Maximum possible subsidence} = \frac{\gamma}{\gamma_l} H = 0.75H \tag{11}$$

Thus, the empirical number of 75% is understood. Note that this 75% rule is a consequence of increasing buoyancy force with subsidence. Its numerical reproduction is not possible without consideration of large displacement.

Studies on case histories as described above are always valuable and important. There is, however, a shortcoming that nothing is monitored on subsoil behavior during shaking. To further investigate the nature of ground displacement, the author and the Public Works Research Institute conducted a collaboration study by using a 6-meter-long shaking table facility. One of the test results (Sasaki et al., 1992) is presented in Fig.59 to show that the observations in Figs. 53 and 55 are correct. Note that the lateral displacement which is demonstrated by the distortion of colored sand in Fig.59 is continuous in the vertical direction. Therefore, it was concluded that the liquefaction-induced ground displacement is a consequence of large shear strain of sand which is softened by generation of excess pore water pressure. This point was consistently confirmed by additional five tests (Sasaki et al., 1992). Another finding was that the development of lateral displacement is terminated at the end of shaking. See also a centrifugal model tests on gravity quay wall in which lateral displacement of grid points as shown by triangles (▽) suggests continuous displacement in the vertical direction (Fig.60). Displacement was terminated in this test at the end of shaking as well.

Figure 56. Excavation of Tokachi River dike after 1993 Kushiro Oki earthquake, Hokkaido, Japan.

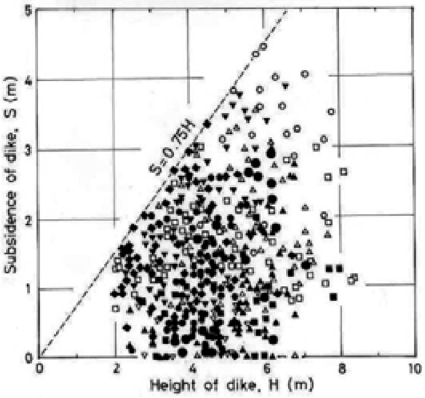

Figure 57. Empirical correlation between subsidence of river dike (S) and original height (H) (after TCMSERS, 1996).

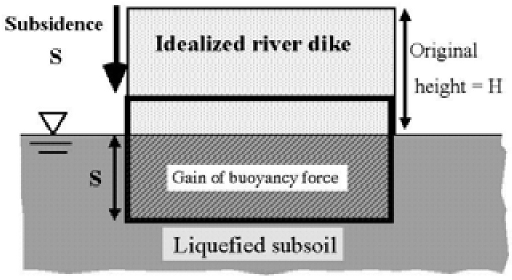

Figure 58. Equilibrium between gravity force and buoyancy force after subsidence of river dike.

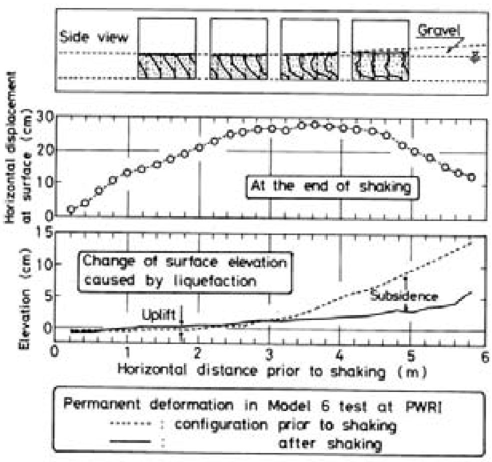

Figure 59. Deformed shape of liquefied slope with unliquefiable surface crust (1-G shaking table test by Sasaki et al., 1992).

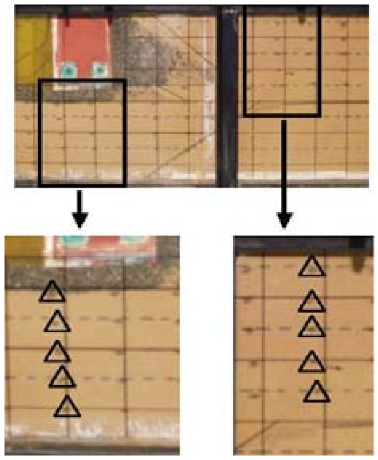

Figure 60. Centrifugal model tests on lateral displacement of gravity quay wall model.

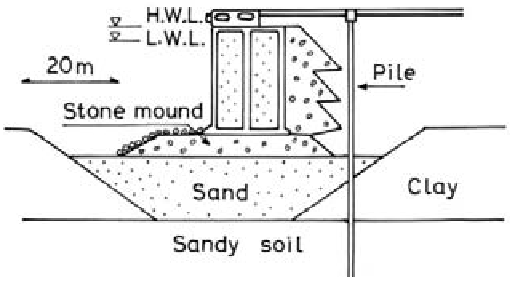

Figure 61. Cross section of gravity quay wall in Port Island of Kobe.

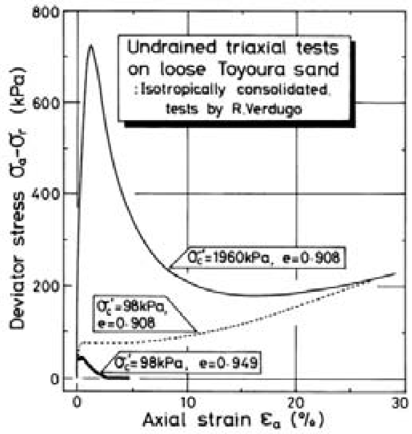

Figure 62. Undrained triaxial compression tests under different effective stress levels at different densities.

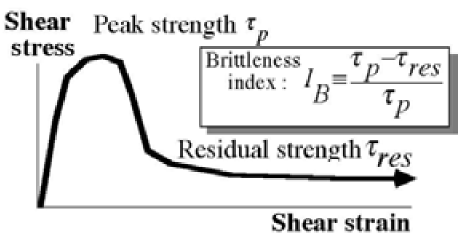

Figure 63. Definition of brittleness index by Bishop et al. (1971).

In contrast to the author's opinion that liquefaction-induced permanent displacement is a consequence of large strain in softened sand, there is to date a different idea. It is therein supposed that a thin film of water is formed under a less permeable soil layer as a consequence of pore pressure migration and that a soil mass above the water film translates smoothly due to strain localization (Fiegel and Kutter, 1994; Kokusho, 1999; Malvick et al., 2004, Yoshimine et al., 2004). The interesting feature of this idea is that large displacement is able to develop after the end of shaking because a water film is formed after the migration of pore water. This feature has seldom been observed in tests on uniform soil deposit. To verify the existence of less permeable soil layer in reality, Kokusho and Fujita (2002) investigated the cross section of Niigata subsoil which liquefied and translated laterally during the 1964 earthquake. It was found by them that there is a continuous layer of less permeable soil which supports the idea of water film as a causative mechanism of large displacement.

The water-film mechanism is characterized by an existence of long and continuous layer of less pervious soils. The conducted model tests installed such a layer in a direction along which soil translation was easy to occur. It seems that such a situation is likely to exist in natural deposits of soils where sedimentation process occasionally produces a silty layer. In contrast, artificial land reclamation where liquefaction damage is significant may not have a continuous silty layer because employed materials are sandy or gravelly, and soils are placed site by site, making a continuous layer to be difficult to be formed. An example of the author's opinion is found in the foundation of a gravity quay wall in Kobe harbor where the original marine clay was replaced by cohesionless soils (Fig.61) and large displacement occurred upon the earthquake in 1995 (Fig.20). Another example is the vertical subsidence of building foundation (Figs. 13 and 14) in which a vertical silty layer is unlikely.

It seems therefore that there are several mechanisms which make subsoil very soft and induce large deformation. This situation is similar to instability of slopes which is induced by many mechanisms such as filtration of ground water, removal of soil near the bottom, and overloading at the top. It is not a good idea to insist one of the mechanisms being superior to others. Based on this idea, the present text is going to deal with development of large strain in liquefied sandy ground in place of the water-film approach.

The following part is going to introduce a series of 1-G shaking table tests which was conducted on the nature of liquefied sandy ground undergoing lateral displacement. The advantage of 1-G shaking tests is that it can employ larger models at lower cost than centrifuge tests. However, it is often argued that the reduced stress level under 1-G gravity field may affect the stress-strain behavior of tested sand as compared with reality. To overcome this difficulty, it has been proposed to use looser sand for testing. Fig.62 was drawn by using test data by Verdugo and Ishihara (1996). Firstly, two tests on specimens with void ratio of 0.908 were conducted under isotropic consolidation pressures of 1960 kN/m^2 and 98 kN/m^2, respectively. Although the density was identical, the shape of stress-strain curve changed from a strain-softening type to monotonic increase of stress level. Hence, two specimens have to be considered to be different materials although they are physically same. It is not appropriate, therefore, to run model tests under reduced pressures with identical density of soil. Then, Fig.63 further indicates that the strain-softening behavior under higher pressure was reproduced under lower pressure by making sand looser (void ratio=0.949). Thus, the stress-strain behavior is governed by a combination of two factors which are stress level and density. It is possible to cancel the effects due to change of one factor by adjusting the other factor.

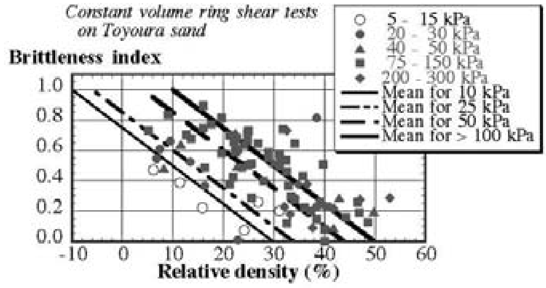

Figure 64. Relationship between effective stress level and relative density of sand with constant brittle index (data by Vargas, 1998).

Prior to 1-G shaking table tests, discussion is made of the superimposed effects of stress level and density on the stress-strain behavior. The steady-state theory has been insisting on the importance of undrained strain softening in the development of large deformation (for example, Poulos et al., 1984; Sladen et al., 1985; Vaid and Chern, 1985; Kramer and Seed, 1988; Castro et al., 1992; Ishihara, 1993). Referring to this idea together with the simplicity, the present study uses Bishop's brittleness index, IB, which is illustrated in Fig.63, as a key parameter. Based on ring shear tests on Toyoura sand, maintaining constant height of a sample, Fig.64 was drawn. This figure illustrates the variation of relative density which maintains the constant brittleness index under varying stress level. When the effective stress level is reduced from the in-situ range of, for example, 100 kN/m^2 down to 5 kN/m^2 in a model (scale of 1/20), the relative density should be reduced by 20% so that similar brittleness index may be maintained. Thus, the following 1-G shaking table tests were conducted employing reduced density of Toyoura sand (Toyota et al., 2004).

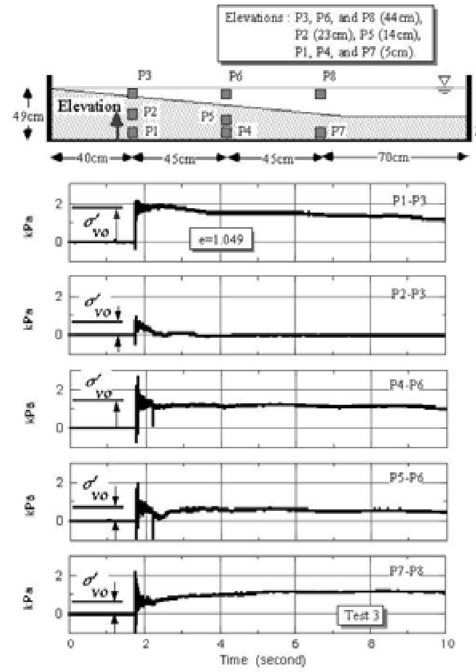

Figure 65. Time history of excess pore water pressure during flow under gravity with very low density of sand (-20% relative density or void ratio = 1.049).

A very loose deposit of Toyoura sand, whose relative density was -20% in the extreme case, was prepared in a container with two kinds of slope inclination; 10% and 20% gradients. The illustration at the top of Fig.65 indicates the model of 20% slope as well as the location of embedded pore pressure transducers. The time history of lateral displacement was recorded near the P2 transducer (Fig.66).

In the first stage of the tests, a study was made of flow displacement of liquefied sand under static gravity force. To achieve this goal, a model ground was shaken by a hammer impact in the transverse horizontal direction (normal to the figure). After causing 100% development of excess pore water pressure in the model of extremely loose sand (relative density=-20% in Fig.65), the transverse shaking decayed quickly within 0.2 second and the flow displacement of the slope occurred under gravity force only. Note further that the impact shaking did not affect the soil displacement in a kinematical sense because the direction of motion was perpendicular to the direction of soil displacement.

Fig.67 demonstrates the temporal development of deformation of the model. This model of extremely low density achieved a horizontal configuration after about three seconds. This implies that the model ground lost its shear rigidity or strength completely and that the stability or force equilibrium was obtained by a horizontal configuration. Another important finding is that the flowing slope did not exhibit any oscillatory motion as water would do. This suggests an energy dissipation mechanism in the model slope. In the structural dynamic terminology, this situation is called over-damping with the critical damping ratio greater than unity. Moreover, the duration time of flow was longer than the time which a perfect liquid without rigidity or rate-dependent nature would take for lateral oscillation.

The time history of excess pore water pressure in the model is presented in Fig.65. It is important to note that the pore pressure records of individual piezometers included the effects of water waves which was generated by the flow of soil. To remove this component, the pore pressure difference between the subsoil and the surface water (for example, P1-P3) was plotted in this figure. It is seen that pore pressure achieved 100% development everywhere. A careful examination of the pore pressure records may find that P1-P3 near the top of the slope is slightly lower than the initial effective stress (σ_{vo}'), while that near the bottom (P7-P8) exceeded the initial effective stress in the later stage of flow. This is a consequence of the changed shape of the model (Fig.67) in which the decreased thickness of soil near the top reduced the total overburden pressure at the location of P1, while conversely the overburden pressure at P7 increased. This change of total stress induced change in pore pressure due to nearly undrained conditions. Such a phenomenon occurred because pore pressure transducers were fixed to vertical rods and their elevation was held constant throughout the tests.

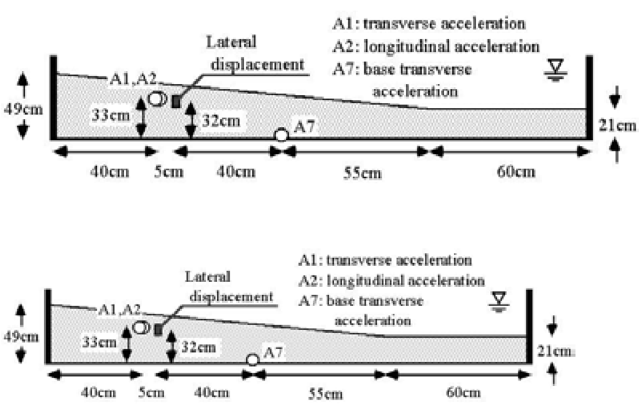

Figure 66. Location of lateral displacement transducer.

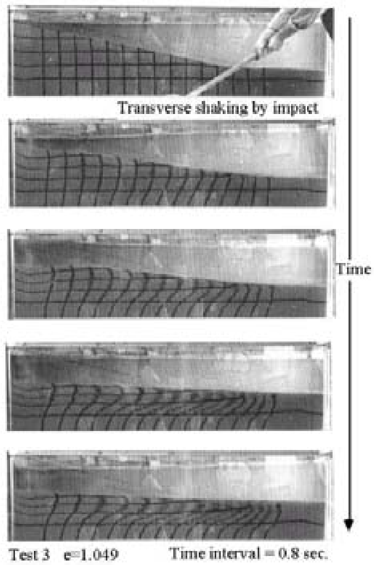

Figure 67. Temporal development of flow failure in model slope with -20% relative density of Toyoura sand.

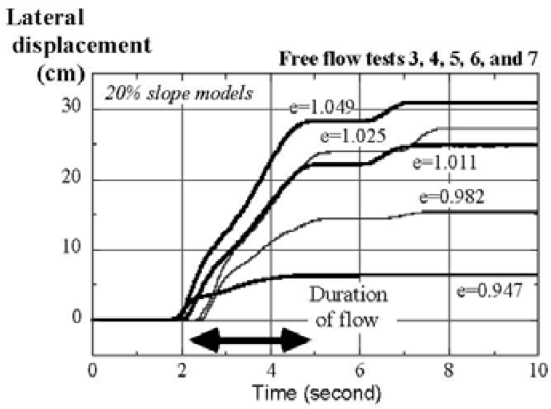

Figure 68. Effects of density of sand on time history of lateral displacement during free flow.

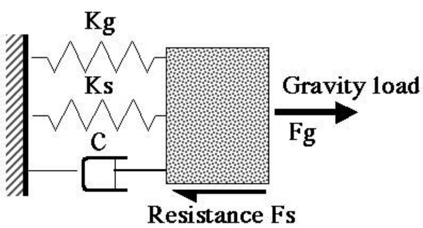

Figure 69. Idealization of free flow of liquefied slope by single-degree-of-freedom model.

Similar tests on free flow of liquefied slope were carried out with varying density of sand. Fig.68 shows that denser sand develops less extent of displacement. What is noteworthy is the fact that flow displacement started at 2 seconds and was terminated at 4.5 to 5 seconds, thus the duration time is nearly independent of density. Although the three loosest cases (void ratio = 1.049, 1.025, and 1.011) had a second stage of flow due to pore pressure redistribution, this period of time is eliminated from the present discussion. When the density was higher than those employed in these tests (relative density being greater than 10%) , free flow was negligible. By referring to Fig. 64 on effective stress effects, it may be said that real sandy deposits with relative density greater than 40% are unlikely to flow freely under static force.

The reduced displacement for higher density of sand in Fig. 68 suggests two possibilities;

- denser sand has greater shear rigidity, or
- denser sand has greater shear strength under undrained conditions.

Discussion is made of these possibilities from the viewpoint of a simplified model of one degree of freedom (Fig.69);

$$m\frac{d^2u}{dt^2} + c\frac{du}{dt} + k_s u = F_g - k_g u - F_r \qquad (12)$$

where u stands for the magnitude of displacement, m the mass of flowing soil, c the possible rate-dependent energy dissipation, k_s the shear rigidity of sand, F_g the load induced by gravity, -kgu the reduction of gravity load due to decreasing slope with the development of displacement (Fig.67), and F_r the possible shear strength of liquefied sand. Fig.70 illustrates the results of example calculation of Eq. 12 in which an overdamped response was produced by maintaining the viscous term of c;

$$c = 2\sqrt{mk_g} \times 10 \qquad (13)$$

In Fig.70, two groups of response are seen; the one showing the effects of increased rigidity of sand (K_s), and the other with the effects of increased shear strength (F_r). The Control Case had both K_s and F_r equal to zero. Firstly, both groups are able to reproduce the observed behavior of liquefied slope in Fig. 68 in which the increased properties decrease the displacement. There is an essential difference between two groups, however, that the time at the completion of displacement (90% completion is employed in the illustration) changes with increasing K_s (see △), but is held unchanged for increasing F_r (see ○). Since only the latter group is able to reproduce the observed fact of constant duration time of flow (Fig. 68), the present study concludes that the free flow of liquefied slope is accompanied by varying (undrained) shear strength of sand. Moreover, the elongated duration of flow can be reproduced by the use of rate-dependent (viscous) mechanism. Note that the change of shear strength cannot elongate the duration time of flow (Fig.DP).

Model tests were further carried out with continued horizontal shaking. Shaking was generated in either transverse or longitudinal direction of the model (Fig.71). While the longitudinal shaking is commonly employed in similar studies, the transverse shaking is characterized by the fact that the shaking does not generate a significant inertial effect on the flow phenomenon. Thus, this kind of dynamic test is similar to the aforementioned free flow tests in a mechanical sense. There is, however, a remarkable difference in the magnitude of lateral displacement. Fig.72 exhibits one of the test results in which a model of -7% relative density (void ratio = 1.000) was subjected to a continued shaking of 200-300 Gal with 3Hz. The ultimate displacement was greater than what happened for similar sand density after impulse shaking and free flow in which a horizontal configuration was achieved. This difference is related with the elongated state of high pore water pressure (Fig.73).

The elongated duration of lateral displacement is the important feature of continued shaking. Fig.74 illustrates the case in which the amplitude of longitudinal excitation increased gradually at 3Hz. Pore water pressure was maintained high and the lateral displacement at the place of the displacement transducer (Fig.66) was able to develop up to 30cm at which the ground surface became nearly level and no more displacement was generated. This is in a clear contrast with the aforementioned impulse shaking in which the lateral displacement was able to develop for a shorter time period (Figs. 74 and 75). The longitudinal shaking tests were thus repeated varying shaking conditions as well as density of Toyoura sand.

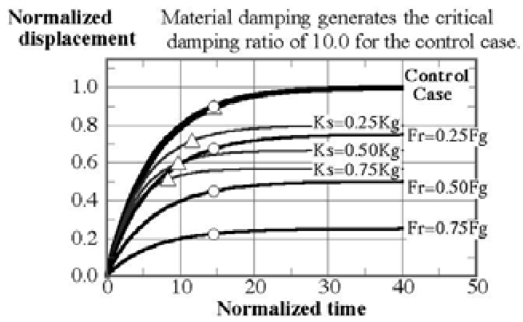

Figure 70. Over-damped behavior of single-degree-of-freedom model.

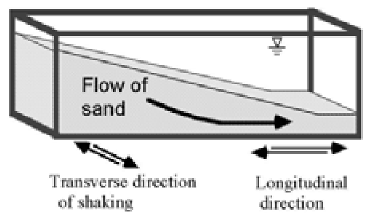

Figure 71. Transverse and longitudinal directions of shaking.

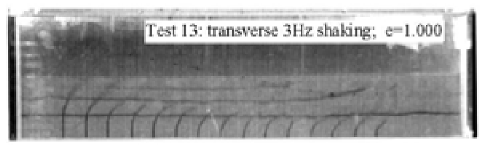

Figure 72. Ultimate configuration of 20% slope model with -7% relative density (void ratio=1.000) subjected to continued transverse shaking.

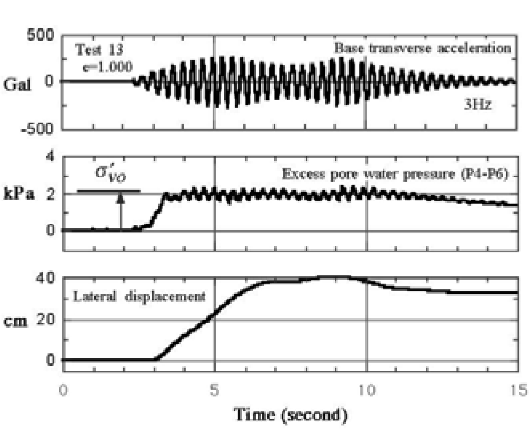

Figure 73. Response of 20% slope model to 3Hz transverse shaking (relative density = -7%).

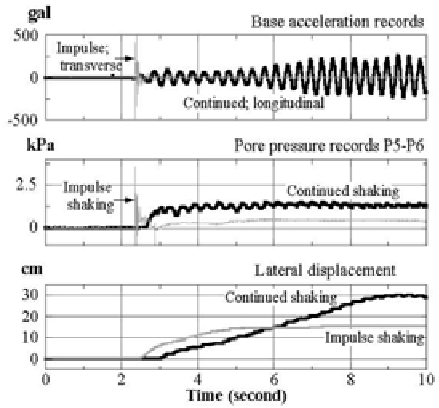

Figure 74. Response of 20% slope model to 3Hz longitudinal shaking (relative density=-3%).

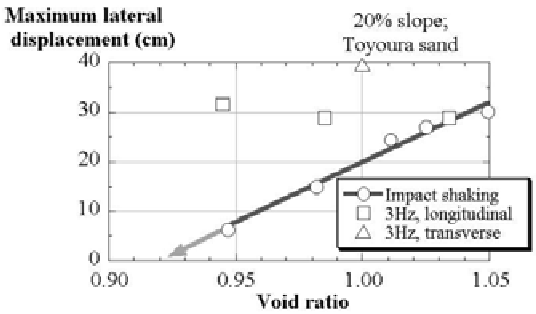

Figure 75. Maximum displacement caused by impact or 3-Hz continued shaking.

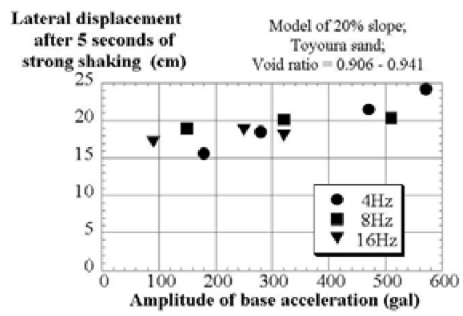

Figure 76. Effects of nature of base shaking on residual displacement.

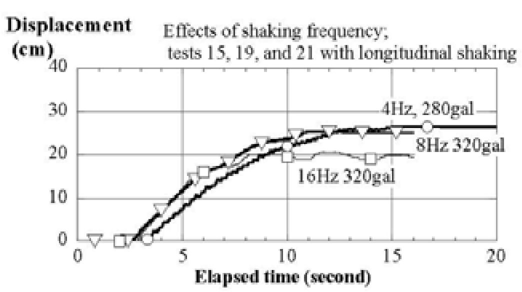

Figure 77. Effects of void ratio on time history of lateral displacement.

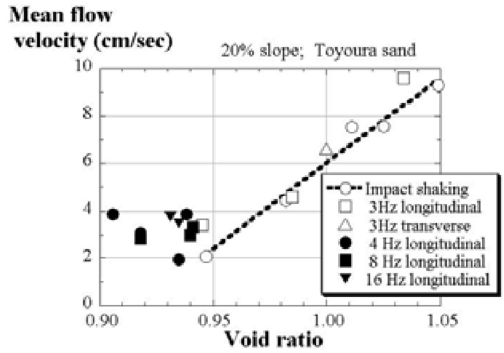

Figure 78.. Effects of shaking frequency on mean flow velocity (e=0.918 - 0.940).

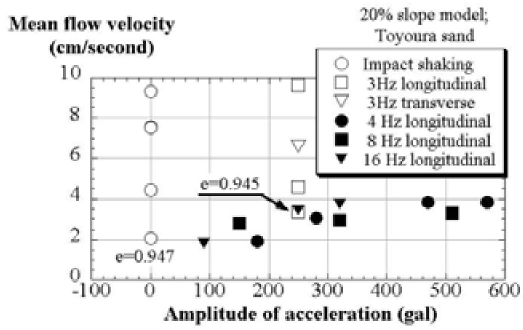

Figure 79. Effects of shaking acceleration on mean velocity of lateral soil flow.

Effects of the intensity and frequency of continued longitudinal shaking on the development of lateral displacement are going to be studied in what follows. Since the ultimate and maximum possible displacement is held constant at around 30cm irrespective of the type of longitudinal shaking, the magnitude of the displacement at the end of shaking cannot demonstrate the effects of the nature of shaking. Fig.76, therefore, employs the displacement at 5 seconds after the initiation of shaking, intending to examine the variation of flow velocity. It is therein shown for the studied range of sand density that the effects of base shaking is less important. This finding is consistent with the field experience that the soil movement occurred in the direction of slope under the influence of static gravity force (Fig.53).

Fig.77 compares the development of displacement for different shaking frequencies, while maintaining density of sand and intensity of shaking similar. The flow velocity is thus unchanged by the shaking frequency. In combination with Fig.76, it may be stated that shaking does not play a major role in development of lateral displacement when subsoil is liquefied. The chief role of shaking is to trigger liquefaction. This is in contrast with the accumulation of strain which occurs in unliquefied subsoil (Fig.49).

Fig.78 compares the variation of mean flow velocity when the void ratio changed. The mean flow velocity was obtained by dividing the residual displacement by the elapsed time to attain it. In spite of the varied shaking acceleration, there is a single trend as seen in this figure. The velocity decreases as the sand becomes denser. When sand was very loose, the velocity data from impact shaking and continued shaking were similar. Thus, the nature of shaking is not important in lateral flow of loose sandy slope. In contrast, when the void ratio is less than 0.92 under the reduced stress level of 1-G model, an impact shaking would not be able to generate flow displacement, as was already discussed in Fig.75. When sand was denser, lateral displacement was able to develop only by continued shaking.

Finally, Fig.79 exhibits the effects of the intensity of base acceleration on the velocity of soil flow. This figure employs the same data set as in Fig.78. Although the acceleration increases the rate of flow when sand was relatively denser (solid symbols), the major role is not yet played by the acceleration. When sand was extremely loose, velocity was greater, whether model was shaken by impact or continued excitation.

1-G model tests should be run at reduced density of sand in order to take into account the effects of confining pressure. In consequence of the tests, it was concluded that the density of sand affects the rate and the magnitude of residual displacement, and that the continued shaking is needed for a significant displacement to occur in relatively denser sand. It was further shown that the intensity of shaking and frequency are less important. On the other hand, the material properties of liquefied sand that governs the magnitude and rate of displacement are undrained shear strength and possible rate dependency. In case of very loose sand, the tested slope models became level after flow, suggesting that liquefied sand has neither shear rigidity nor shear strength. Consequently, the slow and monotonic (over damped) development of displacement can be understood only by the concept of viscosity.

6 LABORATORY SHEAR TESTS ON ACCUMULATION OF SHEAR DEFORMATION UNDER CYCLIC LOADING

This section introduces the recent knowledge on behavior of sandy soil undergoing cyclic loading which was obtained by laboratory shear testing.

Conventionally, most of the experimental studies on cyclic behavior of loose sand have been conducted by assuming a horizontal layered ground. Hence, there was no static shear stress and the cyclic shear stress was loaded equally in positive and negative directions; i.e., two-way loading. A typical example of test results is presented in Fig.80. As is well known, the increase of the tangent shear modulus (gradient of stress-strain curve) after 0.02 shear strain (2% strain) in Fig.80(a) is due to decreasing pore pressure or increase in effective stress (Fig.80(b)).

In case of slopes that develop residual strain after cyclic loading, the deformation develops as schematically illustrated in Fig.81. In case of liquefaction in loose sand, the dynamic component of strain is smaller than the residual one and, therefore, is not important. In contrast, when subsoil does not liquefy, the residual strain can develop in consequence of unloading and reloading of cyclic deformation (Fig.49).

The knowledge obtained from shear tests such as Fig.80 is true in more realistic conditions. Fig.82 illustrates a deformed shape of a gravity-type quay wall model which was subject to liquefaction in both backfill and foundation. Being intended to investigate the causative mechanism of large deformation of quay walls in Kobe Harbor area, sandy deposit was placed under the wall. Moreover, the density of sand was made looser than reality in order to compensate for the effects of reduced stress level (Fig.64). Since shaking occurred in the longitudinal direction of the model in Fig.82, the directions of the initial static shear stress and the cyclic stress were identical, making one-dimensional conditions.

Fig.82 clearly indicates that the distortion of the quay wall was associated with large shear deformation of surrounding soils. Since there was no silty layer in this model, no water-film phenomenon occurred. Ghalandarzadeh et al. (1998) experimentally reproduced the stress-strain and stress-path diagrams of the foundation soil under the quay wall model of Fig.82. Fig.83 indicates the results. In the course of shaking, the stress-strain diagram (Fig.83(a)) shows the accumulation of deformation with the number of loading cycles. The stress-path diagram in Fig.83(b) shows that this strain accumulation occurred when the stress state stayed near the failure line. Noteworthy is that deformation of the model ceased at the end of shaking, because the mechanism of strain accumulation due to cyclic loading (similar to Fig.47) was terminated. This is consistent with findings by Okamura et al. (2001) in centrifugal tests.

(a) Shear stress-strain behavior

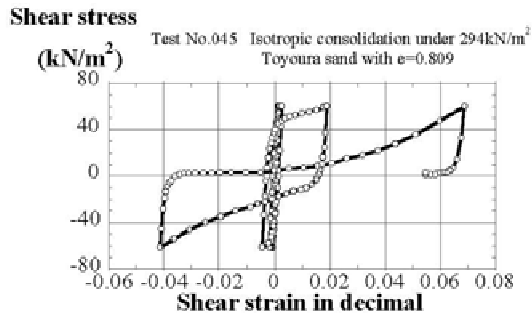

(b) Stress path diagram

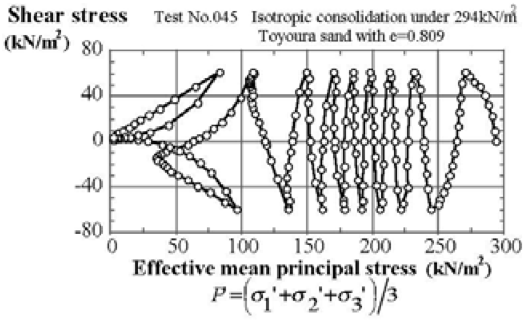

Figure 80. Undrained cyclic shear test on loose Toyoura sand.

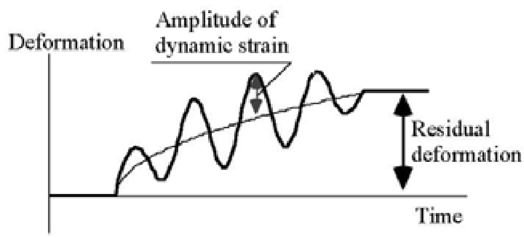

Figure 81. Schematic illustration of strain accumulation due to cyclic shear loading.

The preceding sections concerned with the loading condition in which the initial static shear stress and the cyclic component occur in the same direction. This situation may be called one-dimensional. In the recent times, in contrast, the engineering interests in more complicated loading conditions have increased. Although the final target of loading conditions is the one in a three-dimensional stress-strain space, the degree of freedom of the stress space therein is six and cannot be produced by existing soil testing machines. For example, the conventional triaxial apparatus can control only two stress components, and the torsional shear apparatus has three independent stresses (axial, lateral, and torsional components), or four, if internal and external lateral stresses are controlled independently. In this respect, the present discussion is focused on the stress-strain behavior in a two-dimensional condition.

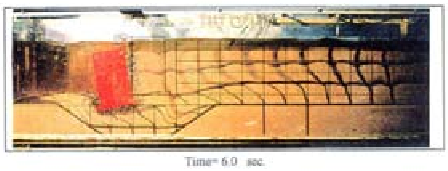

Figure 82. Deformed shape of gravity quay wall model after 1-G shaking table test (Ghalandarzadeh et al., 1998).

(a) Shear stress-strain behavior

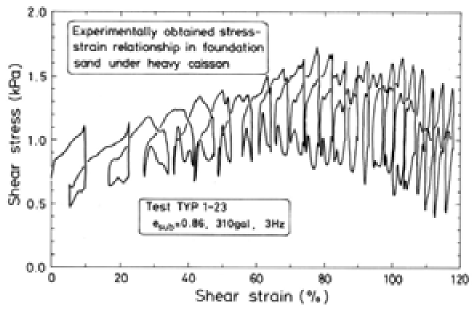

(b) Stress path diagram

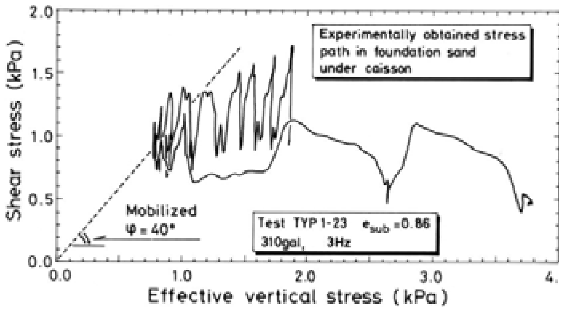

Figure 83. Reproduced behavior of sand under gravity quay wall in 1-G shaking test (Ghalandarzadeh, 1998).

There are two important types of two-dimensional stress conditions during seismic loading. Fig.84 illustrates them. The first situation in Fig.84(a) occurs in a vertical cross section of subsoil, for example, under a heavy structure such as dikes, oil storage tanks, and buildings without deep foundation. The significant stress difference between the vertical and horizontal stresses, σ_v-σ_h, is generated by the static gravity, which is then superimposed by cyclic shear stress in the horizontal plane, τ_{vh}. Fig.85 shows an example of this kind of loading in which the vertical compression increases with the cyclic loading of shear stress. Since the direction of shear stress and the direction of strain accumulation are perpendicular to each other, they are independent of each other in an energy sense. Fig.86 illustrates the translation of Mohr's effective stress circle in this test. Although the effective stress was held high during the cyclic loading, the tested specimen was not in a stable condition. Due to small translation to the left, the Mohr's stress circle came to a position at which the mobilized friction angle was 45.6 degrees. Thus, shear failure became imminent.

Interesting behavior can be found in the case of two-dimensional loading in a horizontal plane (Fig.84(b)). Being otherwise called multi-directional, this type of loading is closer to a real earthquake loading that has both East-West and North-South accelerations simultaneously. Fig.87 shows the two-dimensional acceleration record which was obtained in the campus of Kobe University during the earthquake in 1995. Since this campus is situated in a mountain area, the subsurface condition is rigid. It may be seen in this figure that the intensity of NS and EW components are similar.

The same earthquake was recorded in the Port Island in Kobe Harbor as shown in Fig.88. Out of four sets of records obtained at different depths, two of them at the ground surface and 16 meters below the surface are presented in this figure. Note that the latter one was obtained below the artificial fill which liquefied during the earthquake. Since the liquefied artificial fill could not fully transfer the dynamic shear stress towards the surface, the acceleration at the surface was weaker than at the bottom. By comparing Fig.87 and Fig.88 further, it is found that the Port-Island records had a stronger component in the NW-SE direction. This feature is probably due to the location of the site which was at a few kilometers away from the seismic fault (directivity of motion). The campus of Kobe University was much closer to or nearly above the fault and was probably free from such a phenomenon.

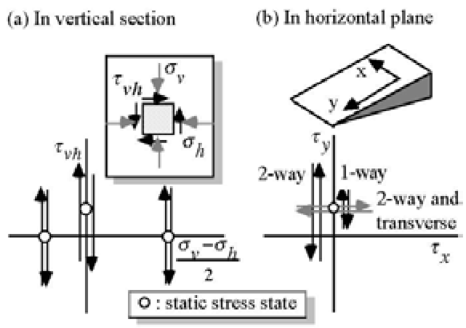

Figure 84. Two-dimensional stress states subjected to seismic loading.

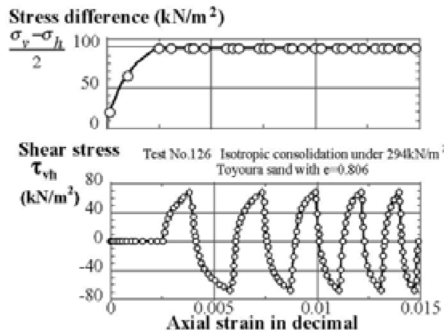

Figure 85. Vertical compression induced by superposition of stress difference in vertical and horizontal directions and cyclic shear stress in horizontal plane.

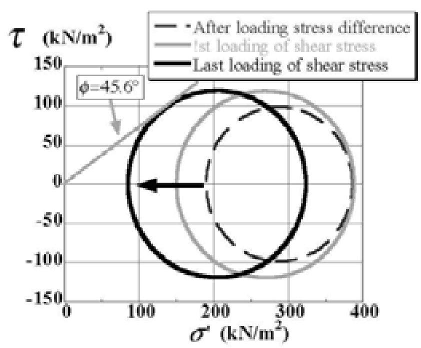

Figure 86. Mohr's stress circles during the test in Fig.85.

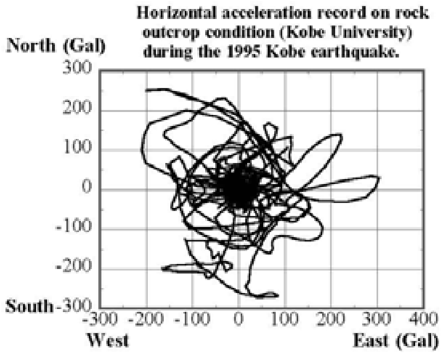

Figure 87. Two-dimensional acceleration record in Kobe University Campus in 1995 (obtained by Committee of Earthquake Observation and Research in the Kansai Area).

(a) At the ground surface

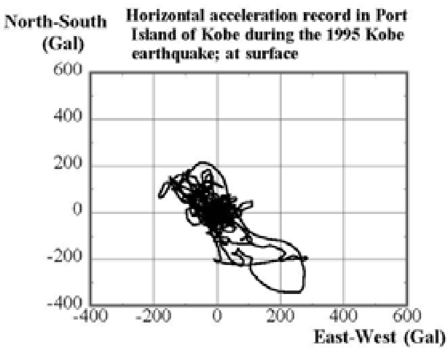

(b) At 16 meters below the surface

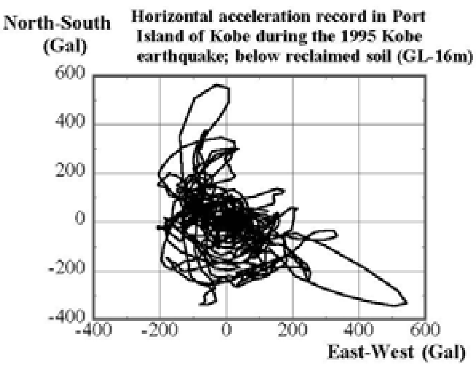

Figure 88. Two-dimensional acceleration time histories in Port Island of Kobe during 1995 earthquake (recorded by Development Bureau of Kobe City Government).

Experimental studies have shown that, in case that there is no initial static shear, the two-dimensional loading induces volume contraction or triggers liquefaction more easily than conventional one-dimensional loading (Pyke et al., 1975; Seed et al., 1978; Ishihara and Yamazaki, 1980; Kammerer et al., 2004).

An interesting feature is found in the effects of superimposing a second acceleration component in a direction perpendicular to the initial static shear; see the two-way and transverse loading in Fig.84(b). A stress time history, composed of monotonic strain-controlled loading in the y direction superimposed by cyclic loading in the x direction, was applied in a drained manner to compacted specimens of Yurakucho sand which is an alluvial material in the Tokyo downtown area. Fig.89 illustrates an experimental device which generated two-directional simple shear loading.

Fig.90 shows the volume change during shear. Since the relative density of the specimens exceeded 100%, volume expansion or positive dilatancy was going to start in the phase of monotonic shear in the y direction (between the origin and ○). When superposition of the cyclic loading in the x direction was initiated at the points of ○, however, a significant extent of volume contraction (positive volumetric strain) occurred. This transition of positive dilatancy to negative one (volume contraction) is equivalent in undrained shear with higher pore water pressure and greater deformation. Thus, although positive dilatancy in conventional one-dimensional loading exhibited the development of rigidity and shear strength in undrained conditions (Fig.80), their effects should not be relied on too much in two-dimensional conditions.

Figure 89. Two-directional simple shear apparatus (Horie, 2002).

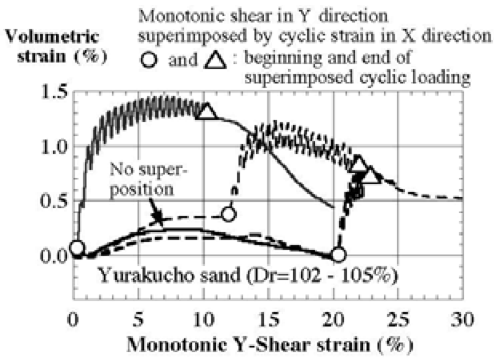

Figure 90. Volume change of dense sand specimen undergoing multi-directional simple shear (Horie, 2002).

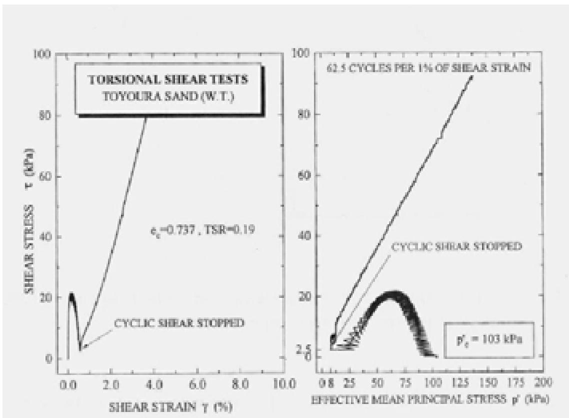

Figure 91. Effects of undrained superposition of cyclic loading on monotonic shear in independent directions (Meneses et al., 1998 and 2000).

Meneses et al. (1998 and 2000) carried out undrained shear tests in which two-dimensional loading was produced in a torsion shear device. A monotonic torsional shear was superimposed by cyclic loading of axial stress in which triaxial compression and extension were repeated. Fig.91 shows that , after the end of stress superposition, strain softening behavior and development of excess pore water pressure are changed to strain hardening behavior with increasing effective stress. Thus, the effects of stress superposing are important.

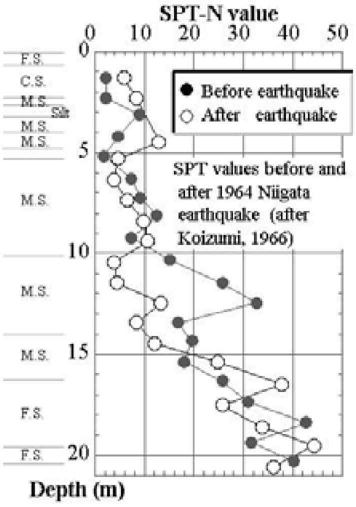

Figure 92. Change of SPT-N before and after 1964 Niigata earthquake (Drawn based on figure by Koizumi, 1966)

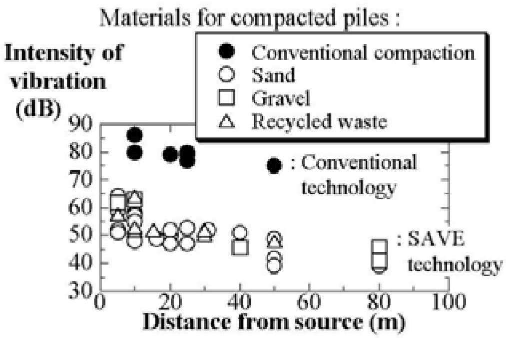

Figure 93. Reduced level of ground vibration by new kind of sand compaction pile installation (Data by Fudo Construction Company).

Figure 94. Liquefaction in unimproved part and no liquefaction in densified part of Lukan land reclamation site, Taiwan (Kaiyo Kogyo Company).

7 PROTECTION OF GEOTECHNICAL STRUCTURES FROM LIQUEFACTION-INDUCED GROUND DISPLACEMENT

The conventional approach to mitigate liquefaction-induced hazards has been soil improvement. After the 1964 Niigata earthquake, Koizumi (1966) reported an increase of SPT-N in shallow sandy soils, while N value decreased in lower more stable soils (Fig.92). This finding led to an idea of critical N value above which liquefaction is unlikely. Since then, densification became the most important measure to avoid risk of liquefaction. Upon the 1995 Kobe Earthquake, the central part of Port Island in Kobe Harbor did not have significant damage of liquefaction in consequence of different types of sand densification (Yasuda et al., 1996). Although sand compaction pile had long been a very important method to densify sand, it had a big problem of heavy noise and ground vibration. This shortcoming, however, was solved by new development as illustrated in Fig.93. On the other hand, as an economical measure to densify sand, the effect of dynamic consolidation by using impact loading was validated during the 1999 ChiChi earthquake in Taiwan (Fig.94).

In addition to sand densification, grouting in a grid shape proved its good performance during the Kobe earthquake (Tokimatsu et al., 1996) The effects of gravel drain were validated as well in Kushiro Harbor of Japan in 1993.

The recent research needs have been focused on protection of existing structures from liquefaction problems. Since the ground surface is occupied by structures, available area is limited. In urbanized areas, moreover, ground displacement and vibration upon installation of mitigative measure are not a good idea. Hence, some of the conventional soil improvement technologies are difficult to be used.

The review of past liquefaction damage in the previous chapter revealed that the essence of damage lies in the excessive displacement. The basic philosophy of performance-based design will rely on seismic displacement which is kept within allowable extents. In this line, the author has made efforts to verify the effects of installing embedded sheet pile walls in order to reduce the liquefaction-induced displacement.

The use of embedded wall was suggested by an experience during the 1995 Kobe earthquake. Fig.95 shows that a building foundation surrounded by embedded walls survived the quake although nearby buildings were affected by ground displacement. Those walls were installed for excavation of the foundation as a common practice when the building was constructed. Not being designed as a permanent structure, those walls cannot be taken into account in seismic design as a mitigation measure. They have, however, good effects because the displacement of foundation soil is prevented by these stable underground walls.

Figure 95. Intact foundation of building surrounded by embedded walls (Shimagami Pumping Station, Kobe, 1995; Photo by J.Koseki).

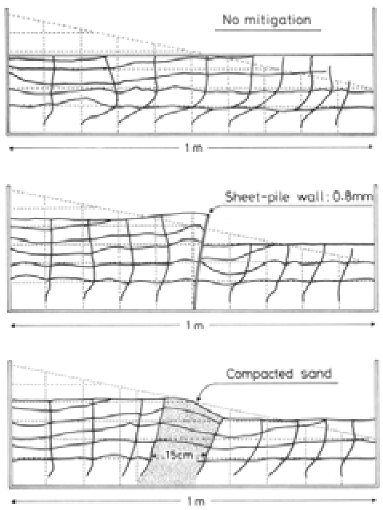

Figure 96. Mitigation of liquefaction-induced ground displacement by embedded walls.

(a) Sheet pile model

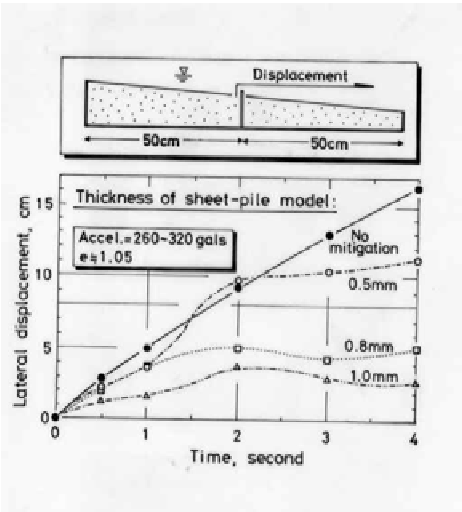

(b) Compacted sandy wall.

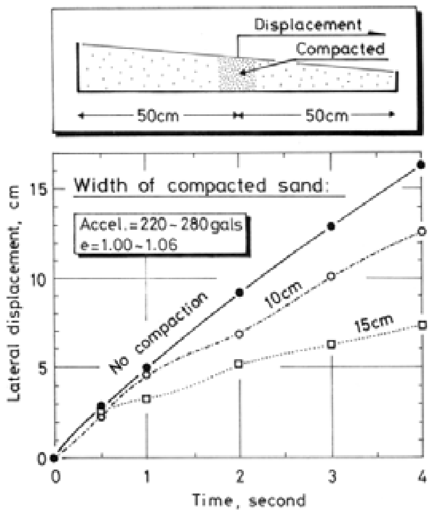

Figure 97. Effects of wall thickness on mitigation of lateral displacement.

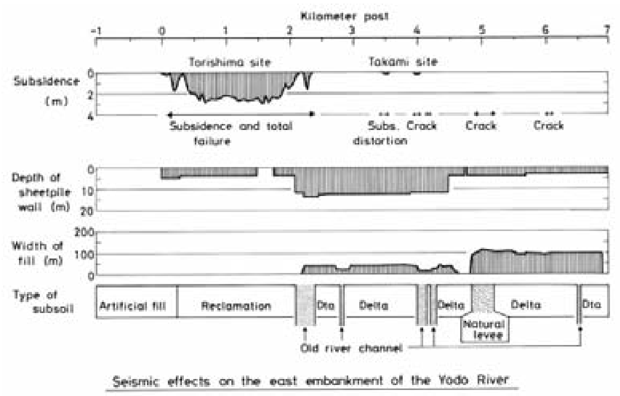

Figure 98. Variation of subsidence along Yodo River dike (data by then Ministry of Construction).

Figure 96 illustrates one of the earliest attempts to demonstrate the effects of an embedded wall on mitigation of lateral ground displacement caused by liquefaction (Kogai et al., 2000; Towhata et al., 2000). After shaking in the longitudinal direction, the model slope without mitigation as shown at the top of the figure became level. The maximum horizontal displacement was around 15 cm. The second model with a model sheet pile wall was able to reduce the displacement to 5 cm or less. Note that this good result was obtained because the bottom tip of the wall was stable, fixed at the bottom of the container. A similarly good result was obtained by the use of compacted sandy wall as well; see the bottom of the figure. The mitigative effects of a wall obviously depend on its rigidity; better mitigation for thicker walls as illustrated in Fig.97.

The use of embedded wall has been investigated for mitigation of subsidence of embankment. Before detailed discussion, it is meaningful to review the damage of Yodo River dike in 1995 (Fig.21). From the viewpoint of performance, the behavior of a river dike is considered satisfactory unless flooding occurs as a consequence of shaking. Minor subsidence could be restored within a reasonably short period of time.

Fig.98 illustrates the variation of dike subsidence along the river channel. As reported by Matsuo (1996), the subsidence was significant only in Torishima area. The less affected dike in Takami area has three differences. Firstly, the subsoil is composed of natural deltaic deposit which is probably more aged than that in Torishima area. Field experiences as well as laboratory tests demonstrated the effects of aging on increase in liquefaction resistance of sand (Mulilis et al., 1977; Tatsuoka et al. 1988).

Age of soil is not the only one reason for different seismic performances. The subsoil in Torishima-Takami area used to be swampy several hundred years ago and, similar to Dagupan City of the Philippines, the subsoil there may not be very aged yet. Hence, it is meaningful to look for more reasons for the good performance of the Takami dike. The second difference between Torishima and Takami is the depth of sheet pile walls (Fig.98) which were installed to reduce seepage flow under the dikes. Note that those walls were not intended to reinforce the dike structurally. In Takami, the depth of wall was 10 m which was sufficient to reach the bottom of sandy layer. Thus, a situation similar to Fig.97 was unintentionally created. On the contrary, the sheet pile in Torishima was much shorter, leading to less reinforcing effects. The third difference is the existence of berm on the river side of Takami dike (Fig.98). It should be recalled that placement of a berm near the bottom of a slope is a common practice to improve stability. It seems therefore that embedded walls and placement of berms are helpful in mitigating instability of dikes and embankments subjected to subsurface liquefaction.

(a) Before shaking

(b) After shaking

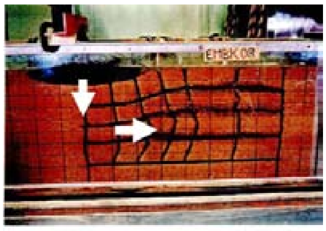

Figure 99. 1-G shaking test on embankment subjected to subsurface liquefaction without mitigation.

(a) Location of sheet pile model.

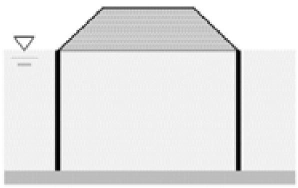

(b) Subsidence of embankment model with sheet piles after shaking.

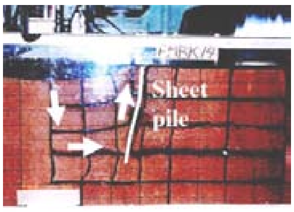

Figure 100. 1-G shaking test on embankment with sheet piles subjected to subsurface liquefaction.

The first series of tests on dike and embankment were carried out on a 1-G shaking table by using a container of 2 meter in length (Towhata et al., 1998; Mizutani et al., 1999 and 2001). Fig.99 shows the configuration of a model prior to and after shaking. Taking into account the effects of reduced stress level in and the shorter natural period of a 1-G small model, this series of tests employed extremely loose sand and shaking at 10Hz that was higher than the predominant frequency of real seismic acceleration. The model embankment was 10 cm high and made of unliquefiable gravel which was underlain by split sheets of fence in order to prevent gravel grains from falling down into liquefied subsoil. The subsidence of the embankment was measured at the bottom of the gravel fill so that the compaction of gravel fill might not be included in the record. The deformed shape in Fig.99(b) clearly shows that the subsidence of the embankment was associated with the lateral displacement of liquefied subsoil. Thus, it appeared promising to install sheet pile walls beside the embankment and prevent the lateral displacement.

An embankment with sheet pile walls under the toes of the slopes was tested as illustrated in Fig.100. Two model sheet pile walls were made of aluminum plates with their bottoms fixed to the base of the container. This implies that sheet piles in reality should penetrate into unliquefiable soil layers. Moreover, the model sheet piles were installed beyond the embankment slope (Fig.100(a)) because river engineers in practice are afraid of leakage of water through possible cracks in a dike produced by pile penetration. After shaking with 120 Gal and 10 Hz for 12 seconds, the embankment model was distorted as shown in Fig.100(b). Although the model sheet pile was distorted by the earth pressure difference, it prevented the outward displacement of subsoil. Consequently, the liquefied subsoil moved up towards the toe of the embankment. The time history of measured subsidence is plotted in Fig.101. It is remarkable that the subsidence was reduced by sheet pile installation to nearly 1/3 of that without mitigation.

Additional tests were performed by using the amplitude of acceleration equal to 0.25 Gal and the duration time of 25 seconds. Since the shaking frequency was reduced to 3Hz, the displacement amplitude became greater than the one in Fig.101. The use of 3 Hz for a small model test may not be realistic because 3 Hz is a typical prototype earthquake motion. However, together with the elongated duration, it was intended to exert very significant shaking to the model.

Results are shown in Fig.102. Sheet piles could not mitigate the subsidence. One reason for this poor performance is the large displacement at the top of sheet piles which opened cracks between sheet piles and the embankment model. A substantial amount of sand boil was ejected through them, and large subsidence was induced. To solve this problem, additional gravels bags were placed upon the location of cracks (berms) in order to prevent sand boiling. This idea worked to some extent as shown by the third time history in Fig.102. However, the mitigative effects are around 30% only.

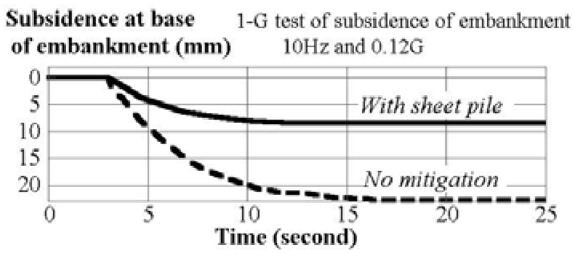

Figure 101. Mitigative effects of sheet pile installation in time history of subsidence.

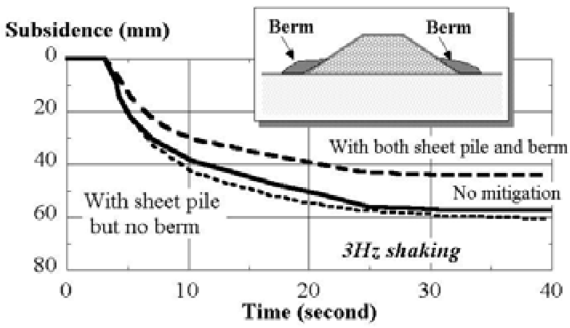

Figure 102. Effects of reduced shaking frequency on time history of subsidence.

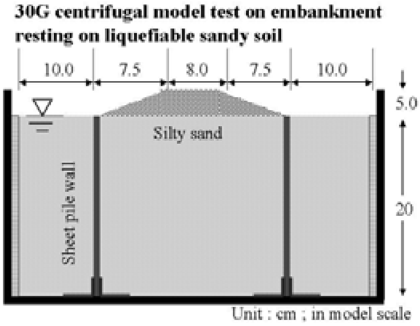

Figure 103. Configuration of centrifugal test model of embankment.

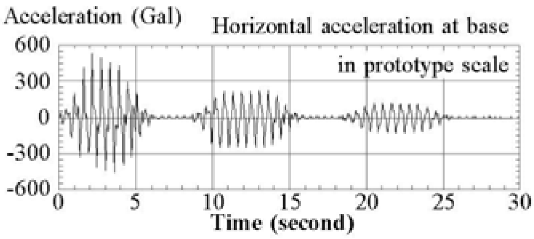

Figure 104. Time history of base shaking in centrifugal tests on embankment.

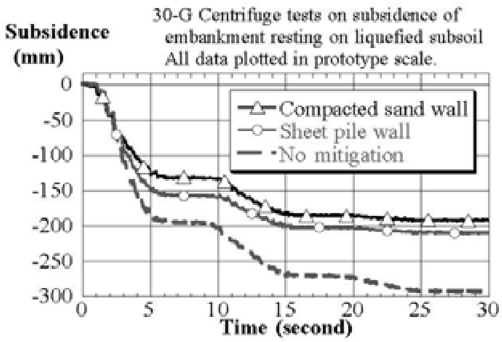

Figure 105. Time history of subsidence of embankment model measured by centrifugal tests with and without mitigation.

Model tests on embankment were continued under 30G centrifugal field (Alam et al., 2004a, 2004b, and 2004c). Fig.103 demonstrates the configuration of a model in which embankment was made of 1-mm lead shots and was placed upon liquefiable fine loose sand. The location of embedded sheet pile walls for mitigation is illustrated as well. Since the centrifugal tests generated the effective stress level similar to the prototype, there was no need to employ unrealistically low density of sand as practiced in 1-G tests.

In the present case, fine cohesionless sand (Gs=2.618, D_{50}= 0.028mm and fines content = 92.8%) was collected from the Tottori-Takenouchi site where liquefaction occurred in 2000. This sand was mixed with water under vacuum, put in a container, and consolidated under centrifugal gravity. It seems that this model preparation reproduced the natural sedimentary process. Since the permeability of this material was as low as 6.84×10^{-7} m/second, there was no need to use viscous liquid as the pore fluid. Shaking was of harmonic type with 60 Hz and 3 stages (Fig.104). The amplitude of acceleration was reduced with intermission as carried out by Okamura et al. (2001) in order to see the effects of shaking on development of ground deformation.

Figure 106. Example of chemical factory.

Figure 107. Small drilling machine for compaction grouting in narrow basement floor.

Fig.105 demonstrates the time history of the subsidence of embankment with and without mitigations. Two kinds of mitigative measures were employed. The first one was the use of aluminum sheet piles with the model thickness of 6mm and the elastic modulus of E= 70 GN/m^2, while the other mitigation was made by compacted sand wall in which 50mm-thick (model scale) wall of Toyoura sand was installed at the relative density = 90%. Both mitigative measures reduced the subsidence to two thirds of the unmitigated subsidence. It is interesting that subsidence occurred only during shaking, indicating the importance of cyclic stress application on development of large soil deformation. This finding is consistent with Okamura et al. (2001).

Mitigation of liquefaction-induced subsidence is an urgent problem for oil storage tanks in chemical factories and oil refineries in Japan. This is because many existing tanks were constructed when the safety regulation was less strict and at present the government is going to apply stricter seismic design codes to old ones. Sand compaction is not a practical mitigation. This is because existing factories are fully occupied by tanks and pipes (Fig.106), and, hence, ground vibration upon soil compaction is not appropriate. One of the earliest ideas was the use of gravel drains whose installation would not significantly cause ground displacement or vibration. Kimura et al. (1997), therefore, conducted centrifuge model tests to demonstrate the mitigative effects of underground unliquefiable walls made of gravel drains.

There are more problems to be solved in oil storage tanks. Since most chemical factories are full of tanks and pipes, big construction machines for sand compaction or gravel drain installation may not be able to enter. Hence, it was desired to construct an embedded wall around the foundation of a tank by using small machines. One of the solutions to this task is compaction grouting (Fig.107).

Yonekura and Shimada (1992) showed that colloidal silicate grout can uniformly seep into sandy soil and maintains its strength for many years without weathering and deterioration. It appears that this grouting material is not poisonous and, therefore, satisfies the environmental requirement for a permanent ground improvement. Gallagher and Mitchell (2002) worked on a similar material. Since this material has a very small size of colloidal silicate particles, it can seep into minute voids of silty sand for which mitigation of liquefaction is very important. During injection, this grout has a low viscosity, and it solidifies later in ground. Fig.108 demonstrates the tiny injecting tubes of Nasu (2000) who developed a multiple and slow injection to form a uniformly solidified soil column under the ground. On the other hand, Zen et al. (1997) as well as Hayashi et al. (2001) injects the grout from a bore hole.

The improved resistance against liquefaction was studied by Kabashima and Towhata (2000) as well as Towhata and Kabashima (2001) on Toyoura sand which had the colloidal silicate grout injected. A special care was taken of reproducing the stress history which grouted sand experiences in reality. Hence, loose Toyoura sand with relative density of 40% was placed in a cylinder in which sand was saturated with water and was consolidated under the specified vertical stress. The sand specimen was thereinafter had the grout seeped in and the pore water was thus replaced by the silicate liquid. After curing for more than five weeks, the solidification was completed and the sand specimen was moved to a triaxial apparatus. The specimen was consolidated under isotropic or anisotropic stress and was subject to various kinds of shear tests.

Figure 108. Injection tubes for multiple point injection method.

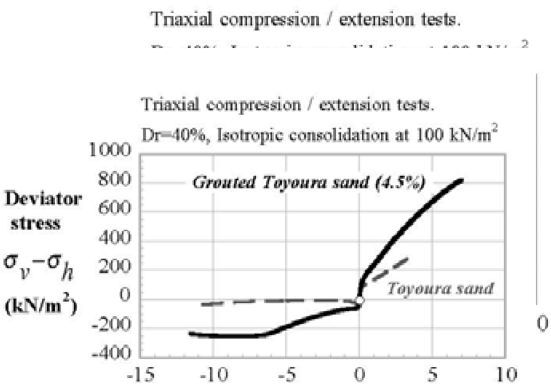

Figure 109. Undrained triaxial tests on grouted Toyoura sand.

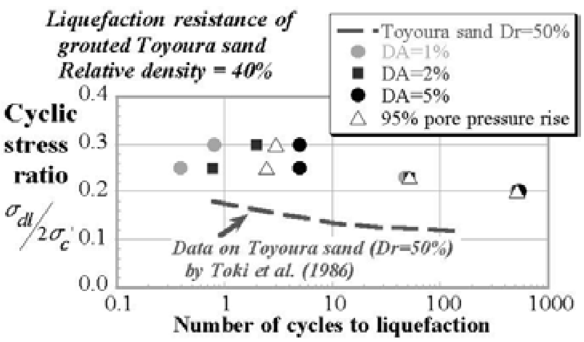

Figure 110. Cyclic triaxial tests on grouted Toyoura sand.

Fig.109 illustrates undrained triaxial compression and extension tests on grouted and unimproved samples. For this test, the density of colloidal silicate grout was 4.5%. It is clearly seen that both rigidity and shear strength of sand were substantially improved. Cyclic triaxial test data in Fig.110 shows the resistance of grouted sand against liquefaction. Although the relative density of the specimens was 40%, the obtained resistance was far greater than that of unimproved Toyoura sand with 50% relative density.

Based on the above findings from laboratory shear tests, 1-G shaking model tests were conducted on mitigation of subsidence of a storage tank model resting on liquefiable subsoil (Isoda et al., 2001). Fig.111 shows the configuration of one of the tested models in which walls of grouted Toyoura sand measured 12.5 cm in width. Note that three more tests were run; one without grouting, one with doubled grouted sand wall (extended outwards), and one with full grouting under the tank in Fig.111. The weight of the tank model was produced by filling it with lead shots which is more appropriate than using water because no undesired sloshing of liquid occurs. The bottom of the tank was covered by plastic sheet without tension so that the intended contact pressure might be uniformly transferred to the foundation. The interface between liquefiable Toyoura sand and grouted sand walls were covered by plastic sheets as well in order to prevent quick propagation of pore water pressure.

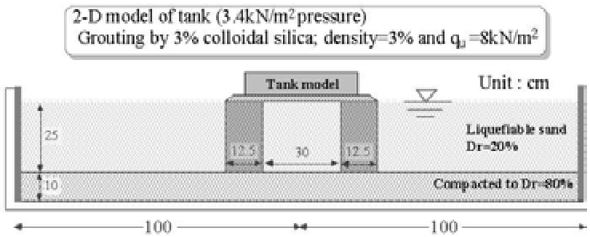

Figure 111. Configuration of two-dimensional tank model with grouted sand walls.

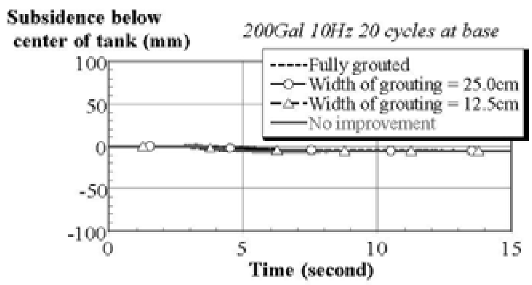

Figure 112. Subsidence at center of tank under 200-Gal shaking.

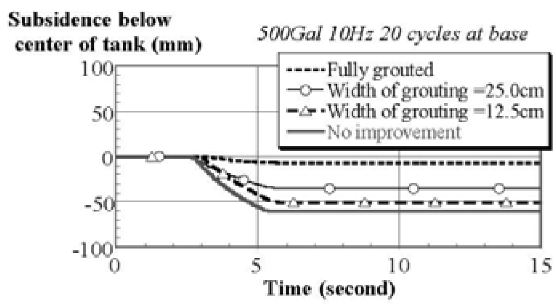

Figure 113. Subsidence at center of tank under 500-Gal shaking.

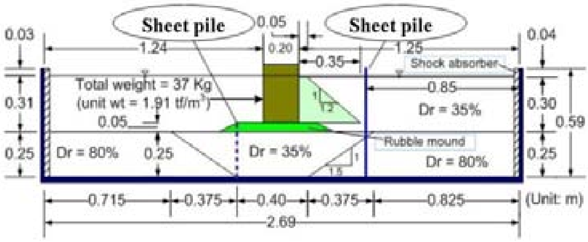

Figure 114. 1-G model of quay wall with sheet piles.

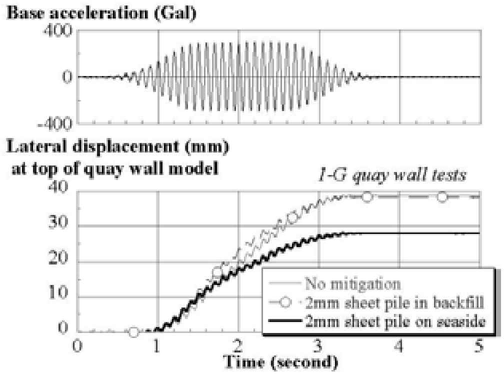

Figure 115. Mitigative effects of sheet pile on lateral displacement of gravity quay wall.

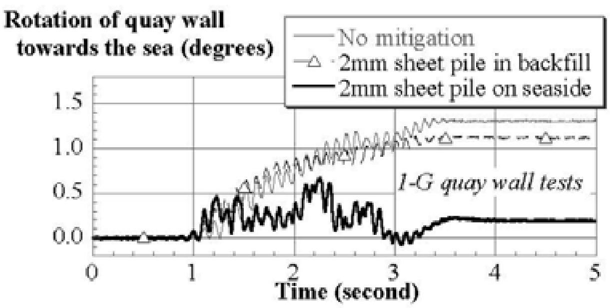

Figure 116. Mitigative effects of sheet pile on seaward rotation of gravity quay wall.

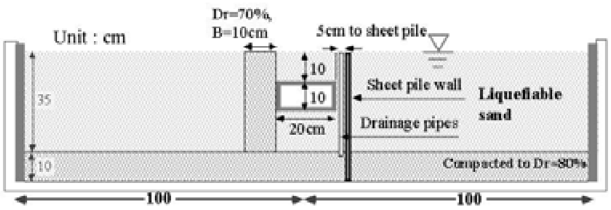

Figure 117. Configuration of 1-G model with and without embedded walls for mitigation.

Two kinds of shaking were applied to the models; 200 and 500 Gal with 20 cycles at 10 Hz. Under the weaker shaking, there was no remarkable difference in the small subsidence at the center of the tank as shown in Fig.112. However, under 500-Gal excitation, the installation of grouted wall was able to reduce the subsidence as illustrated in Fig.113. Note that the extent of mitigative effects was 25 to 40%. Obviously the best mitigation was attained by grouting the whole foundation.

Mitigative effects of sheet pile walls on seismic stability of a gravity quay wall were examined in 1-G shaking table tests. Fig.114 shows the configuration of the employed model. This figure further illustrates the location of sheet piles which were placed in the backfill or in front of the quay. The shaking consisted of 26 cycles at 10 Hz with the maximum amplitude of 300 Gal (see top of Fig.115). While mitigative effects are seen in Fig.115 when a sheet pile was installed on the seaside (front) of a quay wall, a similar wall in the backfill was not effective. This is because the seaward installation prevents the lateral displacement of the foundation sand, and, in contrast, the sheet pile behind the quay cannot be installed in the proximity due to gravelly filter whose mass exerts significant dynamic earth pressure on the wall. Similar difference is seen in Fig.116 in the extent of rotation of the quay wall as well.

Since floating of embedded structure (Figs.15, 16, and 17) is an important problem, mitigation by means of underground walls was investigated by 1-G shaking table models (Towhata et al., 2003). Fig.117 illustrates the configuration of the employed models wherein the location of embedded walls is indicated. The embedded walls were made of either sand compaction or 2-mm aluminum sheet piles and the same kind of wall was installed on both sides of the underground structure. In case of compaction, the width of the wall was either 10 cm or 20 cm. Base shaking of 180 Gal was put in with 1Hz for 12 seconds. An underground structure model which measured 20 cm in width and 10 cm in height was placed at the depth of 10 cm below the surface.

(a) Prior to shaking

(b) After shaking

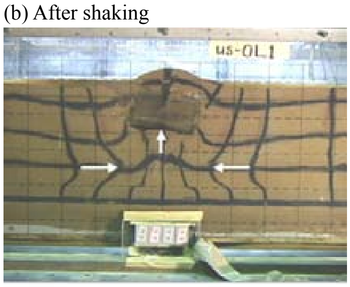

Figure 118. Behavior of embedded structure model without mitigation.

Figure 119. Appearance of embedded structure model with compacted walls on both sides.

Fig.118 indicates the configuration of a model without mitigation. The underground structure floated significantly upon shaking. The displacement of liquefied sand around the structure clearly indicates that sand moved in towards the bottom of the structure and then pushed it upwards. Therefore, it seems promising to install walls that can prevent this soil movement. Fig.119 shows the mitigative effects which were generated by compacted sand walls on both sides of the structure. The thickness of the walls was 10 cm and, by comparing this figure with Fig.118(b), it is clearly seen that floating and ground distortion were reduced. Moreover, tests with sheet pile walls were conducted. The most remarkable mitigation was obtained when drainage pipes were installed between the underground structure and sheet pile; see Fig.120. The insignificant floating which still occurred in this test was mainly caused by the soil movement which was generated downwards between the structure and sheet piles.

Fig.121 compares time histories of floating with and without a variety of mitigations. Note that floating was terminated at the end of 12-second shaking. While floating was reduced to some extent by sheet pile walls, remarkable mitigation was achieved by compacted sand wall and sheet pile walls with drainage pipes.

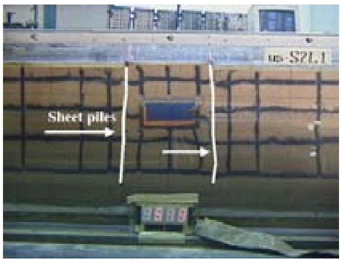

Figure 120. Appearance of embedded structure model with sheet pile walls with drainage.

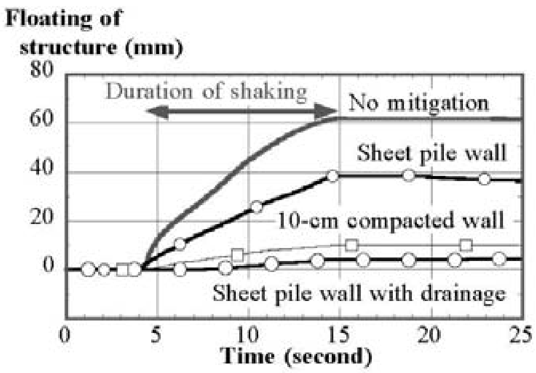

Figure 121. Effects of walls on time history of floating.

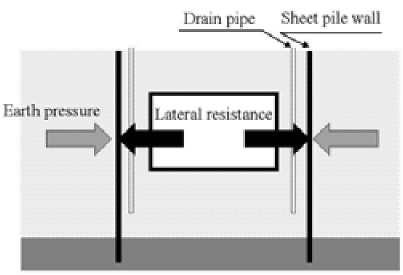

Figure 122. Rigidity of embedded wall improved by structure .

The mitigative effects of sheet pile walls rely on their bending stiffness in both cases of subsidence of embankment and floating of embedded structure. However, the extent of mitigation was significantly different between subsidence and floating. In case of subsidence, this rigidity was developed only by the bending stiffness of sheet piles or shear modulus / strength of compacted sand. In case of floating, conversely, the rigidity was improved by the underground structure which functioned as a rigid column between walls. This feature was further improved by installing drainage and maintaining the subgrade reaction modulus of sand (Fig.122).

8 PILE FOUNDATION SUBJECTED TO LATERAL FLOW OF LIQUEFIED GROUND

There are two important damage mechanisms in pile foundation subjected to liquefaction (Fig.123). The first one is the loss of subgrade reaction and increased bending moment caused by the inertial effects of the superstructure. The second mechanism is the increased lateral pressure which is produced by the lateral flow movement of liquefied ground. The lateral displacement of liquefied subsoil in Niigata triggered bending failure of pile foundation.

Concerning the second mechanism, information obtained by case history study is important. The excavation of damaged pile in Niigata City by Yoshida and Hamada (1990) demonstrated that bending failure occurred at two elevations which were at the top and bottom of liquefied subsoil (Fig.124). This finding implies that the damaged pile was restrained by the pile cap and the unliquefied base soil, and was subjected to lateral displacement at the top without rotation. Obviously this mechanism generated the maximum value of bending moment, leading to bending failure, at those two restraining boundaries. Note that buckling mechanism cannot produce this mode of failure.

In the failure mechanism in Fig.123(b), two kinds of lateral load are important. The one is the passive earth pressure between the pile cap and the unliquefied surface crust. Berrill et al. (2001) excavated a bridge foundation to examine the generation mechanism of this passive earth pressure.
The other kind of lateral load is the one exerted by liquefied subsoil. 1-G model tests by Hamada et al. (1998) as well as Ohtomo (1998) (Fig.125) revealed that the magnitude of bending moment in a pile generated by this type of lateral load has a better correlation with the flow velocity of liquefied ground than the flow displacement. This implies that the interaction between a pile and liquefied sand is better expressed by a rate-dependent mechanism than by a conventional p-y approach in which the load changes with the relative displacement.

(a) Loss of subgrade reaction. (b) Earth pressure caused by lateral flow.

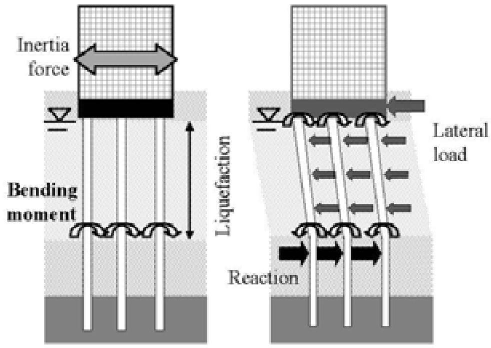

Figure 123. Two kinds mechanism of bending failure in pile foundation subjected to liquefaction.

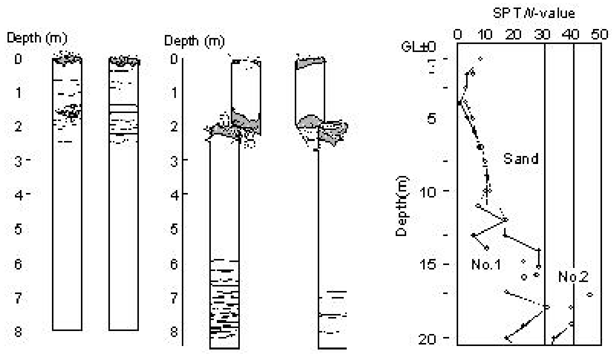

Figure 124. Bending failure of pile foundation caused by subsoil liquefaction in Niigata (Yoshida and Hamada, 1990).

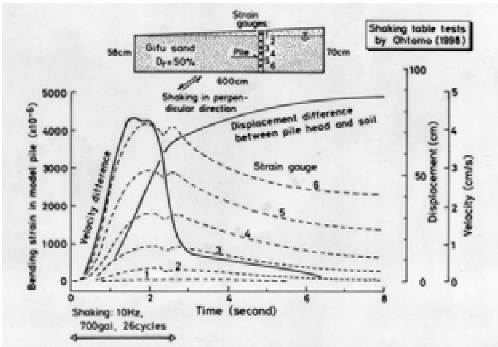

Figure 125. Rate-dependent nature of interaction between pile and lateral flow of liquefied sandy ground (Ohtomo, 1998).

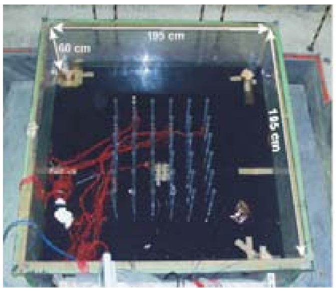

Figure 126. Plan view of 1-G model with 121 piles.

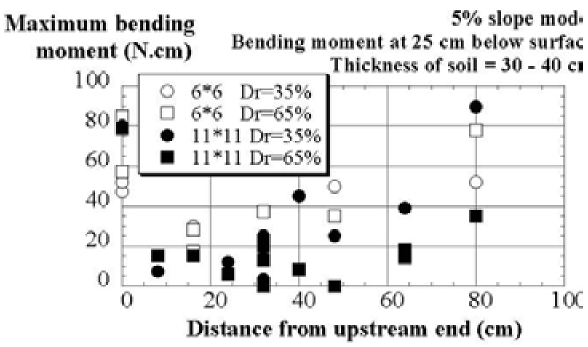

Figure 127. Variation of bending moment across a group pile foundation.

One of the author's interest lies in the retrofitting of existing pile foundation. His attention has also been focused on behavior of a group pile. Thus, a model test was conducted to study the behavior of group pile which consisted of 11*11=121 piles. Fig.126 illustrates a plan view of a tested model in which the model ground of 5% slope measures 195cm*195cm in size and consists of loose Toyoura sand with 35% relative density. The thickness of liquefiable sand changed from 30 to 40 cm in the direction of slope.

Fig.127 illustrates the variation of maximum bending moment in piles measured at 25 cm depth from the surface. It is therein seen that the bending moment takes the maximum value at the upstream and downstream ends of the group pile, while the internal piles are of less magnitude of bending moment. Thus, it is proposed to install additional sacrificing piles, which do not bear the weight of a superstructure, around an existing pile foundation so that the lateral load due to liquefaction is resisted mainly by those sacrificing piles.

9 DYNAMIC EARTH PRESSURE

The practical assessment of seismic earth pressure is one of the most important issues in earthquake geotechnical engineering. The recent increase in intensity of design earthquake (Fig.23) has resulted in the increased magnitude of seismic earth pressure which makes economical design of retaining structures very difficult. In this respect, Koseki et al. (1998) studied this problem experimentally and proposed to use in the conventional Mononobe-Okabe earth pressure theory the friction angle at the peak strength in place of the conventional friction angle at the residual state. Since the angle at the peak strength is greater than the residual one in compacted backfill materials, the newly-calculated earth pressure is lower than the conventional pressure and the size of unstable soil wedge is smaller. This reduced size maintains the earth pressure lower than the conventional one even when strain softening proceeds and the friction angle comes down to the residual value. A further study is continued on direct effects of shaking by Watanabe et al. (2003) among others.

In case of liquefaction, earth pressure has been assessed by combining the hydrostatic pressure as the static component and, for example, the Westergaard (1931) approximate solution of dynamic fluid pressure as the cyclic component. Since the Westergaard theory concerns a rigid dam body, his formula is applicable to a rigid embedded structure. Since some real structure is not very rigid, Tamari and Towhata (2003) showed by shaking model tests that the design dynamic pressure could be reduced by taking account of the flexibility of a structure.

10 EFORMATION CHARACTERISTICS OF LOOSE SAND UNDER LOW EFFECTIVE STRESS

Mitigation of liquefaction-induced damage will be achieved by introducing the idea of performance-based design principle which was addressed in a preceding chapter. Since large and unallowable extent of residual deformation is the essence of liquefaction-induced damage, the performance-based principle will be accomplished by two important issues. The first one of them is the technology that can reduce the residual displacement to an allowable extent, while the second one is a practical tool which can assess the magnitude of displacement. Since the first issue was discussed in the previous chapter, the present and the following chapters are going to discuss the second issue. In particular, the present chapter discusses the deformation characteristics of liquefied sand which is essential in the calculation of deformation.

To date there are many constitutive models which are employed in computer codes for dynamic analysis. One of the possible problems in some of those models is that they were developed in early days when large deformation of liquefied ground did not attract engineering concern. Hence, those models were built without paying much attention to behavior of sand after high pore pressure rise. This problem was partly due to the fact that soil testing machines could not achieve such a large strain as 50% or more which would occur in liquefied subsoil (Fig.82). Since this situation has not drastically changed to date, special efforts have to be made to investigate the behavior of liquefied sand.

To the author's knowledge, there are two kinds of ideas about the nature of liquefied sand. The first one considers liquefied sand as a solid material. Although the Newmark rigid block analogy belongs to this category, it is not suitable to the liquefaction problem, because liquefied sand is not rigid in any sense. More appropriate approach can be found in Yasuda et al. (1992) whose latest idea is illustrated in Fig.128. This approach as shown in Fig.128 is characterized by the use of reduced stiffness which occurs after significant rise of excess pore water pressure. By using experimental data, the extent of stiffness reduction as well as the strain range of this softening has been determined as empirical functions of factor of safety against liquefaction. Since liquefied sand is the target of the analysis, this factor of safety is less than unity. Consequently, two static finite element analyses are conducted by using pre-liquefaction and post-liquefaction reduced moduli, respectively, and the difference in calculated displacements is considered as the liquefaction-induced displacement. It should be recalled that the use of two stiffness values prior to and after shaking was originally developed by Lee (1974) who proposed to determine the reduced stiffness by applying seismic stress history on soil samples.

The author has been working on a second approach to assessment of liquefaction-induced ground deformation in which liquefied sand is considered to be viscous liquid. Viscous liquid stands for either Newtonian or Bingham liquid, depending upon the extent of shear resistance.

The idealization of liquefied sand as viscous liquid originates from the experimental finding in shaking table tests that the rate of flow is slow but the final configuration is level in case of very loose sand. This idealization may be supported further by the time history of bending moment in pile tests (Fig.125) in which the variation of bending moment is more consistent with the time history of flow velocity of liquefied sand than that of displacement.

It was felt that the idea of viscosity had to be verified by a more direct manner by running experiments. The first attempt in this direction was made by pulling an embedded pipe in a sandy ground which was subjected to horizontal shaking on a 1-G shaking table (Vargas and Towhata, 1995; Towhata et al., 1999a). For the testing device, see Fig.129. By pulling a pipe at different velocities in liquefied model ground, the drag force, which stood for the shear stress in the model ground, was recorded and plotted against the velocity of the pipe in Fig.130. Note that the pipe velocity stands for the strain rate in the surrounding sand. As shown in the figure, the drag force increases with the pipe velocity. According to the theory of fluid mechanics (Lamb, 1911), this finding implies that liquefied sand is a viscous material.

Figure 128. Reduced stiffness of sand after liquefaction (after Yasuda et al., 1992).

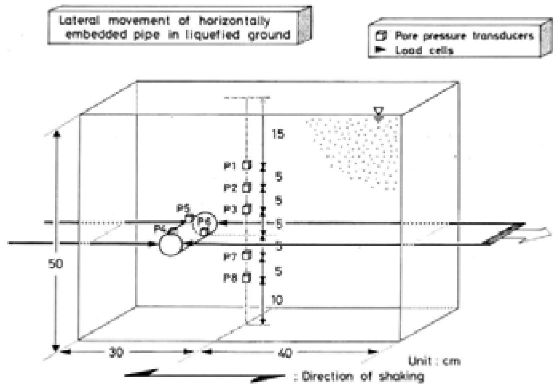

Figure 129. Measurement of drag force exerted by liquefied sandy ground in 1-G shaking table test.

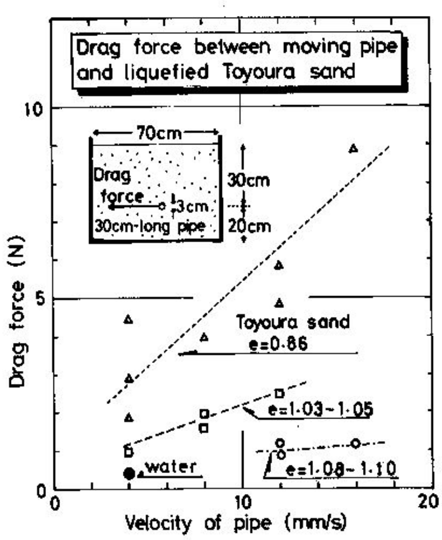

Figurre 130. Relationship between drag force and pipe velocity in 1-G tests on lateral displacement of embedded pipe.

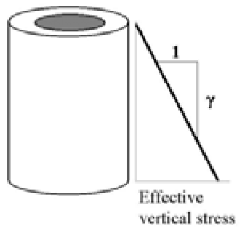

Figure 131. Minimal effective stress near the top of torsion shear specimen.

There were two shortcomings in the pipe-pulling tests;
- the effective stress level was lower than reality, although density of sand was reduced in the tests, and
- the stress-strain state in the liquefied sand was not uniform, making it difficult to interpret the properties of such a nonlinear material as liquefied sand.

In particular, the second shortcoming could be solved only by running shear tests on specimens in place of model tests. The first solution to these problems was therefore torsion shear tests in which a sandy specimen was consolidated under a realistic stress, and then was subjected to pore pressure rise. After liquefaction, shear stress was applied in a monotonic manner at different strain rates so that rate-dependent nature could be detected. This attempt, however, was not successful, because shear deformation was localized at the top of the sample where the effective stress was extremely small after liquefaction and shear strength was minimal in the body of a specimen (Fig.131). Note that the lower part of a specimen had higher effective stress due to gravity or weight of sand grains even after the state of liquefaction. This strain concentration made it difficult to determine the magnitude of strain (Kokeguchi et al., 2001a and 2001b).

The problem lying in torsion shear tests was overcome by running triaxial compression or extension tests in which all the parts of a specimen was uniformly loaded by the applied stress and developed deformation without significant localization of strain. This series of tests were conducted in a torsion shear apparatus in which both triaxial and torsional types of shear were possible (Nishimura et al., 2002; Galage et al. 2005). The torsional shear with up to 25-Hz frequency was possible in this device so that cyclic shear could be superimposed on triaxial compression, if necessary.

The testing was conducted in the following manner.

1) A loose sandy specimen was isotropically conducted under, for example, 100 kN/m^2.
2) The effective stress was then reduced to a specified low level by either increasing the back pressure (pore water pressure) or applying cyclic undrained shear stress.
3) The drainage valve was opened while maintaining the high pore water pressure unchanged.
4) Triaxial compression stress was loaded with the drainage valve open.

The "drained" loading was employed in the 4th stage so that the state of high pore water pressure might be maintained. If the valve is closed, positive dilatancy under low effective stress reduces the pore pressure and increases the effective stress, thus departing away from the research aim of liquefaction. It should be recalled that the state of complete liquefaction, in which the effective stress was null, could not be achieved. This is because some extent of effective stress was necessary in a specimen for the sake of stable behavior of a tested specimen. Therefore, the second stage as described above reduced the effective stress to 5, 10, or 15 kN/m^2, and the measured data was extrapolated to the state of full liquefaction.

Tests were conducted on loose specimens of Yurakucho alluvial sand in Tokyo. Fig.132 illustrates time histories of deviator stress as well as deviator strain in a test in which a specimen of 30.6% relative density was consolidated under 100 kN/m^2, pore water pressure was raised to achieve the effective stress = 5 kN/m^2, and triaxial compression took place in a drained manner. It is seen in Fig.132 that the triaxial compression stress was loaded by stages with measurement of creep deformation between the stages. Note that the pore water pressure and the horizontal effective stress were kept constant during the triaxial compression, while the loading of deviator stress (axial stress) increased the mean effective stress, P'.

Fig.133 shows the stress-strain relationship obtained by assembling the data in the previous figure. It is therein seen that the deviator stress was loaded by stages, followed by the development of creep deformation. Note that the measured deviator stress was not composed fully of a rate-dependent component because the effective stress still greater than zero produced frictional behavior of sand. Therefore, what is called reference curve was drawn in this figure by connecting end points of creep at which the rate of strain was negligible. In other words, the reference curve stands for the frictional behavior of sand without strain-rate effects, and the difference between the measured and reference curves is the rate-dependent component.

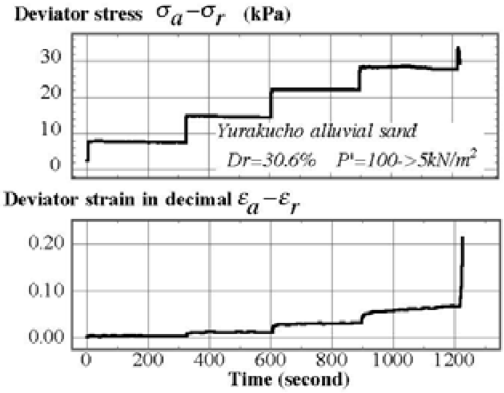

Figure 132. Time histories of deviatoric stress and strain in test on Yurakucho sand with relative density = 30.6% (Galage et al., 2005).

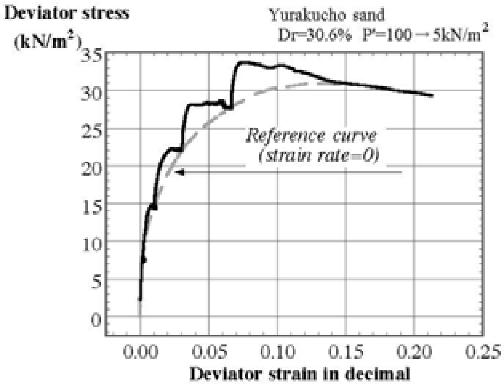

Figure 133. Stress-strain relationship of Yurakucho sand with relative density = 30.6% during stage loading of triaxial compression (Galage et al., 2005).

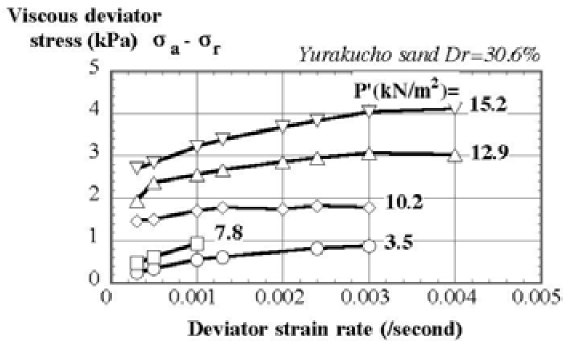

Figure 134. Rate dependent component of deviator stress in loose Yurakucho sand (Galage et al., 2005).

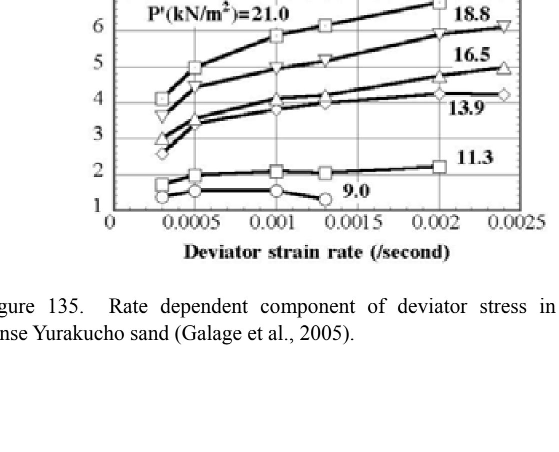

Figure 135. Rate dependent component of deviator stress in dense Yurakucho sand (Galage et al., 2005).

Figs. 134 and 135 demonstrate the rate-dependent stress components thus derived for both loose and dense Yurakucho sand. It is evident that the rate-dependent stress increases with the increase of strain rate as well as the increase of effective mean principal stress, P'. Since the rate-dependent stress and the strain rate are not linearly proportional to each other, although their relationship is nearly linear, it seems that Bingham modelling is more appropriate than Newtonian modelling (Fig.136). Since the research target was the behavior of sand at null effective stress (P'), a further investigation was conducted by triaxial extension which was able to attain a lower value of P'. A special test was performed further by using 1-mm grains of Styrofoam. Having the specific gravity of 1.04, this granular material can achieve very low effective stress without sample instability.

Fig.137 indicates the variation of Bingham properties with the change of effective stress. The viscosity coefficient was determined by

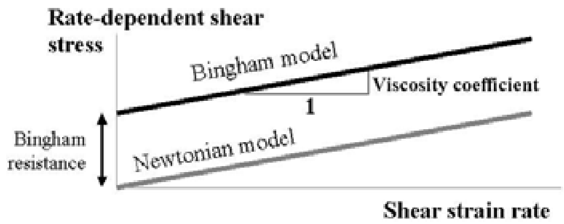

Figure 136. Bingham and Newtonian model of viscous material.

(a) Bingham viscosity coefficient

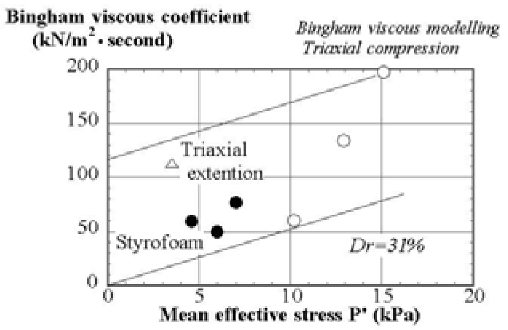

(b) Bingham strength

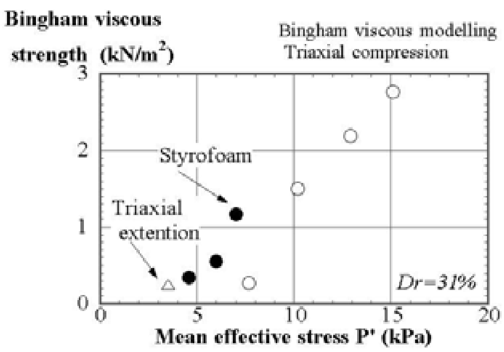

Figure 137. Variation of Bingham material properties with decrease of effective stress.

$$\text{Viscosity} = \frac{\Delta(\text{Rate dependent } \tau)}{\Delta(\text{Rate of strain } \gamma)}$$

$$= \frac{(\text{Rate dependent } \sigma_1 - \sigma_3)/2}{\text{Rate of } \varepsilon_1 - \varepsilon_3} \quad (14)$$

By extrapolating those data towards the state of zero effective stress, it can be stated that the viscosity coefficient lies in the range of less than 100 kN/m^2, while the Bingham strength vanishes. Thus, it seems that liquefied sand with zero effective stress behaves as a Newtonian viscous material.

(a) Bingham viscous coefficient.

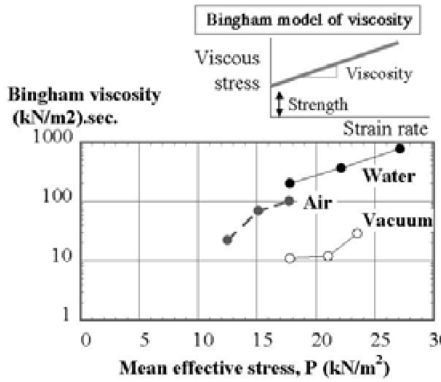

(b) Bingham viscous strength

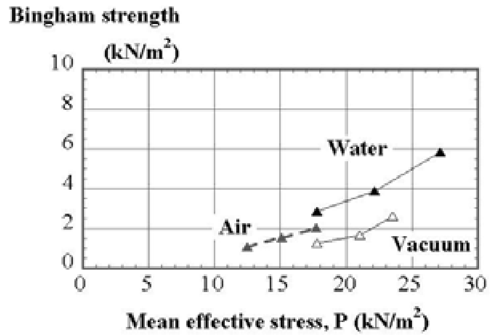

Figure 138. Effects of pore fluid on Bingham viscosity.

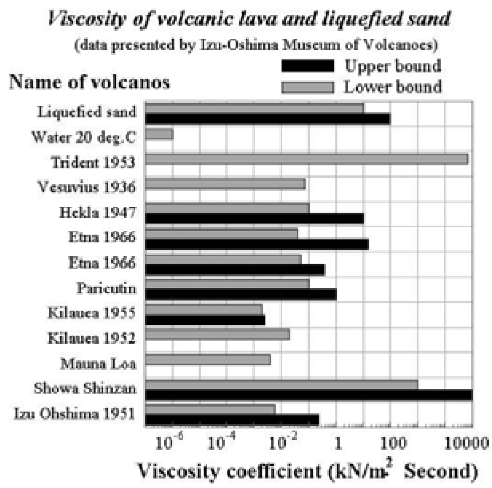

Figure 139. Viscosity of volcanic lava flow (Data by Izu-Oshima Museum of Volcanoes, Japan).

The idea of liquefied sand as a viscous liquid may be difficult to understand conceptually, although experimental findings suggest so. This difficulty mainly comes from the knowledge that liquefied sand consists of rigid grains and water none of which is significantly viscous. To have more insight into the physical back ground of this problem, additional tests were conducted by replacing the pore fluid from water to air and even vacuum. Similar stress history was employed in new tests as in previous ones except that the effective isotropic stress was unloaded prior to shear from 100 kN/m^2 to 10 kN/m^2 in place of 5 kN/m^2 for the stability of some samples. Fig.138 illustrates the variation of Bingham properties with the effective stress. It may be found that the extent of viscosity decreases as the pore fluid changes from water to air and vacuum. This suggests that the effects of viscosity of pore fluid play a very important role in the observed rate-dependent behavior, and this is particularly true of the Bingham viscous coefficient in Fig. 138(a). Most probably, vortex flow of pore fluid upon migration of grains is the source of viscosity. There remains, however, some extent of viscosity even in a vacuum specimen, possibly because some part of observed viscosity stems from interaction between grains. Since intergranular friction is not of rate-dependent nature, the present study supposes that grain-to-gain collision is responsible for this rate-dependency. Same idea has been practiced in studies of debris flow (Egashira and Miyamoto, 2000).

The magnitude of Bingham viscosity coefficient so far observed is of the order of 10 kN/m^2. This is remarkably greater than that of other fluid; for example, viscosity of water at 20 degrees C is 10^{-6} kN/m^2 • second. Volcanology has measured the viscosity of lava flow upon many eruptions in the past. The obtained viscosity ranges from the order of 0.001 to 1000 kN/m^2 • second, depending on the nature of lava (Fig.139). Since some kinds of lava flowed hundreds of meters to kilometers, while the displacement of liquefied sand is merely a few meters at maximum, the greater value of viscosity for liquefied sand is not strange.

11 CALCULATION OF LIQUEFACTION-INDUCED DISPLACEMENT OF GROUND

The assessment of residual displacement caused by subsoil liquefaction plays a very important role in seismic performance design of geotechnical structures. This is particularly true when the design earthquake is rare and strong and also when the situation does not allow soil improvement. The latter is the case with a river dike which is very long but the construction budget is limited. Embedded lifelines have a similar situation for which the land is scarcely owned by the lifeline industries.

It is widely believed that liquefaction-induced displacement can be calculated only by using a sophisticated computer codes together with nonlinear constitutive models. Needed soil data can be obtained by undrained soil sampling and laboratory consolidation as well as (cyclic) shear tests. Those sophisticated approaches were reviewed early in 1994 by VELACS Project (Arulanandan and Scott, 1993).

It should be recalled that most of the practice in hazard assessment of liquefaction can afford costs for only penetration tests. The obtained data is only penetration resistance and basic physical properties such as gradation and Atterberg limits. By using them together with a specified design earthquake, the thickness of liquefiable soil layer and the extent of liquefaction (factor of safety) have been determined. It seems that most of the ordinary projects cannot afford higher costs for advanced soil investigations. Thus, it has been desired to develop economical tools which can assess liquefaction-induced displacement with only currently-available soil data. Although the nonlinear dynamic finite element (FE) analysis based on effective stress principles is a powerful tool, the required cost is substantial. Note, further, that geometric nonlinearity should be taken into account even by a simplified approach as shown by the importance of gravity-buoyancy equilibrium in subsidence of structures (Fig.58).

The aforementioned finite element code by Yasuda et al. (1992) (see Fig.128) seems to satisfy this requirement, while the author has been attempting to develop a simpler method. The relationship between the simple method and sophisticated FE methods is similar to the one between slope stability analysis based on a circular slip surface and a nonlinear FE method. Since the author's numerical formulation is simple, a three-dimensional dynamic analysis with consideration on geometric nonlinearity is possible within reasonable computation time (Orense and Towhata, 1998; Kobayashi and Towhata, 2004).

The essence of the author's method is going to be introduced briefly in this text. Although detailed information is available in Towhata et al. (1992 and 1999b), it may be said that the method is characterized by the following points.

- It idealizes liquefied sand as Bingham or Newtonian viscous liquid as will be shown experimentally later.
- It relies on differential equation which describes the liquefaction-induced displacement and can be solved analytically.
- It takes into the importance of large displacement which changes the magnitude of buoyancy force (Fig.58) and force equilibrium after some displacement.
- Many efforts were made to make the method as simple as possible; these efforts were supported by experimental findings in model and shear tests.

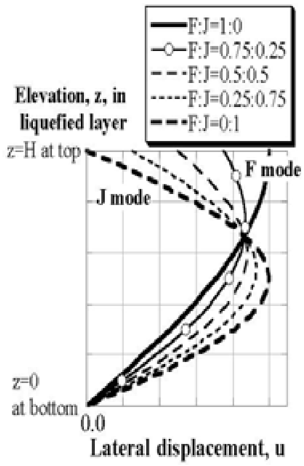

Figure 140. Modes of lateral displacement as observed in shaking model tests.

While FE method employs nodal displacements as unknown variables, which are many in number, the author's method uses the magnitude of two typical displacement modes as the unknown. Fig.140 illustrates the variation of lateral displacement, u, in the vertical direction within a liquefied layer. In this figure, what is called "F" mode is one quarter of a sinusoidal function (angle ranging from 0 to 90 degrees), while "J" mode stands for one half of it (from 0 to 180 degrees). The F mode is predominant in lateral flow of slope model (Fig.67), while the J mode occurs in subsidence of an embankment, for example (Fig.99). The F mode was similarly observed in centrifuge tests by Taboada and Dobry (1998). It seems that a variety of combination of F and J as illustrated in Fig.140 occurs in reality. Thus, the present analysis employs the magnitude of each mode as the unknown variable. Certainly, the magnitude changes with time. Conceptually, Lateral displacement u(t) = F(t) + J(t) (15)

where t designates time. The number of unknowns and the amount of computation are drastically reduced by using modes in place of displacement at nodal points. Note that the thickness of liquefiable soil is determined separately in advance by using SPT or CPT data or others as is practiced everywhere.

The vertical displacement, v, is obtained further by assuming a constant volume (undrained) condition to liquefied soil;

$$\frac{\partial u}{\partial x}+\frac{\partial v}{\partial z}=0 \tag{16}$$

where x and z stand for horizontal and vertical coordinates, respectively. Hence, consolidation settlement is dealt with separately. When there is an unsaturated and unliquefiable soil crust at the ground surface, this part moves together with the liquefied subsoil (Fig.59) and behaves as an elastic horizontal column under compression, while no resistance occurs therein under tension. Thus, all the components of displacement are expressed by the magnitude of F and J.

The theory of Lagrangian equation of motion makes it possible to derive the equation of motion of ground flow in terms of F and J. Conceptually, the kinetic energy, K, of ground, composed of liquefied subsoil and surface crust, is expressed by the time derivatives of F and J, while the potential energy, Q, due to weight of the whole ground and strain in the surface crust is a function of F and J. Moreover, when liquefied subsoil is considered as a viscous liquid, as studied in the previous chapter, the strain energy is negligible, while the energy dissipation per unit time, D, is a function of time derivatives of F and J. Hence, the Lagrangian equations of motion are given as

$$\begin{aligned}
&\frac{d}{dt}\left\{\frac{\partial(K-Q)}{\partial\left(\frac{\partial F}{\partial t}\right)}\right\}-\frac{\partial(K-Q)}{\partial F}=-\frac{\partial D}{2\partial\left(\frac{\partial F}{\partial t}\right)}\\
&\frac{d}{dt}\left\{\frac{\partial(K-Q)}{\partial\left(\frac{\partial J}{\partial t}\right)}\right\}-\frac{\partial(K-Q)}{\partial J}=-\frac{\partial D}{2\partial\left(\frac{\partial J}{\partial t}\right)}
\end{aligned} \tag{17}$$

The principle of this derivation is identical with what is employed in the energy approach to FE dynamic analysis. Since "Q" includes strain energy, it is possible to take into account the mitigative effects of sheet pile and compacted sand walls in which the strain energy increases with distortion.

Eq.17 is integrated with time over the duration of strong shaking and, at the end of strong shaking, the displacement makes the final stop as shown by model tests (Figs. 83 and 105). The temporary idea of "strong shaking" is the acceleration of not less than 50 Gal. This magnitude of acceleration is the one which is needed to maintain the state of flow deformation and was chosen tentatively as the mean between zero and 100 Gal. The value of 100 Gal stands for an empirical idea of the threshold acceleration which triggers liquefaction in loose sand. Moreover, the flow is assumed to start at the time of the maximum acceleration at which the thickness of liquefied soil is finally determined. This idea gives several tens of seconds for the ground movement to occur. For an example, see Fig.141 on 1964 Niigata earthquake record at the Kawagishi-Cho liquefaction site. Fig.142 is a summary of available earthquake motion records in which the duration of time between the peak acceleration and the end of strong (>50 Gal) is plotted against the seismic magnitude. Detailed studies on duration of strong motion were performed by Gutenberg and Richter (1956); Housner (1965), Newmark and Rosenblueth (1971), Lee and Chan (1972), Kawashima et al. (1985); Bommer and Martinez (1999), and Wang et al. (2002) among others.

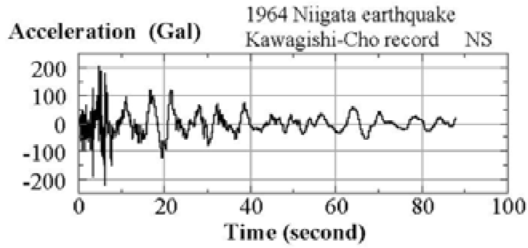

Figure 141. Long duration of Kawagishi-Cho record in 1964 Niigata earthquake (data by Kudo et al., 2000).

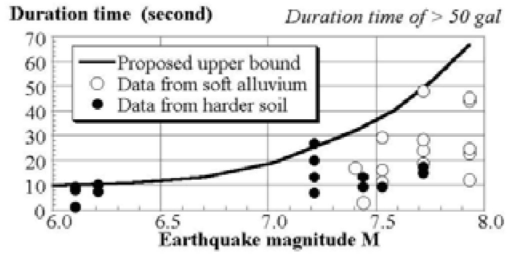

Figure 142. Elapsed time between maximum acceleration and end of strong acceleration (>50Gal) (Okada et al., 1999).

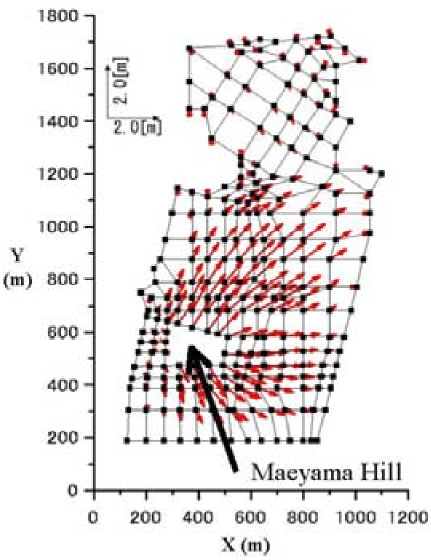

Figure 143. Three dimensional dynamic analysis on flow displacement of liquefied slope around Maeyama Hill in Noshiro during 1983 Nihonkai-Chubu earthquake.

The proposed method of displacement analysis has been applied to many situations. For example, Fig.143 illustrates the lateral displacement around a small Maeyama Hill in Noshiro City during the 1983 Nihonkai-Chubu earthquake in Japan; see Fig.53 for the observed displacement. The magnitude and direction of displacement are consistent between calculation and observation. The calculated displacement could be put in a deformation analysis on embedded pipelines for stress analysis. Secondly, Fig.144 indicates the displacement around the north half of Kobe Port Island where the maximum lateral displacement exceeded 5 meters (Inagaki et al., 1996). Detailed displacement distribution behind a quay wall was calculated as shown in Fig.145.

The lateral displacement of a quay wall is a significant problem not only to the operation of harbors but also to facilities in the backfill area (Fig.19). This is because the liquefied backfill soil translates laterally together with the unstable quay wall. Examples of potentially vulnerable structures are pile foundation as well as embedded lifelines. In this respect, it is important to assess the range of affected area during an earthquake. The present study considers that the quay wall displacement triggers the propagation of displacement into level backfill land. The rate of propagation, V_f, was obtained by analytical studies done by Towhata et al. (1999)

$$V_f=\sqrt{\frac{2g\left(ET+\frac{4\gamma H^2}{\pi^2}\right)}{\gamma H+2P}} \tag{18}$$

in which g stands for the gravity acceleration, E the elastic modulus of surface unliquefied crust, T the crust thickness, γ the unit weight of liquefied sand, H the thickness of liquefied sandy layer, and P the overburden pressure due to the crust. When the backfill soil is subject to tension, as is the case of quay wall backfill, $E=0$ is reasonable. An example calculation of this equation with γ=20kN/m^3, H=10m, T=1m, P=16kN/m^2, and E=0 gives V_f=8.3m/sec.

Figure 145 presents two kinds of calculation of temporal development of subsidence in the backfill area. The first kind of calculation is by means of Eq.18, and the second one by the numerical method as shown by Eq.17. It is found in this figure that the range of significant subsidence obtained by the numerical method is in good agreement with the simple calculation by Eq.18. Moreover, the calculation was made of past case histories in which the range of affected backfill area is available in literature (Yasuda et al., 1997). The wave propagation was assumed to continue between the time of the peak acceleration and the time at which the acceleration magnitude becomes less than 50 Gal. The results are shown in Fig.146 in which the calculation by Eq.18 and case histories are consistent.

At the end of this chapter, the results of centrifuge and 1G model tests on mitigation of ground displacement are reproduced by the proposed method of calculation. Two kinds of centrifugal tests on subsidence of embankment and lateral displacement of gravity quay wall together with 1G tests on floating of embedded structure are investigated. Fig.147 illustrates a 30G model of an embankment which rests on a liquefiable sandy deposit. This sandy deposit was made of alluvial sand with fines which liquefied in Yonago of Japan during an earthquake in 2000. The void ratio of the completed model was 1.053. Since the fines content of 93% in this sand drastically reduced the permeability of this soil to 6.84*10^{-7} m/sec., which is significantly low as compared with that of ordinary alluvial sand, no further effort was made to reduce the permeability from the viewpoint of similitude. Hence, distilled de-aired water was employed as the pore fluid. The ground water table was situated at the surface of this deposit. In contrast, the model embankment was made of coarse lead shots which was free of meniscus action and, hence, did not absorb ground water. The bottom of the embankment had pieces of metal nets which prevented lead shots from sinking into liquefied subsoil. The measured "subsidence" in this study stands for the one at the bottom of the embankment. Harmonic shaking occurred in the longitudinal direction with the amplitude of 15 G (model scale), the frequency of 50 Hz, and the duration of 0.15 seconds (model scale). According to the measured pore water pressure records, liquefaction was achieved in the top 70 mm of the liquefiable sandy deposit.

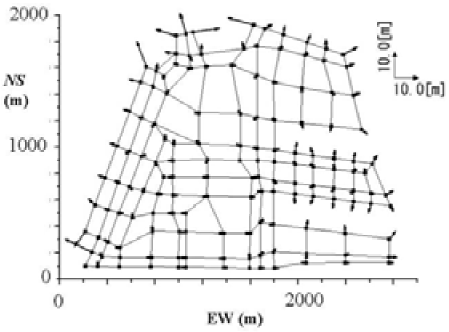

Figure 144. Three dimensional dynamic analysis on lateral displacement of quay walls around Kobe Port Island during 1995 Kobe earthquake.

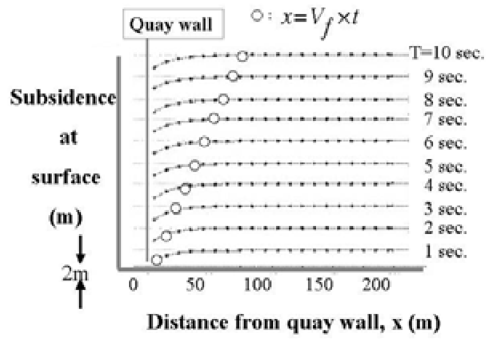

Figure 145. Example calculation on range of backfill which is affected by quay wall.

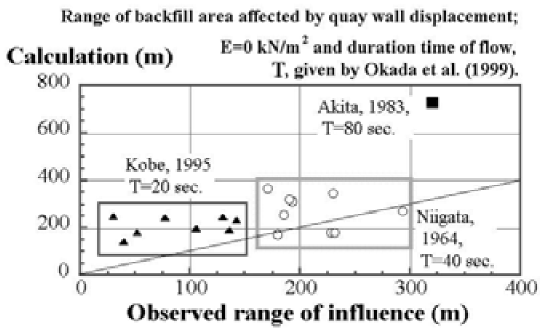

Figure 146. Range of backfill affected by past earthquakes and simple calculation.

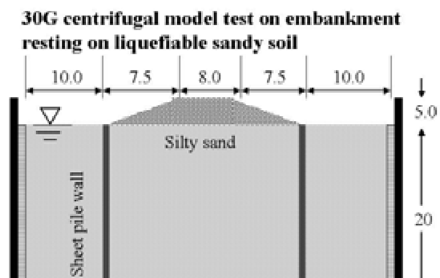

Figure 147. Model of embankment in 50G centrifuge test.

The aim of the first analysis on the model in Fig.147 is the determination of appropriate viscosity coefficient of liquefied subsoil which gives good agreement between calculated and observed subsidence. By comparing calculated and observed subsidence in Fig.148, it can be stated that the viscosity coefficient of around 30 (kN/m^2).sec is the most appropriate value. Note that this value is consistent with the findings in laboratory tests in Fig. 137(a).

The next stage of analysis on embankment was performed on the mitigative effects of sheet pile walls which were installed below the bottom of the slope of the embankment (Fig.147). By using the same viscosity and thickness of liquefied subsoil, Fig.149 was obtained. The calculated extent of mitigation is much more significant than observation. This is probably because the calculation assumed a fixed bottom boundary condition that no rotation occurs in sheet piles at the interface between liquefied and unliquefied layers, while the real sheet piles penetrated into unliquefied but soft silty subsoil which allowed translation and rotation to some extents. Thus, the tested sheet piles were able to deform more than assumed in the calculation, leading to more subsidence of the embankment.

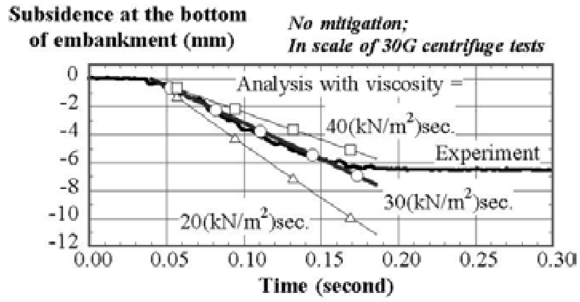

Figure 148. Calculated and observed subsidence of embankment resting on liquefied ground.

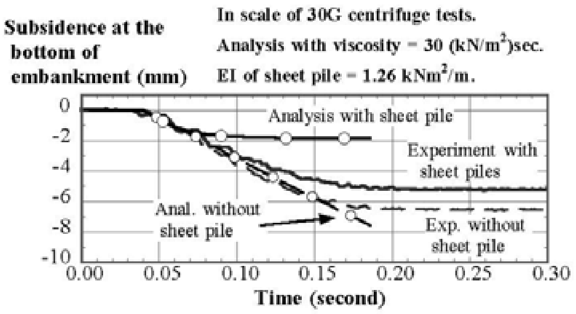

Figure 149. Calculation on mitigative effects of sheet pile walls on subsidence of embankment resting on liquefiable subsoil.

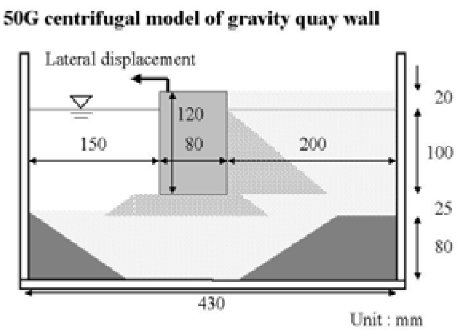

Figure 150. Numerical analysis on lateral displacement of gravity quay wall which was tested in 50G centrifugal field.

The second series of analysis was conducted on 50 G model tests on lateral displacement of gravity quay wall (Fig.150). Both backfill and foundation were made of loose Toyoura Sand with the relative density of 40 % so that these parts would liquefy upon shaking. Shaking occurred in the longitudinal direction with amplitude of 20G (model scale) and 100 Hz for 0.3 seconds (model scale). Calculations with a family of viscosity coefficient (Fig.151) exhibits that 10 (kN/m^2).sec gives the best agreement between calculated and observed translation of the quay wall. Again, this value is consistent with the aforementioned laboratory tests (Fig. 137(a)).

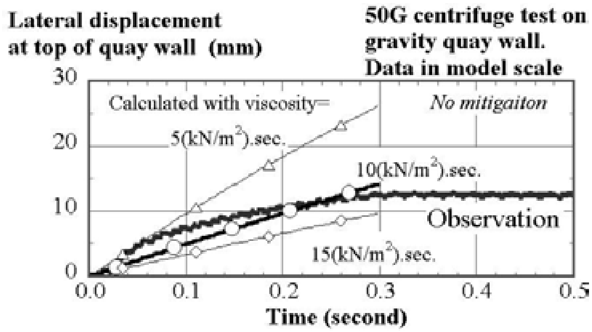

Figure 151. Calculated and observed histories of lateral displacement in model of gravity quay wall.

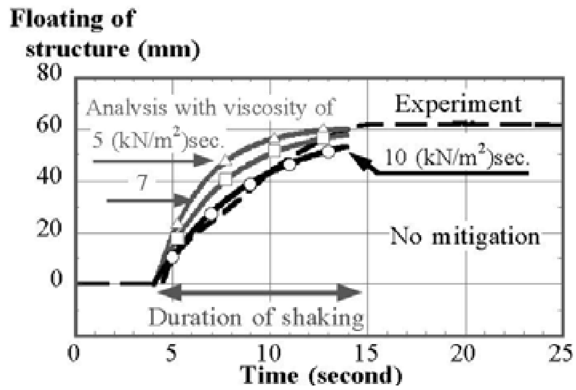

Figure 152. Prediction of floating of embedded structure.

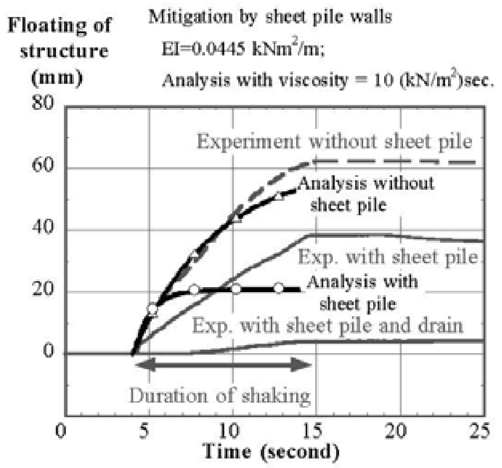

Figure 153. Prediction of mitigative effects of sheet pile walls on floating of embedded structure.

The third analysis was made of floating of embedded structures with and without sheet pile installation. Fig.152 compares the calculated time histories with different viscosity coefficients with the observed floating in a 1G model test (Fig.118). Among the assumed viscosity values, 10(kN/m^2)sec. seems to give the best matching with observation. This optimum value of viscosity is consistent with the experimental value in Fig.137(a), although it is smaller than other optimum values in centrifugal tests due possibly to the reduced consolidation pressure in 1G tests. By using this particular value of viscosity, Fig.153 compares the mitigative effects obtained by model tests and analyses. Although there is still difference, the analysis on mitigation is not much different from the experiments.

12 FUTURE TOPIC

The conventional approach of geotechnical earthquake engineering which has been taken in the past decades concerns seismic behavior of specified individual structures. For example, one particular embankment is studied from the viewpoint of seismic behavior and, in case that a significant damage is expected, a seismic retrofitting is practiced. The recent earthquake in Niigata-Chuetsu in 2004, however, revealed that different approach is needed.

Fig. 154 shows a situation of damaged road embankment in a mountainous village in the epicentral area. Although the village had a good road network prior to the quake, it was destroyed at many places by collapse of embankment as well as failure of nearby mountain slopes. Consequently, the local transportation was abandoned, evacuation by land transportation became impossible, and the whole inhabitants were forced to leave the village. The problems encountered may be summarized as what follows;

- The soft tertiary geological setting made slope failure to occur at many places leading to blockage of land transportation.
- Embankment resting upon small valley deposits collapsed easily upon strong shaking.
- Although efforts are needed to protect transportation from natural hazards, it is financially difficult to improve the seismic toughness of the road everywhere in the village.

Figure 154. Destroyed road embankment in Yamakoshi Village in Niigata-Chuetsu, 2004.

The present discussion focuses its attention on local transportation. In order to improve the post-earthquake situation in local communities with a limited budget, the following actions are recommended.

- Trunk roads should be selected and more budget should be allocated to them for their seismic retrofitting. The aim of the retrofitting is that all the communities in the concerned area should have an appropriate approach to at least one road after a strong earthquake.
- Selection of trunk roads should take into account the idea of network that the probability of seismic collapse of two routes in a single event is much less than that of one route.
- The said probability should be assessed by detailed prediction on intensity of future earthquakes as well as geotechnical assessment of seismic behavior of earth structures.
- In addition to retrofitting, quick restoration of induced damage is another good measure to reduce the probability of transportation blockage. Therefore, provision for this, inclusive of materials, budget, and human resources, is encouraged.
- To promote involvement of local inhabitants, education on risk of future earthquake as well as idea of quick restoration should be practiced.
- To further assist the post-earthquake restoration, an emergency information network should be constructed so that people and local government can share information on damage extent and its distribution. It is desired that this network has sensors to monitor displacement of embankment and slopes along trunk roads. An example of such a network has already been in operation in other field of geotechnical earthquake engineering (Shimizu et al., 2005).

13 CONCLUDING REMARKS

The present text described recent developments of geotechnical earthquake engineering with due reference to those in early days, paying attention to situation in other kinds of disaster mitigation technologies. With special attention paid to liquefaction problems, the following conclusions are drawn.

1) The essence of liquefaction-induced damage lies in the unallowable magnitude of residual displacement.
2) For the performance-based principle of seismic design in the field of geotechnical engineering, a methodology to determine the allowable displacement was proposed, in which the allowable time of restoration is decided first, followed by the allowable displacement.
3) Recent engineering concern is focused on seismic retrofitting of existing structures.
4) Several attempts were addressed for mitigation of liquefaction-induced deformation of geotechnical structures.
5) To facilitate the prediction of liquefacit0on-induced displacement with and without mitigative measures, laboratory tests were conducted on deformation characteristics of sand under low effective stress near liquefaction.
6) Test results shows that sand under low effective stress behaves like Bingham viscous liquid, and, in the extreme case of null effective stress and liquefaction, it behaves like Newtonian viscous liquid.
7) Simple but still mathematically rigorous method of deformation analysis was developed which idealizes liquefied sand as Bingham or Newtonian viscous liquid. This method of analysis is equivalent with a large-deformation formulation of nonlinear dynamic analysis in the time domain.
8) During development of this method of analysis, a special care was taken so that it would work with data which is easily available in ordinary liquefaction studies.
9) The proposed method of analysis was used to replicate the observed deformation in real earthquake events as well as laboratory model tests in centrifugal and 1G fields.

ACKNOWLEDGMENT

It is the author’s pleasure to express his sincere thanks to people and institutions which made invaluable contributions to the development of the studies that are introduced in this report.

Most laboratory tests and numerical studies were conducted by former and present students and visiting researchers at the geotechnical engineering laboratory, the University of Tokyo. Among many of them, the author would mention the names of Mr. K. Sugo, Dr. R. Verdugo, Dr. W. Vargas-Monge, Dr. R. Orense, Dr. M. Yoshimine. Mr. K. Yamada, Dr. Y. Tamari, Dr. H. Toyota, Dr. T. Uchimura, Mr. Y. Kogai, Mr. K. Amimoto, Mr. J. Kohchi, Mr. T. Maeda, Mr. K. Watanabe, Dr. A. Ghalandarzadeh, Dr. T. Mizutani, Mr. N. Shinkawa, Mr. T. Nasu, Mr. Y. Kabashima, Mr. S. Imamura, Dr. J. Meneses, Mr. K. Horie, Mr. A. Shimokawa, Mr. H. Matsumoto, Mr. H. Isoda, Dr. Y. Kobayashi, Mr. S. Kokeguchi, Mr. N. Nakai, Mr. H. Ishida, Dr. H. Shahnazari, Dr. M. Mohajeri, Mr. S. Nishimura, Mr. C. Galage, Mr. T. Honda, Dr. V. Sesov, Mr. Alam Jahangir, and Mr. H. Sato. Important information was supplied on testing method by Prof. T. Iwadate of Tokyo Metropolitan University. Discussion on analytical methods with Dr. N. Yoshida of OYO Corporation has always been fruitful. The study on paleoliquefaction was first introduced to the author by Prof. S. Mori of Ehime University. Collaborations with external institutes were extremely productive. Those institutions are the Public Works Research Institute as well as Prof. Y. Sasaki and Dr. K. Tokida, the Association for the Development of Earthquake Prediction with Mr. J. Ikeda, Dr. K. Harada of the Fudo Construction Company, Mr. Y. Ohno of the Toa Corporation, Mr. N. Harada of the Zenitaka Corporation, and Dr. S. Tamate of the National Institute of Industrial Safety. Moreover, the technical committee 4 of the International Society of Soil Mechanics and Geotechnical Engineering under the chairmanship of Prof. W.D.L. Finn has encouraged the author to study the basic principle of performance-based seismic design for earth structures.

Financial supports given by the Ministry of Education, Culture, Sports, Science and Technology and the Japan Iron and Steel Federation are deeply appreciated. The interview study on allowable displacement was made possible by the enthusiastic contribution by Dr. S. Yasuda of Tokyo Denki University, Dr. A. Tateishi of Taisei Corporation and many members of a research subcommittee of the Earthquake Engineering Research Committee, Japan Society of Civil Engineers. Important information of lateral displacement was supplied by the Noshiro Municipal government. Earthquake motion records during the 1995 Kobe earthquake were obtained and supplied by the Committee of Earthquake Observation and Research in the Kansai Area as well as the Development Bureau of Kobe City Government. Detailed study on seismic behavior of earth fills made by Prof. J. Koseki, the University of Tokyo, and Dr. M. Tateyama of Railway Technical Research Institute is respected. Last but not least, the author always relies on French translation of this text by Mr. S. Ronteix. The author expresses his sincere thanks to those assistances and supports supplied to him over many decades.

REFERENCES

Alam, M.J., Towhata, I., Honda,T., and Fukui, S. (2004a) Mechanism of liquefaction process under embankment without and with a mitigation measure studied by dynamic centrifuge testing, Proc. South East Asian Geotechnical Conference, Bangkok, 905-910.

Alam, M.J., Fukui, S., Towhata, I., Honda, T., Tamate, S., Tanaka, T., Uchiyama, J., and Yasuda, A. (2004b) Centrifuge model tests on mitigation effects of underground walls on liquefaction-induced subsidence of embankment, Proc. 11th Int. Conf Soil Dynamics and Earthquake Engineering and the 3rd Int. Conf. Earthquake Geotechnical Engineering, Berkeley, Vol.2, 537-544.

Alam, M.J., Honda, T., Towhata, T., Tamate, S., Fukui, S., Yasuda, S., and Tanaka, T. (2004c) Behavior of liquefaction mitigative measures of foundation soil under earth embankment, Proc. IS-Osaka, Engineering Practice and Performance of Soft Deposits, 343-348.

Amick, P. and Gelinas, R. (1991) The search for evidence for large prehistoric earthquakes along the Atlantic Seaboard, Science, Vol.251, 655-658.

Arulanandan, K. and Scott, R.F. (1993) Verification of numerical procedures for the analysis of soil liquefaction problems, Publ. Balkema,

Berrill, J.B., Christensen, S.A., Keenan, R.P., Okada, W., and Pettinga, J.R. (2001) Case study of lateral spreading forces on a piled foundation, Geotechnique, Vol.51, No.6, 501-517.

Bishop, A.W., Green, G.E., Garga, V.K., Andresen, A., and Brown, J.D. (1971) A new ring shear apparatus and its application to the measurement of residual strength, Geotechnique, Vol.21, No.4, 273-328.

Bommer, J.J. and Martinez-Pereira, A. (1999) The effective duration of earthquake strong motion, Journal of Earthquake Engineering, Vol.3, No.2, 127-172.

Castro, G., Seed, R.B., Keller, T.O. and Seed, H.B. (1992) Steady-state strength analysis of Lower San Fernando Dam slide, Journal of Geotechnical Engineering, ASCE, Vol.118, No.3, 406-427.

Clague, J.J., Naesgaard, E., and Sy, A. (1992) Liquefaction features on the Fraser delta: evidence for prehistoric earthquake, Canadian Geotechnical Journal, Vol.29, 1734-1745.

Clague, J.J., Naesgaard, E., and Nelson, A.R. (1997) Age and significance of earthquake-induced liquefaction near Vancouver, British Columbia, Canada, Canadian Geotechnical Journal, Vol.34, 53-62.

Egashira, S. and Miyamoto, K. (2000) Mechanism of debris flow Monthly Magazine of Japanese Geotechnical Society, Vol.48, No.8, 46-52 (in Japanese).

Fiegel, G.L., and Kutter, B.L. (1994) Liquefaction-induced lateral spreading of mildly sloping ground, Journal of Geotechnical Engineering ASCE, Vol.120, No.12, 2236-2243.

Florin, V.A., and Ivanov, P.L. (1961) Liquefaction of saturated sandy soils, Proc. 5th ICSMFE, Vol.1, 107-111.

Galage, Chaminda, P.K., Towhata, I., and Nishimura, S. (2005) Laboratory investigation on rate-dependent properties of sand undergoing low confining effective stress, accepted by Soils and Foundations.

Gallagher, P.M. and Mitchell, J.K. (2002) Influence of colloidal silica grout on liquefaction potential and cyclic undrained behavior of loose sand, Soil Dynamics and Earthquake Engineering, Vol.22, 1017-1026.

Ghalandarzadeh, A., Orita, T., Towhata, I., and Fang, Y. (1998) Shaking table tests on seismic deformation of gravity quay walls, Soils and Foundations, Special Issue on Geotechnical Aspects of the January 17 1995 Hyogoken-Nambu Earthquake, No.2, Soils and Foundations, 115-132.

Gutenberg, B. and Richter, C.F. (1956) Earthquake magnitude, intensity, energy and acceleration (second paper), Bull. Seism. Soc. Amer., Vol.46, No.2, 105-146.

Hamada, M., Yasuda, S., Isoyama, R., and Emoto, K. (1986a) Generation of Permanent ground displacements Induced by soil liquefaction Proc. JSCE, No.376/III-6, 211-220 (in Japanese).

Hamada, M., Yasuda, S., Isoyama, R., and Emoto, K. (1986b) Study on liquefaction-induced permanent ground displacements and earthquake damage, Proc. JSCE, No.376/III-6, 221-229 (in Japanese).

Hamada, M., Oono, M., Kitamura, K., and Komatsu, H. (1998) Lateral force exerted on pile by lateral flow of liquefied sand – effect of surface unliquefied crust, Annual Conference of JSCE, Vol.1 (in Japanese).

Hayashi, K., Zen, K., Yamazaki, H., and Hayashi, N. (2001) A large soil stratum test on the permeability and the improved strength of new solution type chemical grout, Proc. JSCE, No.694/III-57, 221-228 (in Japanese).

Horie, Y. (2002) Study on behavior of soil subjected to cyclic loading by simple shear test and site investigation, Master thesis, Univ. Tokyo.

Housner, G.W. (1965) Intensity of earthquake ground shaking near the causative fault, Proc. 3rd WCEE, Vol.III, 94-115.

Hwang, J.H., Yang, C.W., and Chen, C.H. (2003) Investigation on soil liquefaction during the Chi-Chi earthquake, Soils and foundations, Vol.43, No.6, 107-123.

Inagaki, H., Iai, S., Sugano, T., Yamazaki, H., and Inatomi, T. (1996) Performance of caisson type quay walls at Kobe Port, Soils and Foundations, Special Issue on Geotechnical Aspects of the January 17 1995 Hyogoken-Nambu Earthquake, 1, 119-136.

Ishihara, K. and Yamazaki, F. (1980) Cyclic Simple Shear Tests on Saturated Sand in Multi-Directional Loading, Soils and Foundations, Vol.20, No.1, 45-59.

Ishihara, K. (1993) Liquefaction and flow failure during earthquakes,

Geotechnique, Vol.43, No.3, 351-415.
Isoda, S., Nakai, N., Orense, R., and Towhata, I. (2001) Mitigation of liquefaction-induced uplift of underground structure by using sheet pile wall, Proc. Soil Improvement Conference, Singapore, 70-77.
Japan Society of Civil Engineers (2000) Report of Technical Subcommittee on Earthquake Resistant Design of Geotechnical Structures subjected to Strong Seismic Motion, Earthquake Engineering Research Committee, Subcommittee Report (in Japanese).
Japanese Geotechnical Society (2004) Photographs of Niigata Earthquake, CD ROM publication.
Japan Road Association (2002) Specifications for Highway Bridges, Part V.
Kabashima, Y. and Towhata, I. (2000) Improvement of dynamic strength of sand by means of infiltration grouting, Proc. 3rd International Conference on Ground Improvement Techniques -2000, Singapore, 203-208.
Kammerer, A.M., Seed, R.B., Wu, J., Riemer, M.F. and Pestana, J.M. (2004) Pore pressure development in liquefiable soils under bi-directional loading conditions, Proc. 11th Int. Conf. Soil Dynamics and Earthquake Engineering and the 3rd Int. Conf. Earthquake Geotechnical Engineering, Berkeley, Ed. T. Nogami and R.B. Seed, Vol.2, 697-704.
Kawashima, K., Aizawa, K., and Takahashi, K. (1985) Duration of strong motion acceleration records, Structural Engg. and Earthquake Engg., JSCE, Vol.2, No.2, 161-168.
Kawasumi, H., Morimoto, R., Umemura, H., Okamoto, S., and Kubo, K. (1968) General Report on the Niigata earthquake of 1964, Publ. Tokyo Electrical Engineering College Press, Plate 22.
Kimura, T., Takemura, J., Hiro-oka, A., Okamura, M., and Matsuda, T. (1997) Countermeasures against liquefaction of sand deposits with structures, Proc. First Int. Conf. Earthquake Geotechnical Engineering (IS Tokyo 95), Vol.3, publ. Balkema, 1203-1224.
Kobayashi, Y. and Towhata, I. (2004) Three-dimensional analysis on subsidence of shallow foundation resting on liquefied ground, 13th World Conference on Earthquake Engineering, Vancouver, Paper Number 1232.
Kogai, Y., Towhata, I., Amimoto, K., and Hendri Gusti Putra (2000) Use of embedded walls for mitigation of liquefaction-induced displacement in slopes and embankments, Soils and Foundations, Vol.40, No.4, 75-93.
Koizumi, Y. (1966) Changes in Density of sand subsoil caused by the Niigata earthquake, Soils and Foundations, Vol.6, No.2, 38-44.
Kokeguchi, K., Shimokawa, A., Kohchi, J., and Towhata, I. (2001a) Post liquefaction torsion shear tests on sand with various strain rates, Proc. 4th Int. Conf. Recent Advances in Geotechnical Earthquake Engineering and Soil Dynamics, 2001, San Diego, Paper Number 1.16.
Kokeguchi, K., Shimokawa, A., Kohchi, J., Towhata, I., and Yoshikawa, A. (2001b) Experimental study on strain-rate dependency in post-liquefaction behaviour of sand, Proc. JSCE, No.680/III-55, 97-107 (in Japanese).
Kokusho, T. (1999) Water film in liquefied sand and its effect on lateral spread, Journal of Geotechnical and Geoenvironmental Engineering, ASCE, Vol.125, No.10, 817-826.
Kokusho, T. and Fujita, K. (2002) Site investigation for involvement of water films in lateral flow in liquefied ground, Journal of Geotechnical and Geoenvironmental Engineering, ASCE, Vol.128, No.11, 917-925.
Koseki, J., Tatsuoka, F., Munaf, Y., Tateyama, M., and Kojima, K. (1998) A modified procedure to evaluate active earth pressure at high seismic loads, Soils and Foundations, Special Issue on Geotechnical Aspects of the January 17 1995 Hyogoken-Nambu Earthquake, No.2, Soils and Foundations, 209-216.
Kramer, S.L. and Seed, H.B. (1988) Initiation of soil liquefaction under static loading conditions, Journal of Geotechnical Engineering, ASCE, Vol.114, No.4, 412-430.
Kramer, S.L. and Paulsen, S. (2004) The prediction of reinforced slope performance during earthquakes, Proc. 11th Int. Conf. Soil Dynamics and Earthquake Engineering and the 3rd Int. Conf. Earthquake Geotechnical Engineering, Berkeley, Ed. T. Nogami and R.B. Seed, Vol.2, 275-282.
Kudo, K., Uetake, T., and Kanno, T. (2000) Re-evaluation of nonlinear site response during the 1964 Niigata earthquake using strong motion records at Kawagishi-cho, Niigata city, Proc.12th WCEE, Paper number=0969, Auckland.
Lamb, H. (1911) On the uniform motion of a sphere through a viscous fluid, Philosophical Magazine and Journal of Science, Vol.21, No.121, 112-121.
Lee, K.L. and Chan, K. (1972) Number of equivalent significant cycles in strong motion earthquakes, Proc. Int. Conf. Microzonation for Safer Construction Research and Application, 609-627.
Lee, K.L. (1974) Seismic permanent deformations in earth dams, Report to NSF, Project GI38521.
Makdisi, F.T. and Seed, H.B. (1978) Simplified procedure for estimating dam and embankment earthquake-induced Deformations, Proc. ASCE, Vol.104, GT7, 849-867.
Malvick, E.J., Kutter, B.L., Boulanger, R.W., and Feigenbaum, H.P. (2004) Post-shaking failure of sand slope in centrifuge test, Proc. 11th Int. Conf. Soil Dynamics and Earthquake Engineering and the 3rd Int. Conf. Earthquake Geotechnical Engineering, Ed. Nogami and Seed Vol.2, 447-455.
Masing, G. (1926) Eigenspannungen und Verfestigung beim Messing, Proc. 2nd Int. Cong. on Applied Mechanics, 332-335 (in German).
Maslov, N.N. (1957) Questions of seismic stability of submerged sandy foundations and structures, Proc. 4th ICSMFE, Vol.1, 368-372.
Matsuo, O. (1996) Damage to River Dikes, Soils and Foundations, Special Issue on Geotechnical Aspects of the January 17 1995 Hyogoken-Nambu Earthquake, 1, 235-240.
Meneses, J., Ishihara, K., and Towhata, I. (1998) Effects of superimposing shear stress on the undrained behavior of saturated sand under monotonic loading, Soils and Foundations, Vol.38, No.4, 115-127.
Meneses, J., Ishihara, K. and Towhata, I. (2000) Flow failure of saturated sand under simultaneous monotonic and cyclic stresses, Journal of Geotechnical and Geoenvironmental Engineering, ASCE, Vol.126, No.2, 131-138.
Mizutani, T., Towhata, I. and Anai, K. (1999) Shaking table tests on seismic behavior of sheet pile quay walls subjected to backfill liquefaction, Proc. 11th Asian Regional Conf. Soil Mechanics and Geotechnical Engineering, Seoul, Vol.1, 551-554.
Mizutani, T., Towhata, I., Shinkawa, N., Ibi, S., Komatsu, T., and Nagai, T. (2001) Shaking table tests on mitigation of liquefaction-induced subsidence of river dikes, Proc. 16th ICSMGE, Istanbul, Vol.2, 1207-1210.
Mohajeri, M. and Towhata, I. (2003) Shake table tests on residual deformation of sandy slopes due to cyclic loading, Soils and Foundations, Vol.43, No.6, 91-106.
Mononobe, N., and Matsuo, H. (1929) On the determination of earth pressure during earthquakes, Proc. World Engineering Conference, Vol.9, 177-185.
Mori, S. and Ikeda, E. (1997) Traces of liquefaction of Tokyo formation sand layer and its consideration, Proc. JSCE, No.582/III-41, 247-263 (in Japanese)
Mulilis, J.P., Mori, K., Seed, H.B., and Chan, C.K. (1977) Resistance to liquefaction due to sustained pressure, Proc.ASCE, Vol.103, GT7, 793-797.
Murakami, H., Kaneko, T., Kimura, H., Razavi, S., and Bando, S. (2004) Displacement-based design of reinforcement method for natural slope, Proc. 11th Int. Conf. Soil Dynamics and Earthquake Engineering and the 3rd Int. Conf. Earthquake Geotechnical Engineering, Berkeley, Ed. T. Nogami and R.B. Seed, Vol.2, 344-350.
Nasu, T. (2000) Development of super multiple points injection method, Proc. 4th Int. Conf. Ground Improvement Geosystems, Helsinki..
Nishimura, S., Towhata, I., and Honda, T. (2002) Laboratory shear tests on viscous nature of liquefied sand, Soils and Foundations, Vol.42, No.4, 89-98.
Newmark, N.M. (1965) Effects of earthquakes on dams and embankments, Geotechnique, Vol.5, No.2, 137-160.
Newmark, N.M. and Rosenblueth, E. (1971) Fundamentals of Earthquake Engineering, Prentice-Hall, 233-236.
Noda, S., Uwabe, T., and Chiba, T. (1975) Relation between seismic coefficient and ground acceleration for gravity quay wall, Report of the Port and Harbor Research Institute, Vol.14, No.4, 67-111 (in Japanese)
Obermeier, S.F., Gohn, G.S., Weems, R.E., Gelinas, R.L., and Rubin, M. (1985) Geologic evidence for recurrent moderate to large earthquakes near Charleston, South Carolina. Science, Vol.227, 408-411.
Ohtomo, K. (1998) Load characteristics of ground lateral flow on in-ground structures, Proc. JSCE, No.591/I-43, 283-297 (in Japanese).
Okabe, S. (1924) General Theory on Earth Pressure and Seismic Stability of Retaining Wall and Dam. Proc. JSCE, Vol.10, No.6, 1277-1330 (in Japanese).
Okabe, S. (1926) General theory of earth pressure and laboratory testings on seismic stability of retaining walls, Proc. JSCE, Vol.12,

No.1, 123-134 (in Japanese).
Okada, S., Orense, R.P., Kasahara,Y., and Towhata, I. (1999) Prediction of liquefaction-induced deformations of river embankments, Proc. 2nd Int. Conf. Earthquake Geotechnical Engineering, Vol.2, Lisbon, 543-548.
Okamura, M., Abdoun, T.H., Dobry, R., Sharp, M.K. and Taboada, V.M. (2001) Effects of sand permeability and weak aftershocks on earthquake-induced lateral spreading, Soils and Foundations, Vol.41, No.6, 63-77.
Orense, R.P. and Towhata, I. (1998) Three dimensional analysis on lateral displacement of liquefied subsoil, Soils and Foundations, Vol.38, No.4, 1-15.
Poulos, S.J., Castro, G., and France, J.W. (1984) Liquefaction evaluation procedure, Proc. ASCE, 111, GT6, 772-792.
Pyke, R., Seed, H.B., and Chan, C.K. (1975) Settlement of sands under multidirectional shaking, Journal of Geotechnical Engineering, ASCE, Vol.,101, GT4, 379-398.
Sangawa, A. (1992) Earthquake Archaeology, Chuko Books, No.1096, ISBN4-12-101096-5, p.53 (in Japanese).
Sano, T. (1916) Seismic resistant design of buildings (Part 1), No. 83-1, Report of Shinsai Yobo Chosa Kai (Research Institute for Mitigation of Earthquake Disasters) (in Japanese).
Sano, T. (1917) Seismic resistant design of buildings (Part 2), No. 83-2, Report of Shinsai Yobo Chosa Kai (Research Institute for Mitigation of Earthquake Disasters) (in Japanese).
Sasaki, Y. (1994) River Dike Failure due to the Kushiro-Oki Earthquake of January 15, 1993, Proc. International Workshop on Remedial Treatment of Liquefiable Soils, Public Works Research Institute, Tsukuba.
Sasaki, Y., Towhata, I., Tokida, K., Yamada, K., Matsumoto, H., Tamari, Y., and Saya, S. (1992) Mechanism of permanent displacement of ground caused by seismic liquefaction, Soils and Foundations, Vol.32, No.3, 79-96.
Seed, H.B., Pyke, R.M., and Martin, G.R. (1978) Effect of multidirectional shaking on pore pressure, Journal of Geotechnical Engineering, ASCE, Vol.104, No.1, 27-44.
Shimizu, Y., Yamazaki, Y., Yasuda, S., Towhata, I., Suzuki, T., Isoyama, R., Ishida, E., Suetomi, I., Koganemaru, K., and Nakayama, W., (2005) Development of real-time safety control system for urban gas supply network, accepted by the Journal of Geotechnical and Geoenvironmental Engineering, ASCE.
Sladen, J.A., D'Hollander, R.D., and Krahn, J. (1985) The liquefaction of sands, a collapse surface approach, Canadian Geotechnical Journal, Vol.22, 564-578.
Taboada-Urtuzuastegui, V.M. and Dobry, R. (1998) Centrifuge modeling of earthquake-induced lateral spreading in sand, Journal of Geotechnical and Geoenvironmental Engineering, ASCE, Vol.124, No.12, 1195-1206.
Talwani, P. and Schaeffer, W.T. (2001) Recurrence rates of large earthquakes in the South Carolina Coastal plain based on paleoliquefaction data, Journal of Geophysical Research, Vol.106, 6621-6642.
Tamari, Y. and Towhata, I. (2003) Seismic soil-structure interaction of cross sections of flexible underground structures subjected to soil liquefaction, Soils and Foundations, Vol.43, No.2, 69-87.
Tatsuoka, F., Kato, H. Kimura, M. and Pradhan, T.B.S. (1988), Liquefaction strength of sands subjected to sustained pressure, Soils and Foundations, Vol.28, No.1, 119-131.
TCMSERS, Technical Committee for Mitigation of Seismic Effects on River Structures (1996) Report, Ministry of Construction.
Toki, S., Tatsuoka, F., Miura, S., Yoshimi, Y., Yasuda, S., and Makihara, Y. (1986) Cyclic undrained triaxial strength of sand by a cooperative test program, Soils and Foundations, Vol.26, No.3, 117-128.
Tokimatsu, K., Mizuino, H., and Kakurai, M. (1996) Building damage associated with geotechnical problems, Soils and Foundations, Special Issue on Geotechnical Aspects of the January 17 1995 Hyogoken-Nambu Earthquake, 1, 219-234.
Towhata, I., Sasaki, Y., Tokida, K., Matsumoto, H., Tamari, Y. and Yamada, K. (1992) Prediction of permanent displacement of liquefied ground by means of minimum energy principle, Soils and Foundations, Vol.32, No.3, 97-116.
Towhata, I., Mizutani, T., Anai, K. and Nakamura, S. (1998) Shaking table tests on liquefaction-induced distortion of sheet-pile quay wall, Proc. 13th Southeast Asian Geotechnical Conference, Taipei, 735-740.
Towhata, I., Vargas-Monge, W., Orense, R.P. and Yao, M. (1999a) Shaking table tests on subgrade reaction of pipe embedded in sandy liquefied subsoil, Soil Dynamics and Earthquake Engineering Journal, Vol.18, No.5, 347-361.
Towhata, I., Orense, R.P. and Toyota, H. (1999b) Mathematical principles in prediction of lateral ground displacement induced by seismic liquefaction, Soils and Foundations, Vol.39, No.2, 1-19.
Towhata, I., Kogai, Y., and Amimoto, K. (2000) Use of underground walls for mitigation of liquefaction-induced lateral flow, CD ROM Proc. GeoEng2000 Conf., Melbourne.
Towhata, I. and Kabashima, Y. (2001) Mitigation of seismically-induced deformation of loose sandy foundation by uniform permeation grouting, Proc. Earthquake Geotechnical Engineering Satellite Conference, XVth Int. Conf. Soil Mechanics and Geotechnical Engineering, Istanbul, 313-318.
Towhata, I., Nakai, N., Ishida, H., Isoda, S., and Shimomura, T. (2003) Mitigation of Liquefaction-Induced Floating of Embedded Structures by Using Underground Walls, Proc.12th Asian Regional Conference on Soil Mechanics and Geotechnical Engineering, Singapore, 335-338.
Toyota, H., Towhata, I., Imamura, S., and Kudo, K. (2004) Shaking table tests on flow dynamics in liquefied slope, Soils and Foundations, Vol.44, No.5, 67-84.
Usami, T. (1996) Damaging earthquakes in Japan, Univ. Tokyo Press, ISBN 4-13-060712-X (in Japanese).
Vaid, Y.P. and Chern, J.C. (1985) Cyclic and monotonic undrained response of saturated sands, Advances in the art of testing soils under cyclic conditions, ASCE, 120-147.
Vargas, W.M. (1998) Ring shear tests on large deformation of sand, Ph.D. Thesis, Univ. Tokyo.
Vargas-Monge, W. and Towhata, I. (1995) Measurement of drag exerted by liquefied on buried pipe, Proc. IS-Tokyo '95 First International Conference on Earthquake Geotechnical Engineering, publ. Balkema, Vol.2, 975-980.
Verdugo, R. and Ishihara, K. (1996) The steady state of sandy soils, Soils and Foundations, Vol.36, No.2, 81-91.
Wang, G.-Q., Zhou, X.-Y., Zhang, P.-Z., and Igel, H. (2002) Characteristics of amplitude and duration for near fault strong ground motion from the 1999 Chi-Chi, Taiwan earthquake, Soil Dynamics and Earthquake Engineering, Vol.22, 73-96.
Watanabe, K., Munaf, Y., Koseki, J., Tateyama, M. and Kojima, K. (2003) Behaviors of several types of model retaining walls subjected to irregular excitation, Soils and Foundations, Vol.43, No.5, 13-27.
Westergaard, H.M. (1931) Water pressure on dams during earthquakes, Transactions of ASCE, Paper No. 1835, 418-433.
Yasuda, S., Nagase, H., Kiku, H., and Uchida, Y. (1992) The mechanism and a simplified procedure for the analysis of permanent ground displacement due to liquefaction, Soils and Foundations, Vol.32, No.1, 149-160.
Yasuda, S., Ishihara, K., Harada, K., and Shinkawa, N. (1996) Effect of soil improvement on ground subsidence due to liquefaction, Soils and Foundations, Special Issue on Geotechnical Aspects of the January 17 1995 Hyogoken-Nambu Earthquake, 1, 99-107.
Yasuda, S., Ishihara, K., Harada, K., and Nomura, H. (1997) Factors which affected the area of lateral flow that occurred in the ground behind quaywalls, Proc. 2nd Conf. on Earthquake disasters in Hanshin-Awaji area, JSCE, 113-120 (in Japanese).
Yonekura, R. and Shimada, S. (1992) Long term durability of chemical grouts, Monthly Magazine of Japanese Geotechnical Society, Vol.40, No.12, 17-22 (in Japanese).
Yoshida, N., and Hamada, M. (1990) Damage to foundation piles and deformation pattern of ground due to liquefaction-induced permanent ground deformation, Proc. 3rd Japan-U.S. Workshop on Earthquake Resistant Design of Lifeline Facilities and Countermeasures for Soil Liquefaction, San Francisco, 147-161.
Yoshimine, M., Nishizaki, H., Amano, K., and Hosono, Y. (2004) Flow deformation of liquefied sand under constant shear load, Proc. 11th Int. Conf. Soil Dynamics and Earthquake Engineering and the 3rd Int. Conf. Earthquake Geotechnical Engineering, Ed. T.Nogami and R.B.Seed, Vol.1, 420-427.
Zen, K., Yamazaki, H., Hayashi, K., Yoshikawa, R., Fujisawa, N., and Nagoshi, T. (1997) A field test on chemical grouting at Niigata, Proc. 32nd Japan National Conf. Geotechnical Engineering, Kumamoto, 2347-2348 (in Japanese).